2020-03-25

Solvent Diffusion in a Solvent/Water/Bitumen System

Cavanzo Balcazar, Emilio Andres

UNIVERSITY OF CALGARY

Solvent Diffusion in a Solvent/Water/Bitumen System

by

Emilio Andres Cavanzo Balcazar

A THESIS

SUBMITTED TO THE FACULTY OF GRADUATE STUDIES

IN PARTIAL FULFILLMENT OF THE REQUIREMENTS FOR THE

DEGREE OF MASTER OF SCIENCE

GRADUATE PROGRAM IN CHEMICAL ENGINEERING

CALGARY, ALBERTA

MARCH, 2020

Abstract

Thermal heavy oil recovery processes use steam and therefore are energy intensive and emit significant amounts of greenhouse gases. One option to reduce steam usage is a solvent-assisted process where a hydrocarbon solvent is co-injected with steam. A potential issue for solvent-assisted processes is the effect of the condensing steam on the mass transfer rate of solvent into the heavy oil. This thesis focuses on the diffusion of solvent into the bitumen when a layer of condensed water is present.

The diffusion experiments were performed in 2.2 cm diameter glass vials. Water layers with thicknesses from 0.25 to 2 cm were placed over bitumen and excess solvent was placed over the water. The diffusion rate of the solvent through the water was determined from the change in height of the bitumen layer. A cathetometer was used to measure the changes in water and bitumen heights. The diffusion of toluene, cyclohexane, *n*-pentane and *n*-heptane into two bitumens from different source reservoirs was evaluated at temperatures from 20 to 80°C. Solvent diffusion rates were calculated from the change in the height of the water+bitumen layers and the emulsification rates were determined from the additional change in height of the bitumen layer. The water content in the bitumen was verified by Karl Fischer titrations and micrography. The solvent diffusion rates were modeled with a 1D steady state diffusion model using diffusivity and solubility values for solvent in water taken from the literature.

It was found that surfactants naturally present in bitumen were responsible for water-in-oil and oil-in-water spontaneous emulsification. At 20°C, the measured diffusion rates were consistent with the predicted diffusion rates and the water was a significant barrier to mass transfer. At 60°C, the diffusion rates were significantly higher than predicted possibly due to convection induced from small thermal gradients in the temperature bath but also due to gravity instability. The rate of emulsification rates and time to gravity instability correlated to the solvent mass transfer rates. It is expected that at steam temperatures the water will pose little barrier to mass transfer because gravity instability, convection, and emulsification will dominate.

Acknowledgments

Doing a masters at the University of Calgary has been an extraordinary journey. I would like to acknowledge my supervisor, Dr. Harvey Yarranton, for giving me the opportunity to be a member of your research group. I learned from you the importance of having strong fundamentals to analyze any problem and solve it successfully, also the value of paying attention to the small details which can make a significant difference in the final result. Thank you for all your guidance and advices. You have all my admiration and respect. I truly consider you a role model personally and professionally.

I want to acknowledge my Co-supervisor Dr. Apostolos Kantzas, for giving me specific and fundamental ideas for solving many challenges that I faced during my research. Also you help me to interpret the data obtained from my experiments. Thanks a lot for your guidance and feedback.

I am really grateful to the two lab managers of our research group. Florian, I learned from you the importance of asking basic and fundamental questions of a specific phenomenon, that's the easiest way to find the real problem and solve it, also how important is being and thinking simple to analyze any problem. For me these teachings are invaluable and I will always keep them in mind. Elaine, thanks for helping me with the Karl Fischer measurements and the micrographs, I really appreciated it.

I want to extend my gratitude to my friends currently in our research group: Nicolay, John, Javier, Daniela and Jairo, I really enjoyed all the good times we passed together, the parties and the soccer games, thank you for your friendship. I am also grateful to other current and previous members of the research group: Francisco, Amir, Nicson, Franklin, Andres, Yulman and Yoshi. Thank you to some others with whom I shared good times at the university: Andres, Pradeep, Ajay, Diego, Mario, Jonas, Mohy, Anderson, Jesus, Camilla and Javier.

Finally, I would like to give a special acknowledgment to the Canada First Research Excellence Fund (CFREF) for funding this project.

Dedication

To God, thanks! All my life is yours!

To my dad Luis Emilio and my mom Luz Amparo, this is just for you.

To my brother Juan Jose and my sister Maria Jose

I love you!

Table of Contents

List of Tables

List of Figures and Ilustrations

List of Symbols, Abbreviations and Nomenclature

Upper Case Symbols

A : Cross sectional area [cm^2]

A^* : Fitting parameter of the bitumen density correlation

B^* : Fitting parameter of the bitumen density correlation

C_A : Concentration of species A [g/cm^3]

C_{AB0} : Initial concentration of species A in B [g/cm^3]

C_{Aeq} : Solubility of species A in B [g/cm^3]

$C_{CO2,o}$: Concentration of CO_2 in the oil phase

$C_{CO2,w}$: Concentration of CO_2 in the water phase

$C_{s,w}^{eq}$: Solubility of solvent in water

CI : Confidence interval

$C7$: *n*-heptane

$C5$: *n*-pentane

CH : Cyclohexane

D_{AB} : Diffusivity of species A in B [cm^2/h]

D_{BA} : Diffusivity of species B in A [cm^2/h]

D_{SW} : Diffusivity of the solvent in water [cm^2/h]

D^* : Fitting parameter of the bitumen density correlation

E_b : Correction factor of the bitumen volume

E_w : Correction factor of the water volume

F^* : Fitting parameter of the bitumen density correlation

G^σ : Gibss free energy

G : Apparent gravity

J_{Ax} : Mass flux of species A in the x direction [g/cm^2h]

J_{Bx} : Mass flux of species B in the x direction [g/cm^2h]

K_1 : Integration constant

K_2 : Integration constant

L : Film thickness [cm]

P : Pressure of the system [MPa]

S : Entropy

SG : Specific gravity of the bitumen

T : Temperature

T_{bp} : Average boiling point of the bitumen [°R]

V_{dome} : Volume of the bitumen dome [cm^3]

$V_{b,avg}$: Volume of the bitumen layer based on the uncorrected average height [cm^3]

$V_{w,avg}$: Volume of the water layer based on the uncorrected average height [cm^3]

V_b : Corrected average bitumen volume [cm^3]

V_w : Corrected average water volume [cm^3]

V_s : Volume change of the combined bitumen and water layer [cm^3]

V_t : Volume change of the combined bitumen and water layer at a give time [cm^3]

$V_{b,t=0}$: Initial volume of the bitumen layer [cm^3]

$V_{w,t=0}$: Initial volume of the water layer [cm^3]

$V_{t,t=0}$: Volume of the combined bitumen and water layer at t=0 [cm^3]

V_b^0 : Mass-based bitumen layer volume [cm^3]

V_w^0 : Mass-based water layer volume [cm^3]

ΔV_w : Change in water layer volume [cm^3]

W_k : Watson – *K* parameter

W : Water

Lower Case Symbols

a : First parameter of the dome fitted function

$a_{i,s}$: NRTL model interaction parameter

b : Second parameter of the dome fitted function

$b_{i,s}$: NRTL model interaction parameter

c : Concentration

c_s : Concentration of solvent

c_{1A} : Concentration of species A in x=0

c_{2A} : Concentration of species A in x=L

$c_{i,s}$: NRTL model interaction parameter

h_w : Water layer height [cm]

h_{bl} : Uncorrected left height of the bitumen layer [cm]

h_{br} : Uncorrected right height of the bitumen layer [cm]

h_{bc} : Uncorrected center height of the bitumen layer [cm]

h_{wc} : Heigth of the centre of the top water layer [cm]

h_{we} : Heigth of the edge of the top water layer [cm]

$\Delta h_{b,avg}$: Average thickness of the bitumen layer [cm]

$\Delta h_{w,avg}$: Average thickness of the water layer [cm]

Δh_{wc} : Thickness of the center of the water layer [cm]

Δh_{we} : Thickness of the edge of the water layer [cm]

k : Wavenumber

k_{pc} : Partition coefficient

m_A : Mass diffused of species A

m_b *:* Measured mass of bitumen [g]

m_w *:* Measured mass of water [g]

n : Number of experimental measurements

n_i : Number of moles of species *i*

r : Radial location of dome fitted function

s : Standard deviation of a set of measurements

t : Time [h]

w_A : Mass fraction of species A

w_w : Mass fraction of water in the bitumen layer

$w_{w,max}$: Maximum value of the water content in bitumen

x : Distance in the x direction

x_i : Solubility of water in bitumen as a mole fraction

$\bar{x}$: Average of a set of experimental measurements

y : Distance in the y direction

$\overline{y}$: Average independent variable

z : Distance in the z direction

Greek Symbols

ρ : Density of the mixture [g/cm^3]

ρ_1 : Density of the upper fluid [g/cm^3]

ρ_2 : Density of the lower fluid [g/cm^3]

ρ_b : Density of the bitumen [g/cm^3]

ρ_w : Density of the water [g/cm^3]

ρ_s : Density of the solvent [g/cm^3]

α : Significance level

∞ : Infinite dilution

γ : Mean interfacial tension

γ_i^{∞} : Infinite dilution activity coefficient of water in bitumen

μ_i : Chemical potential of component i

$\alpha_{i,s}$: NRTL model interaction parameter

$\tau_{s,i}$: NRTL model interaction parameter

τ_{is} : Interaction parameter between the water and bitumen

σ : Growth rate of the instability

λ : Wavelength of the periodic instability

Superscripts

∞ : Infinite dilution

Subscripts

avg : Average

b : Bitumen

c : Center of the water and/or bitumen layer

e : Edge of the water and/or bitumen layer

i : Component *i*

l : Left of the water and/or bitumen layer

pc : Partition coefficient

r : Right of the water and/or bitumen layer

s : Solvent

w : Water

Abbreviations

ARD : Absolute Relative Deviation

API : American Petroleum Institute

CSI : Cyclic Solvent Injection

ES-SAGD	: Expanding Solvent Steam Assisted Gravity Drainage
IFT	: Interfacial Tension
LASER	: Liquid Addition to Steam for Enhancing Recovery
W/O	: Water in oil emulsion
O/W	: Oil in water emulsion
SAGD	: Steam Assisted Gravity Drainage
SARA	: Saturates, Aromatics, Resins and Asphaltenes
SAP	: Solvent Aided Process
VAPEX	: Vapor Extraction Process

CHAPTER ONE: INTRODUCTION

Heavy oils and bitumen are defined as oils with a specific gravity below 20 and 10 °API, respectively (Veil and Quinn, 2008). Heavy oil and bitumen viscosities range from 100 to over a million mPa.s at standard conditions. For convenience, heavy oil will be used to refer to both heavy oil and bitumen unless otherwise indicated. Heavy oil reservoirs are located throughout the world and one of the largest deposits is in Alberta. Alberta has $280 \cdot 10^9$ m^3 of heavy oil in place of which $50 \cdot 10^9$ m^3 is currently recoverable. The production of heavy oil from Alberta in 2018 was $453 \cdot 10^3$ m^3/d (AER, 2019).

At *in situ* conditions, the viscosity of many heavy oils can exceed 10000 mP.s. The key to producing heavy oil is to mobilize it in the reservoir, that is, lower its viscosity sufficiently such that it flows readily in the reservoir to a production wellbore. Methods to reduce heavy oil viscosity include: 1) heating the bitumen to a sufficiently high temperature; 2) dissolving solvent in the bitumen to dilute it; 3) inducing a compositional change of the oil that leads to a mobile oil phase, for example by precipitated out asphaltenes or by *in situ* upgrading (Gates and Chakrabarty, 2008; Bayestehparvin *et al*., 2018; Butler *et al*., 1981; Orr, 2009).

The predominant heavy oil recovery process in Alberta is steam-assisted gravity drainage, or SAGD. SAGD was proposed as an *in situ* heavy oil recovery method in the 1970s (Butler *et al.*, 1981) and consists of a pair of two horizontal wells, an injector above a producer, which are drilled into the lower part of a formation. Both wells and the formation between them are first heated by circulating steam through each well. When contact is established between the two wells, steam injection is continued in the upper well, creating a steam chamber at a saturated steam temperature. The steam chamber rises above the injector in the reservoir and decreases the viscosity of the surrounding oil viscosity due to transfer of latent heat from the steam to the cold heavy oil. Meanwhile, bitumen and condensed steam are drained by gravity along the sides of the steam chamber to the lower horizontal well. (Butler, 1987; Butler, 1998; Ji *et al.*, 2015). However, there are some environmental issues with SAGD including the requirement of large volumes of fresh

water for steam generation and the emission of carbon dioxide from the burning of fuel for steam generation (Faradonbeh *et al.*, 2016).

One option to reduce the use of steam is to replace it, or some fraction of it, with a solvent. Dilution with solvent can achieve comparable viscosity reduction to heating with less energy and water usage. Solvent based processes such as VAPEX, N-Solv, and CSI completely replace the steam while solvent assisted processes such as ES-SAGD, SAP and LASER partially replace the steam (Bayestehparvin *et al.*, 2018). This thesis is focused on solvent-assisted processes where both steam and solvent can condense in the reservoir.

In a solvent assisted SAGD process, a pure hydrocarbon solvent or a mixture of solvents is co-injected with the steam at a low solvent concentration as shown in Figure 1.1 (Nasr and Ayodele, 2007). Lin *et al.* (2014) pointed out that the solvent should be chosen such that the solvent and water condensed at similar conditions in order for heat and mass transfer to occur simultaneously at the boundary between the vapor chamber and the untouched heavy oil. According to this criteria, *n*-hexane and *n*-heptane are ideal solvents because their saturation temperatures are similar to that of steam (Orr, 2009); however, they have never been used on a field scale project because they are expensive compared with propane and butane. Experimental evaluations and numerical simulations have shown that solvents ranging between butane and *n*-heptane are the best for application during an solvent assisted SAGD process (Gates and Chakrabarty, 2008; Govind *et al.*, 2008; M. Keshavarz *et al.*, 2014; Keshavarz *et al.*, 2015; Khaledi *et al.*, 2015; Orr, 2009). Of these solvents, only butane has been applied with technical success, increasing the overall oil recovery factor, decreasing the SOR (Steam-Oil-Ratio), and achieving more than 70% solvent recovery in two field projects: 1) an SAP pilot at Senlac thermal facility of EnCana Corp. in 2002 with an average increase in oil production rate from 300 to 480 m^3/d for the well pair after the solvent was aided and a SOR reduction from 2.6 to 1.6 m^3/m^3; 2) an SAP pilot at Christina Lake by EnCana Corp. in 2004 with an increase in the oil production rate from 95 to 210 m^3/d and a SOR reduction from 5 to 1.6 m^3/m^3.

Other field projects have used mixed solvents and diluents. For example, the LASER pilot in Cold Lake by Imperial Oil and ExxonMobil in 2002 used a pentane plus fraction diluent decreasing the SOR from 3.4 to 2.6 m^3/m^3. The ES-SAGD pilot operated by NEXEN in Long Lake used Jet B (carbon numbers from $C_7 - C_{12}$) but did not obtain any incremental oil recovery or reduction in SOR (Memarzadeh, 2015; Lin *et al*, 2014). Typical operating pressures in the aforementioned projects ranged from 1.5 to 2.5 MPa and, according to numerical and experimental studies, temperatures at the interface ranged from 150 to 250°C (Keshavarz *et al*., 2015; Ji *et al.*, 2015).

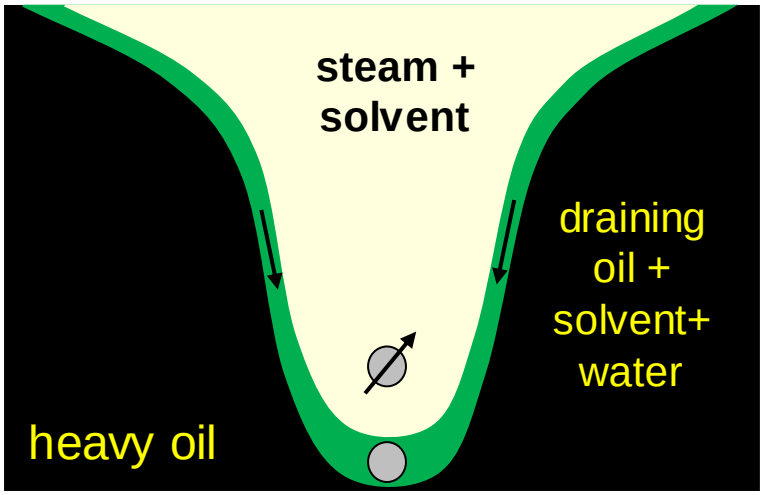

Figure 1.1. Scheme of the SA-SAGD method in the steam/solvent/bitumen chamber.

A significant uncertainty with such steam assisted processes is the nature of the material that condenses; that is, does a uniform liquid phase form, two liquid phases, or an emulsion? The scenarios that can occur in the interface depend on the volatility and the volume of injected solvent and are shown in Figure 1.2. If a highly volatile solvent such as propane is co-injected, then steam will most likely condense preferentially. However, if a heavier solvent such as *n*-heptane is injected then the solvent will condense preferentially. If two liquid phases condense, water-in-solvent and solvent-in water emulsions can form during this process. The type and composition of the liquid phase(s) will affect the mass transfer rates and the success of the process. Ideally, the solvent would be in direct contact with the oil either as a solvent-rich phase or a substantial concentration in a water-rich phase.

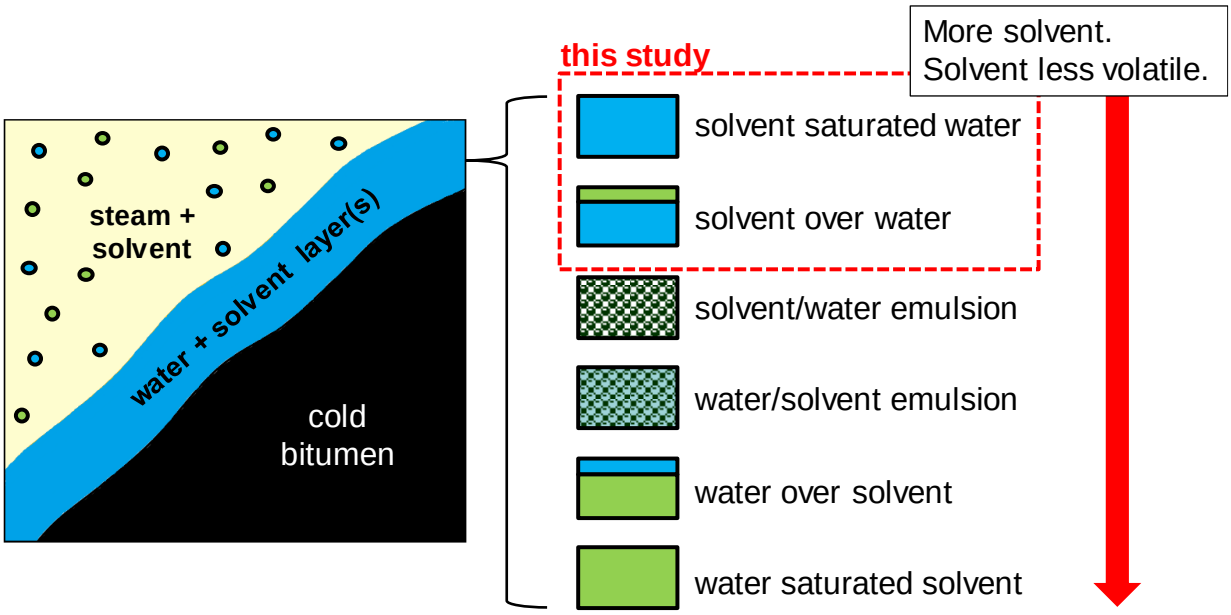

Figure 1.2. Possible scenarios that can be present at the steam/bitumen interface during the application of a solvent assisted-SAGD method.

Co-condensation of the solvent and steam forming a single liquid layer over the bitumen has been proposed for solvents with similar saturation temperatures as steam, such as hexane, heptane, and dodecane (Lin *et al.*, 2014; Orr, 2009; Li and Mamora, 2010). The condensed fluid with these solvents will have a high solvent content, minimizing the blocking effect of the water in the film and improving the production performance relative to more volatile solvents. Jha *et al*. (2013) performed a numerical study on steam-solvent processes for a wide range of alkanes (from propane to *n*-decane). They observed only a single condensed liquid phase at all conditions examined. They found that, as the temperature drops near the steam chamber boundary, the condensed fluid had a low solvent content and initially formed a water barrier over the bitumen. As the temperature decreased toward the chamber boundary and more steam condensed, the vapor phase became richer in solvent and the solvent content in the condensed fluid increased.

Dong (2011) proposed an algorithm to estimate the equilibrium temperature and solvent fraction in the vapor phase at the boundary of the steam chamber. He found that, for a hexane/steam system and over a large range of solvent fractions in the vapor phase, the condensed fluid was initially water-rich. The solvent content in the condensed fluid increased only when its concentration in the vapor was very high. As observed by Jha *et al*. (2013), the solvent fraction in the vapor phase

increased as more steam condensed leading to an increased solvent content in the condensed fluid as the process progressed. Dong also noted that when the edge of the chamber was oriented such that gravity drained the condensing water away from the interface, a high solvent concentration interacted with the oil (*i.e.*, at the upper portions of the steam chamber). However, if the edge of the chamber was oriented such that gravity drained the condensing water towards the interface, a layer of liquid water blocked solvent from interacting with the oil, creating a resistance between solvent and bitumen in the lower portion of the steam chamber (Dong, 2011).

When steam and solvent condense as two liquid phases, water-in-oil emulsions may form. Doan *et al*, (2007) conducted scaled SAGD experiments and observed that the produced fluid after breakthrough consisted of single-phase condensate and water-in-oil emulsions. Mohammadzadeh and Chatzis (2009) conducted flow visualization experiments and confirmed that water-in-oil emulsions can form *in-situ* during a SAGD process. They reported water droplet diameter sizes in the range of 1.1 to 5 um. Ezeuko *et al.* (2012) conducted a simulation study to investigate the effect of emulsion on SAGD and ES-SAGD performance. Their results showed that emulsification increased bitumen mobility and therefore decreased the cumulative steam-oil ratio.

Many investigations have studied the diffusive mass transfer of carbon dioxide through water into crude oil, a factor affecting tertiary CO_2 flooding (Ghoroori *et al*., 2017; Mirazimi *et al*., 2017; Shu *et al*., 2017; Grogan *et al.*, 1987; Muller and Lake, 2007). However, no experimental or analytical/numerical studies were found in the literature for the effect of a water barrier on the mass transfer of a liquid hydrocarbon solvent through water into heavy oil.

1.1 Objectives

This aim of this research is to investigate the effect of a water barrier on the mass transfer of solvent into heavy oil; that is, the scenario where water condenses first followed by condensation of solvent. Spontaneous emulsification and gravity instability are also considered. The specific objectives are to:

1. Develop an experimental methodology to measure diffusion of solvent into bitumen through a water layer. The mass transfer rate of the solvent and water-in-oil emulsification rate will be determined from the changes in volume of the water and bitumen layers.

2. Investigate the effect of the water layer thickness (0.25 to 2 cm), temperature (20 to 80°C), solvent type (toluene, cyclohexane *n*-pentane and *n*-heptane), and the initial condition of the water (unsaturated or presaturated with solvent) on the solvent mass transfer rate and the emulsification rate. Two Western Canadian bitumens are evaluated.
3. Model the solvent mass transfer data using a steady state liquid-liquid diffusion model based on Fick's first law.
4. Assess gravity instability of bitumen visually and by the change in the diffusion rate.

1.2 Thesis Structure

This thesis is divided into five remaining chapters, as outlined below.

Chapter Two begins with a review of diffusive mass transfer theory. The effect of water blocking in CO_2/water/oil micro systems is discussed. Mechanisms for spontaneous emulsification and experimental evidence of spontaneous emulsification of water into heavy oil are presented. Finally, gravity instability in binary liquid-liquid immiscible systems is discussed.

Chapter Three describes the experimental methodology developed in this thesis to measure the solvent and water content in bitumen by examining the change in the solvent/water interface, water and bitumen volume in a solvent/water/bitumen test. The steps take to validate the method and an error analysis are also provided.

Chapter Four presents the property data required to analyze and interpret the mass transfer experiments. The mass transfer and emulsification data are presented at 20 and 60°C including a discussion of the effect of water layer thickness and solvent type. The steady state diffusion model predictions are compared with the solvent mass transfer data. The impact of gravity instability is also discussed. Finally, tests to assess the effect of natural surfactant on spontaneous emulsification are presented.

Chapter Five summarizes the most important results and conclusions from this thesis and provides recommendations for future work in this area.

CHAPTER TWO: LITERATURE REVIEW

The main concepts used to interpret the experiments presented in this thesis are mass transfer, spontaneous emulsification, and gravity instability. This chapter provides a summary of mass transfer theory with emphasis on relevant concepts of steady and unsteady state diffusion. The studies reported in the literature about mass transfer of solvents across layers of water and bitumen are discussed. The fundamentals of emulsions and the mechanisms that control spontaneous emulsification are presented. Finally, two theories that describe gravity instability in immiscible liquid-liquid systems will be described: Rayleigh-Taylor and Marangoni instabilities.

2.1 Mass Transfer Fundamentals

Diffusion is the process where matter is transported from one part of a system to another as a result of random molecular motions (Crank, 1975b; Poiling *et al*.,1987). Cussler (2007) defined it as the net transport of material within a single phase in the absence of mixing, such as by mechanical means or by convection. Both experiments and theory have shown that diffusion can result from pressure gradients, temperature gradients, external force fields, and concentration gradients (Poiling *et al.*, 1987). In this thesis only diffusion driven by a concentration gradient will be considered with no convection, external forces, or reaction.

2.1.1 Steady State Diffusion (Fick's First Law)

Fick (1855) quantified diffusion by adapting the mathematical equation of heat conduction derived some years earlier by Fourier (1822) (Crank, 1975a). He proposed that, in isotropic substances, the rate of transfer of a diffusing substance through unit area of a section is proportional to the concentration gradient measured normal to the section. Therefore, at steady state and without any convection effects, the mass flux is proportional to the concentration gradient and the proportionality factor, D_{AB}, defined as the diffusivity of Component A in Component B. *Fick's First Law* is formulated as follows (Crank, 1975b; Poiling *et al.*, 1987):

$$J_{Ax} = -D_{AB}\frac{dC_A}{dx} \tag{2.1}$$

$$J_{Bx} = -D_{BA}\frac{dC_B}{dx} \tag{2.2}$$

where J_x is the mass flux in the x direction, D is the diffusivity of one component in another, C is concentration, x is distance, and subscripts A and B indicate Components A and B, respectively. The negative sign in this relationship indicates that particles flow from regions of higher to lower concentration (Bird *et al.*, 2002). Steady state diffusion takes place at a constant rate; that is, the number of molecules crossing a given interface is constant with time. In other words, throughout the system dC/dx = constant and $dC/dt = 0$, where t is time (Cussler, 2007).

In a binary mixture of A and B, where substance A is diffusing in one direction through substance B and *vice versa*, and also if the volume change upon mixing is negligible (regular solution), then (Cran and Hartle, 1949; Bearman, 1960):

$$J_{Ax} = J_{Bx} \tag{2.3}$$

For this condition to be satisfied, then (Crank, 1975; Oballa and Butler, 1989):

$$D_{AB} = D_{BA} \tag{2.4}$$

Hence, the behavior of a binary system with no volume change upon mixing can be described using a single mutual diffusivity which is a function of the composition of each component, temperature, and pressure (Crank, 1975; Oballa and Butler, 1989).

Steady diffusion across a thin film is considered in this thesis and is illustrated in Figure 2.1. On each side of the film interface, $0 < x < L$, there is a well-mixed solution of a solvent (Component B) and one solute (Component A). Both of these solutions are dilute but have a different solute concentration. The solute diffuses from the fixed higher concentration located at $x < 0$ on the left-hand side of the film into the fixed less concentrated solution located at $x > L$ on the right-hand side (Cussler, 2007). If there is no material accumulation in the film, combining a mass balance with *Fick's First Law* gives the following equation (Cussler, 2007):

$$0 = D_{AB}\frac{d^2C_A}{d^2x} \tag{2.5}$$

Equation 2.5 is integrated with the following boundary conditions:

$$x = 0, \quad c_A = c_{1A} \tag{2.6}$$

$$x = L, \quad c_A = c_{2A} \tag{2.7}$$

to obtain the following concentration profile (Cussler, 2007):

$$c = c_{1A} + (c_{2A} - c_{1A})\frac{x}{L} \tag{2.8}$$

The flux is found by differentiating this profile (Cussler, 2007) with the following result:

$$J = \frac{D_{AB}}{L}(c_{1A} - c_{2A}) \tag{2.9}$$

The flux is constant because the system is in steady state. Based on the definition of flux, Eq. 2.9 can be rewritten to obtain the mass diffused as follows:

$$m_A = \frac{AtD_{AB}}{L}(c_{1A} - c_{2A}) \tag{2.10}$$

where *m* is the mass diffused, *A* is the cross sectional area, and *L* is the film thickness.

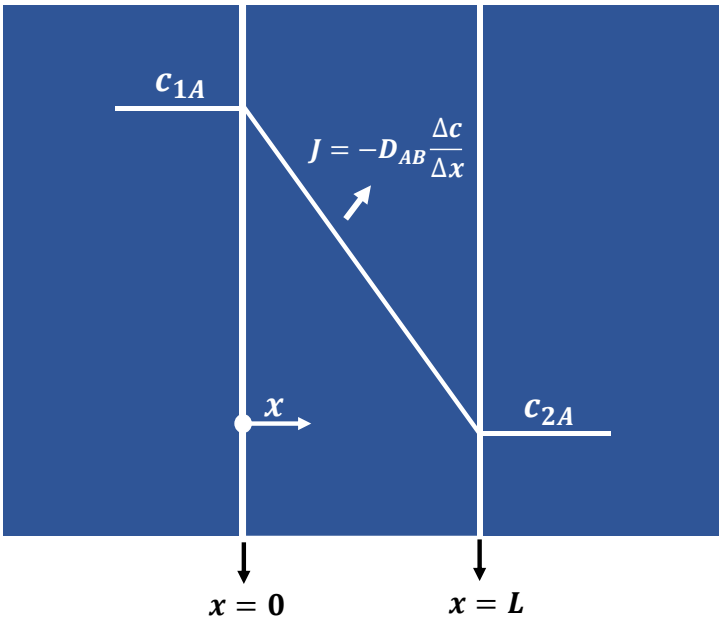

Figure 2.1. Illustration of steady state diffusion through a film between two solutions of a solute (A) in a solvent (B). Adapted from Cussler (2007).

2.1.2 Unsteady State Diffusion (Fick's Second Law)

If mass transfer of Component A through Component B is governed by unsteady state diffusion, then the concentration gradient of *A* in the film will be a function of time, as shown in Figure 2.2. In this thesis, the unsteady state solution was required to estimate the time for the solvent to reach the bitumen through the water layer. This situation is equivalent to diffusion through a semi-infinite slab.

For a dilute liquid solution (constant diffusivity coefficient and density), a mass balance is performed on a control volume and the mass flux term by diffusion is replaced by Fick's First Law to obtain the following continuity equation (Bird *et al.*, 2002):

$$\rho\left(\frac{\partial w_A}{\partial t}\right) = \rho D_{AB}\nabla^2 w_A \tag{2.11}$$

where w is the mass fraction and ρ is the density of the mixture in g/cm³. If diffusion occurs in one direction, then Eq. 2.11 simplifies to *Fick's Second Law*, given by (Bird *et al.*, 2002):

$$\frac{\partial C_A}{\partial t} = D_{AB}\frac{\partial^2 C_A}{\partial x^2} \tag{2.12}$$

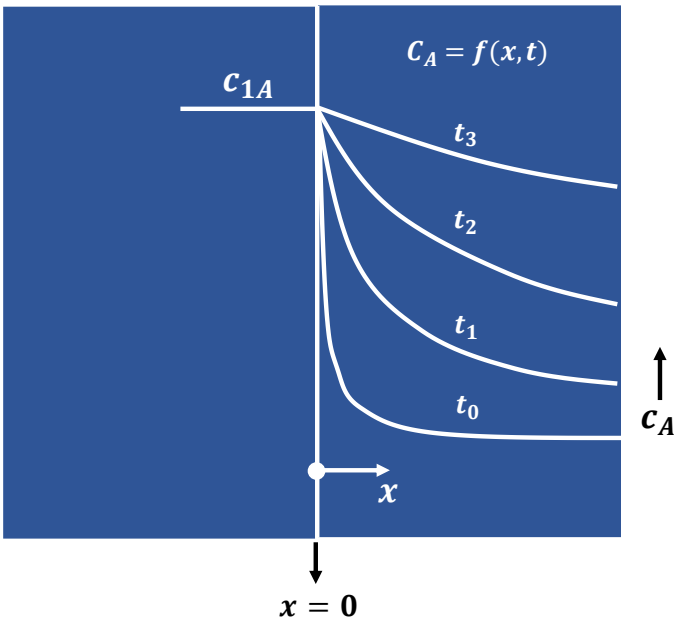

Figure 2.2. Illustration of unsteady state diffusion of a solute (A) in a semi-infinite slab. Adapted from Cussler (2007).

Analytical solutions for Eq. 2.12 can be obtained as long as the diffusivity is assumed to be constant (*i.e.*, independent of concentration) and there is no volume change upon mixing. These two conditions apply in dilute systems (Grimaldos, 2018). Eq. 2.13 is a second order partial differential equation and is solvable by using the combination of variables method where the following integration factor, *y*, is introduced (Bird *et al.*, 2002; Cussler, 2007):

$$y = \frac{x}{\sqrt{4D_{AB}t}} \tag{2.13}$$

The integration factor is substituted for *t* and *x* in Eq, 2.12 to obtain the following expression (Cussler, 2007):

$$\frac{d^2C_A}{dy^2} + 2y\frac{dC_A}{dy} = 0 \tag{2.14}$$

The general solution to Eq. 2.12 is (Bird *et al.*, 2002):

$$C_A = K_1 \int_0^y \exp(-\bar{y}^2)\, d\bar{y} + K_2 \tag{2.15}$$

where $\bar{y}$ is the independent variable, K_1 and K_2 are the integration constants, whose values depend on the initial and boundary conditions.

The solution of relevance for this thesis is for diffusion of a solute (A) into a semi-infinite solution with a solvent (B). In this case, the initial condition is the concentration of the solute in the solution given by:

$$C_A(x > 0, t = 0) = C_{AB0} \tag{2.16}$$

where C_{AB0} is the initial concentration of Solute A in Solvent B and can have any value from zero to the solubility of A in B.

Two boundary conditions are required to solve Eq. 2.15. The first boundary condition is applied at the interface of A and B (x=0 in Figure 2.2) and is given by (Richardson, 2017; Etminan, 2014):

$$C_A(x = 0, t) = C_{Aeq} \tag{2.17}$$

where C_{Aeq} is the solubility of the diffusing Solute A in Solvent B at the system pressure and temperature (Richardson, 2017). At short times when Solute A has not reached the end of the slab, the following infinite acting boundary condition can be applied (Richardson, 2017; Crank, 1975):

$$C_A(x \to \infty, t) = 0 \tag{2.18}$$

Once Solute A has reached the end of the slab, the following finite acting boundary condition is applied (Grimaldos, 2018):

$$\left.\frac{dC_A}{dx}\right|_{x=L} = 0 \tag{2.19}$$

where L is the distance from the interface to the end of the slab.

Dilute Systems: Infinite Acting Solution

The infinite acting solution for dilute systems is given by

$$C_A = C_{AB0} + (C_{Aeq} - C_{AB0})erfc\left(\frac{x}{\sqrt{4D_{AB}t}}\right) \quad (2.20)$$

where *erfc* is the complementary error function. When the concentration of A in B is zero at t=0, Eq. 2.20 simplifies to the following expression (Crank, 1975b):

$$C_A = C_{Aeq}erfc\left(\frac{x}{\sqrt{4D_{AB}t}}\right) \quad (2.21)$$

Eq. 2.21 is valid for isothermal, isobaric one-dimensional diffusion in a dilute isotropic medium (constant diffusivity) without reaction and bulk flow, with no volume change upon mixing, and where the diffusing substance has not reached the bottom of the liquid column; that is, at early time (Grimaldos, 2018). Eq. 2.24 can be used to plot the concentration profile of A in B during the unsteady state period before A reaches B. Solutions for liquid-liquid systems with concentration dependent diffusivity (non-dilute systems) and swelling require numerical models and are outside the scope of this thesis.

2.2 Mass Transfer through Water Films in Carbon Dioxide/Bitumen Systems

Liquid-liquid mass transfer experiments in hydrocarbon/water/bitumen systems have not been reported in the literature. However, a similar phenomenon known as water blocking can occur during miscible flooding where the oil may be prevented from direct contact with a gas (rich in CO_2) by a water barrier, Water blocking has been widely studied experimentally using micromodels, analytically, and numerically (Grogan and Pinczewski, 1987; Muller and Lake, 2007; Grogan *et al.* 2007; Mirazimi *et al.* 2017; Bijeljic *et al.*, 2003; Shu *et al.*, 2017; Fayazi and Kantzas, 2018; Lin and Huang, 2007; Ghoroori *et al.*, 2017; Vali *et al.*, 2011).

Water blocking affects the microscopic displacement efficiency of reservoirs during application of tertiary CO_2 injection after a waterflood. The bulk of the residual oil is left behind the CO_2 displacement front, trapped by water, and therefore inaccessible to flowing CO_2 channels. Eventually, CO_2 diffuses through the water barrier progressively swelling both the oil and water phases. If the oil swelling displaces the blocking water completely, direct contact between solvent and oil can be achieved which results in high oil recovery.

Campbell and Orr (1985) studied the recovery of oil with and without the presence of water barriers shielding the oil. They performed a visual experiment with a micromodel in which a mixture of C_9 through C_{13} branched alkanes in a dead-end pore shielded by water was recovered by CO_2, as shown in Figure 2.3. They confirmed that the CO_2 diffused through the water, swelled the residual oil, and displaced the water barrier. They also showed that the efficiency of both first contact and multiple contact miscible displacements were much higher in the absence of water (Campbell and Orr, 1985; Mirazimi *et al.*, 2017).

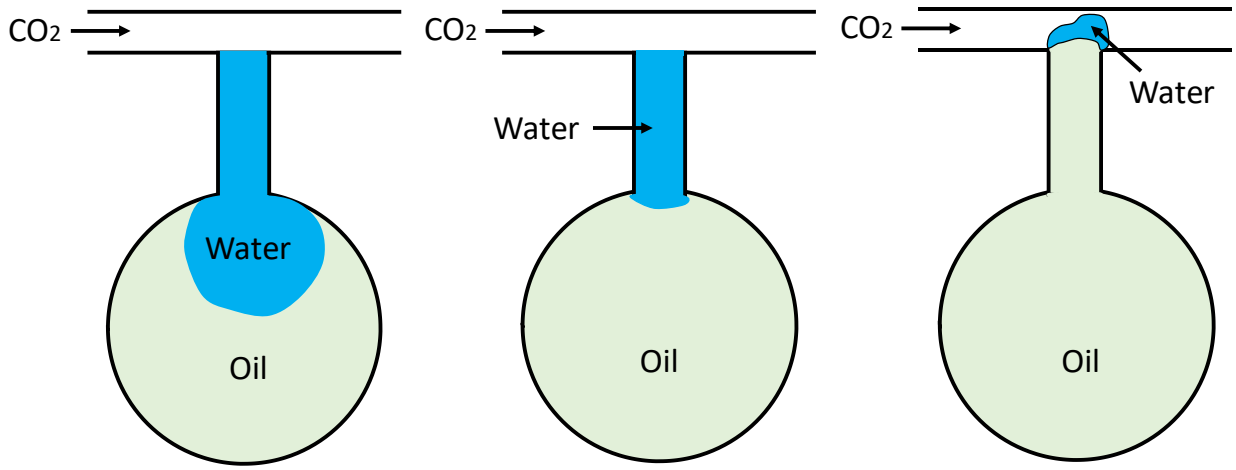

Figure 2.3. Schematic diagram of miscible displacement with CO_2 performed by Campbell and Orr (1985). From left to right: start of CO2 injection; position of water barrier after 18 h; and position of water barrier after 26.5 h. Adapted from Mirazimi *et al*. (2017).

Although water blocking reduces the displacement efficiency in micromodels, the time for water-blocking during carbon dioxide injection at the pore level is relatively short, approximately 1 day for a 100 μm thick water film. The process is relatively rapid because CO_2 has a high solubility in water and diffuses rapidly through the water film. Hence, it appears that water blocking is relatively unimportant for oil recovery via CO_2 injection over the time-scales of a typical recovery scheme of years (Muller and Lake, 2007; Grogan *et al.* 2007; Campbell and Orr, 2007; Grogan and Pinczewski, 1987; Bijeljic *et al.*, 2003).

The mathematical modeling of this diffusion process has been investigated by a number of authors usually by coupling differential equations derived from Fick's laws, the continuity equation, and a moving water/oil interface to simulate the oil swelling. In most cases, an equilibrium CO_2

concentration at the solvent/water interface is set equal to the solubility of CO_2 in water. The concentration of CO_2 on the oil side of the interface is determined through a partition coefficient, k_{pc}, as follows: $C_{CO2,o} = k_{pc} C_{CO2,w}$ (where $C_{CO2,o}$ and $C_{CO2,w}$ are the CO_2 concentrations in the oil phase and water phase, respectively). Hence, the concentration of CO_2 at the oil/water interface has a step change governed by the value of the partition coefficient as shown in Figure 2.4 (Grogan and Pinczewski, 1987; Do *et al.*, 1993; Fayazi and Kantzas, 2018; Muller and Lake, 2007; Riazi *et al.*, 2011; Shu *et al*,. 2017). A variety of methods have been used to solve the mass transfer process and are summarized below.

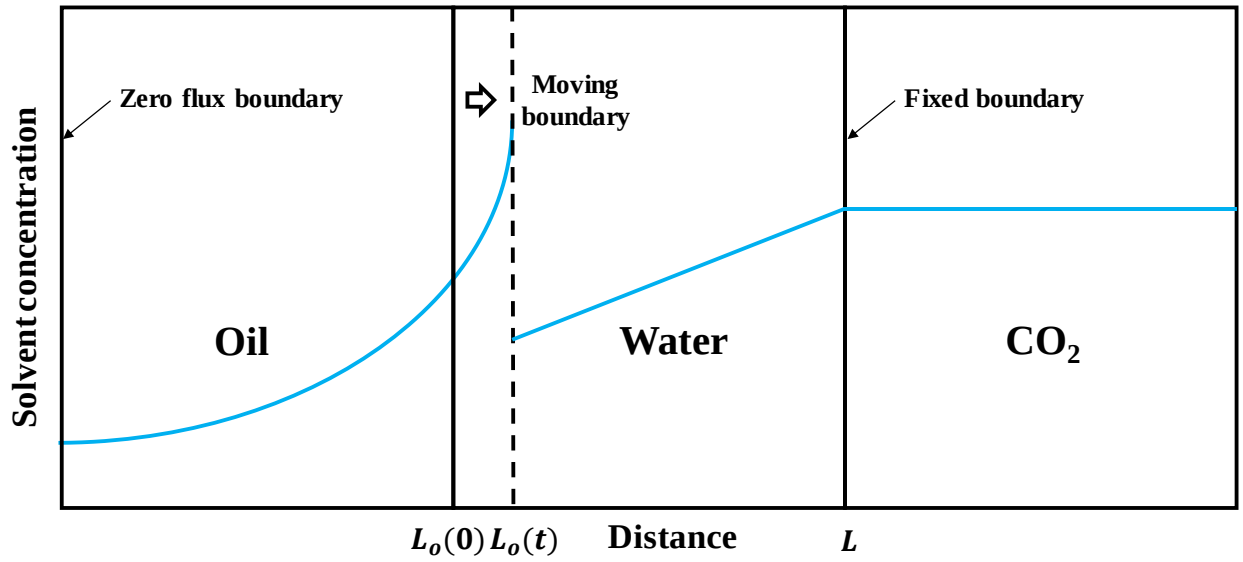

Figure 2.4. Schematic representation of the CO_2 concentration profile in the Fayazi and Kantzas model. Adapted from Fayazi and Kantzas (2018).

Grogan and Pinczewski (1987) proposed a 1-D numerical model that simulated the swelling of residual oil blobs by CO_2 diffusion through a blocking water phase. Their model resulted in a set of coupled highly nonlinear partial-differential equations that constituted a boundary value problem for which the position of the oil/water interface was determined by a numerical solution. They found that the transport of CO_2 through the water phase is the rate-controlling step in swelling the residual oil. They also observed convective mixing and instabilities at both interfaces (CO_2/water and water/oil) as was also observed by Campbell and Orr, these instabilities are most likely the explanation of the enhancement of the mass transfer rate and the high diffusion coefficients reported in their studies.

Muller and Lake (1991) developed a 1-D pore level model simulating diffusion of CO_2 into oil separated by a water film. They calculated the mass flux between the flowing CO_2 and stagnant oil. They used water film thickness as a matching parameter to match the laboratory miscible flood experiments. The results of their model showed that the two dimensionless parameters affecting production of oil in the presence of water blocking are the ratio of the stagnant water/oil volumes and the solvent equilibrium constants at the phase boundaries. They concluded that the diffusivity coefficient of the solvent had little effect on the results.

Do *et al*. (1995) used a system of coupled ordinary differential equations to describe the concentration profiles of CO_2 in oil and water phases. They demonstrated that the water film produced the major mass transfer resistance. They neglected volume changes from mixing of CO_2 with water and oil. Later studies demonstrated that accounted for non-ideal mixing improved the accuracy of this mass transfer model (Mirazimi *et al*. 2017).

Bijelic *et al.* (2003) developed a 1-D diffusion based pore model to simulate the volume change of the oil due to multicomponent mass transfer from the gas phase in the presence of water. They assumed ideal mixing between the gas and the oil and that the hydrocarbon concentrations in the water film were sufficiently low for Fick's first law to be valid. Consequently, they assumed that the concentration profiles within the water were linear and that diffusion was due to concentration gradients only. They found that the rupture times increased with a decrease in the ratio between the initial oil to the initial water film thicknesses and they proved that the rupture time increased with the square of initial length of the water layer. The main advantage of this model is that it does not require a partition coefficient at the water/oil interface. The inputs are pressure, temperature, and fluid composition. Miriazmi *et al*. (2017) later improved the accuracy of this model by accounting for the changes in the partial molar volumes of oil and gas components using the Peng Robinson and Soave-Redlich-Kwong equations of state and considering mass transfer from the surrounding water on the pore body into the shielded oil.

Riazi *et al.* (2011) developed a mathematical model at the pore level to simulate the dynamic process of the oil swelling for two scenarios: oil is separated from a CO_2 source by a water layer, and oil is in direct contact with carbonated water. Water barriers initially prevented the production

of the oil, but swelling of oil ruptured the water layer at later times, which then led to shrinkage of the oil as a result of the extraction of oil components by the CO_2 and the displacement of oil by a film flow mechanism.

Vali *et al.* (2011) proposed a moving mesh method to solve a moving interface method applied to residual oil blobs swelling by CO_2 diffusion through a blocking water phase. They compared the model results with the experimental data from a 2-D glass micromodel and found a good agreement between numerical and experimental results.

Fayazi and Kantzas (2018) used the model developed by Vali *et al*. (2011), extending its application to predict water film rupture times for typical oil and water thicknesses and trapped oil recovery as a function of contact time. They considered a moving interface between oil and water and validated their model against the experimental results obtained by Campbell and Orr (1985).

2.3 Emulsions

Emulsions are almost always formed during crude oil production (Dehghanpour *et al.*, 2014; Ezeuko *et al.*, 2012; Mohammadzadeh and Chatzis, 2009). This section summarizes the fundamentals of emulsions and a phenomena that appears in the tests done in this work, spontaneous emulsification.

2.3.1 Fundamentals of Emulsions

An emulsion is a mixture of at least two immiscible liquids, such as oil and water, in which one liquid is dispersed in the other as droplets. For example, in an oil-in-water (O/W) emulsion, oil droplets are dispersed in a continuous water phase. In a water-in-oil (W/O) emulsion, water droplets are dispersed in a continuous oil phase (Kabalnov, 1998; Tadros, 2009; Schramm, 1992; Becher, 1966; Summer, 1954). Emulsions can be classified as follows (Tadros 2009; Schramm, 1992; Shaw, 1980; Lake, 1989; Becher, 1966; Summer, 1954):

- macroemulsions: these usually have a droplet size range of 0.1–5 μm, averaging 1–2 μm.
- nanoemulsions: these usually have a droplet size range of 20–100 nm. Similar to macroemulsions, they are only kinetically stable.

- micellar emulsions or microemulsions: these have droplets usually in the size range 5–50 nm. They are thermodynamically stable. They are usually formed by the addition of a surfactant to the system which can drop the interfacial tension to values on the order of 10^{-3} to 10^{-4} mN/m.
- Double and multiple emulsions: these are emulsions-of-emulsions (W/O/W and O/W/O).
- Mixed emulsions: these are systems consisting of two different dispersed droplet phases that do not mix in a continuous medium.

Emulsification creates an interface between the oil and water phases. The free energy of the interface is given by (Koretsky, 2004; Fingas *et al*., 1993; Kabalnov, 1998):

$$dG^{\sigma} = -S^{\sigma}dT + Ad\gamma + \sum n_i d\mu_i \tag{2.22}$$

where *G* is the Gibbs free energy, *S* is the entropy, *T* is the temperature, A is the surface area, γ is the mean interfacial tension and n_i is the number of moles of component *i* with chemical potential μ_i. At constant temperature and composition, Eq. 2.22 simplifies to the following expression:

$$dG^{\sigma} = Ad\gamma \tag{2.23}$$

$$\gamma = \left(\frac{\partial G^{\sigma}}{\partial A}\right)_{T,n_i} \tag{2.24}$$

A stable interface has a positive γ; that is, if the interfacial area increases, then G^{σ} increases. A positive interfacial tension and positive free energy indicate that work is required to create the interface.

Consider the system shown in Figure 2.5. A large oil drop of area A_1 is immersed in water (I), which then divides into a large number of smaller droplets (II) with total area A_2 (such that $A_2 >> A_1$) (Fingas *et al*., 1993; Tadros and Vincent, 1983; Schramm, 1992; Shaw, 1980). The change in free energy in going from state I to II is made from two contributions: a surface energy term (positive) that is equal to $\Delta A d\gamma_{12}$ (where $\Delta A = A_2 - A_1$) and an entropy of dispersions term which is also positive (since the production of a large number of droplets is accompanied by an increase in configurational entropy) and is equal to $T\Delta S^{conf}$ (Tadros and Vincent, 1983).

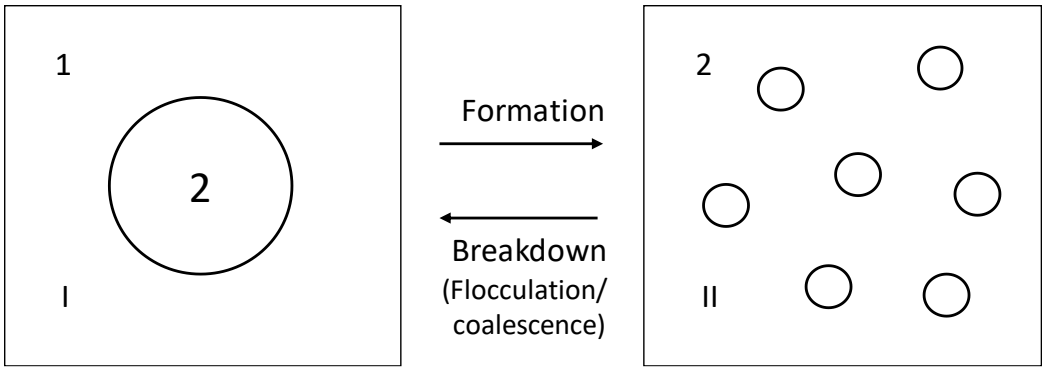

Figure 2.5. Schematic representation of emulsion formation and breakdown. Adapted from Tadros (1987).

From the second law of thermodynamics (Kabalnov, 1998; Moilliet, 1960; Tadros, 2013):

$$\Delta G^{form} = \Delta A\gamma_{12} - T\Delta S^{conf} \quad (2.25)$$

where $\Delta A\gamma_{12}$ is the work done to increase the interfacial area of ΔA, T is the absolute temperature and ΔS is the entropy change due to the system configuration (Silva *et al*., 2017a; Tadros, 2013). In most cases, $\Delta A\gamma_{12} \gg -T\Delta S^{conf}$ meaning that the energy to expand the interface, $\Delta A\gamma_{12}$, is large and positive and cannot be compensated by the small positive entropy of dispersion, $T\Delta S^{conf}$. Hence, ΔG^{form} is positive; that is, the formation of an emulsion is nonspontaneous and the system is thermodynamically unstable and external energy input (such as mechanical or thermal) is required to achieve emulsification (Shahidzadeh *et al.*, 2002; Silva *et al.*, 2017a; Schramm, 1992; Fingas *et al.*, 1993; Isaacs and Chow, 1992). For an emulsion to form spontaneously, $-T\Delta S^{conf} \gg \Delta A\gamma_{12}$, which means that ΔG^{form} must be negative. In general, the addition of a surfactant or a mixture of surfactants is required to reduce the interfacial tension sufficiently for spontaneous emulsification and microemulsion formation (Tadros, 2013; Schramm, 1992; Fingas *et al.*, 1993; Isaacs and Chow, 1992).

While most emulsions are thermodynamically unstable, they can persist for a long time in a metastable state. Nonetheless, emulsion can break or be broken, where breaking refers to the return to separate bulk liquid phases. The mechanisms that govern the breaking process are coalescence, flocculation, creaming and sedimentation, phase inversion, and Ostwald ripening (Araujo *et al*., 2017; Fingas *et al.*, 1993; Langevin *et al.*, 2004; Moilliet, 1960; Sztukowski and Yarranton, 2005; Schramm, 1992; Becher, 1966; Summer, 1954). Coalescence is the merging of two droplets into one and is usually required for complete bulk phase separation. Flocculation is the aggregation of

droplets. Creaming and sedimentation are the accumulation of droplets at the top or bottom of the emulsion drive by gravity separation. Flocculation, creaming and sedimentation bringing the droplets into closer contact where coalescence is more likely. Phase inversion is the flipping of one type of emulsion to another; for example, O/W to W/O, and can lead to more rapid phase separation if the second type of emulsion is less stable. Ostwald ripening is a mass transfer process where the contents of small droplets diffuse towards larger droplets eventually creating a population of large unstable droplets that can easily coalesce. These breaking mechanisms are not relevant for this thesis and not discussed further.

2.3.2 Spontaneous Emulsification

Spontaneous Emulsification at Ultralow Interfacial Tension

As mentioned earlier, negative values of Gibbs free energy lead to spontaneous emulsification (Tadros, 2013; Schramm, 1992; Fingas *et al*., 1993; Isaacs and Chow, 1992). As stated by Gibbs (1878) and can be seen from Eq. 2.25, a negative free energy can be achieved by four different mechanisms: 1) an increase in temperature; 2) an increase the entropy; 3) a reduction in the surface area, and; 4) a reduction in the interfacial tension (IFT). This last mechanism has been widely applied to create water-in-oil emulsions by the addition of surfactants, for example, in enhanced oil recovery (Dawe 1981; Egbogahb and Dawe 1985; Santana-Solano *et al*., 2012; Schechter *et al*., 1975; N. Shahidzadeh *et al*., 1997; Silva *et al*., 2017a; Lake, 1989). The addition of a cosurfactant to an oil-water-surfactant system can drop the IFT to values on the order of 10^{-3} to 10^{-4} mN/m (Schramm, 1992). This dramatic reduction of the IFT facilitates the spontaneous formation of very small water droplets in the oil phase (10 nm or smaller).

Ultralow interfacial tensions (*i.e.*, on the order of 10^{-3} mN/m) have been observed in oil/water/surfactant systems where the emulsion formed spontaneously (Aoki *et al*. 2009; Dawe 1981; Egbogahb and Dawe 1985; Santana-Solano *et al*. 2012; Schechter *et al*. 1975; Shahidzadeh *et al.*, 1997; Shahidzadeh *et al*. 2000; Wu *et al*. 2018). These systems are generally characterized by dispersed droplet diameters less than 10 nm, indicating a microemulsion (Acevedo *et al.*, 2001; Aoki *et al.*, 2009; Santana-Solano *et al*., 2012; Shahidzadeh *et al.*, 2002; Silva *et al.*, 2017b; Wu *et al.*, 2018). Here the required energy to form the emulsion may be derived from the energy of sorption of the surface-active agent at the interface, as well as the energy of solubilization by the

hydrocarbon in the aqueous surfactant micelles (Dawe, 1981). Miller and Scriven (1970) believed that there were other factors besides the ultralow interfacial tension criterion as a mechanism for spontaneous emulsification (*e.g.*, electrical forces in double layers) which can significantly influence stability when the IFT is less than about 1 mN/m.

Lee and Tadros (1982) studied the spontaneous emulsification of emulsifiable concentrates into water at different surfactant concentrations and they found that a minimum of 1% surfactant was necessary to begin emulsification. The lowest IFT they measured was 0.5 mN/m with a surfactant concentration of 2%. They concluded that interfacial instability may occur when the IFT reaches values near of 0.5 mN/m (average droplet size of 3 μm), probably due to the mass transfer of surfactant molecules across the interface.

Silva *et al*. 2017 investigated the spontaneous formation of water droplets in kerosene with the presence of an oil soluble surfactant at concentrations above the critical micelle concentration. The IFT was above 4 mN/m for all the experiments with an average water droplet size of 0.25 μm, proving that there was no need to achieve ultralow IFT to produce spontaneous emulsification. This condition of spontaneous emulsification with IFT values much higher than typical values reported for microemulsions was first discovered by Shinoda and Kunieda (1972) and they called these types of emulsion “swollen micellar solutions.”

In the 1990s, mathematical modelling of spontaneous emulsification in an oil/water system in the presence of a surfactant intensified and these studies concluded from a pure mathematical point of view that Rayleigh-Taylor instabilities might be a mechanism for spontaneous formation of water droplets in oil. For example, Granek *et al*., (1993) developed a mathematical model for spontaneous emulsification which predicted transient negative values of interfacial tension between water and oil in the presence of a surfactant. Long fingers of one phase in the other developed prior to the breakup of the surface and water droplets formed spontaneously. Later, Hu and Granek (1996) found from their mathematical analysis that spontaneous curvature of oil/water interfaces allowed the formation and stability of long fingers (typical Rayleigh-like instabilities) at positive IFTs. Hence, this mechanism may also account for spontaneous emulsification at higher IFT.

Theissen and Gompper (1999) studied the mathematics of spontaneous emulsification using the Lattice-Boltzmann method of an initially flat 2-D oil/water interface and then added surfactant. From their analysis they concluded that the driving force for the emulsification was the diffusion of surfactants at the interface leading to convective transport of oil and water induced by viscous stresses. Their results agreed with Granek *et al.* (1993) that finger-like structures form and grow with a constant velocity.

Spontaneous Emulsification Above Ultralow Interfacial Tension

Spontaneous emulsification can also occur at higher IFT values (Rehbinder, 1957; Silva *et al*., 2017a). There are at least two mechanisms for spontaneous emulsification above low IFT (Davies and Rideal, 1961): interfacial turbulence and diffusion and stranding.

Interfacial Turbulence: The interfacial turbulence mechanism has been reviewed by Lopez-Montilla *et al*. (2002) and Sterling and Scriven (1959). According to Davies and Rideal (1961), spontaneous emulsification produced by interfacial turbulence arises from the mechanical breakup of the interface, which varies according to the intensity of the turbulence. Sterling and Scriven (1959) described the interfacial turbulence as "the agitation of the interface between two unequilibria liquids," which in turn is caused by the Marangoni effect. This phenomena consists of the movement and/or fluctuation of the interface between two immiscible liquids caused by longitudinal differences in the IFT. It was first observed by Thomson (1855) and then formalized by Marangoni (1869).

Marangoni instabilities are caused by local interfacial tension gradients and the presence of unstable density gradients that produce gravitational instabilities (Castor and Somerton, 1977; Mendes-Tatsis and Ortiz, 1992; Slavtchev and Mendes, 2004; Marangoni, 1869; Thomson, 1855; Lord Rayleigh, 1883). The interfacial tension gradients may be created by changes in interfacial concentrations, temperature, or electrostatic charges. The density gradients may be due to variations in temperature caused mainly by heats of solution (Ortiz and Sawistowski, 1973) or volume contraction on mixing (Mendes-Tatsis and Ortiz, 1992). Sørensen (1978) proved from his mathematical analysis that Marangoni instabilities can be coupled with Rayleigh-Taylor

instabilities only when the wavelength of the two instabilities are very closely situated. When the wavelengths coincide, the amplitude of the instability is enhanced. The instability creates interfacial turbulence.

Spontaneous emulsification due to interfacial turbulence was first reported by Ouincke in 1879. The system he studied was lauric acid in oil and he observed that when this solution was placed on top of an aqueous alkali solution, there was spontaneous formation of aqueous droplets on the oil side (Ouincke, 1879). Hutchinson (1947) showed that the diffusion of different alcohols (*n*-propyl, *n*-butyl, *n*-ethyl and *n*-amyl alcohols) across an unstirred benzene-water interface caused convection that led to turbulence at the interface in all cases. He also added a surface active material to the interface that minimized the turbulence and slowed the mass transfer rates. Davies and Wiggill (1959) studied the mass transfer on diluted acetic acid and benzene in static conditions with and without the presence surface active agents. They observed spontaneous emulsification of acid on benzene dispersed by interfacial turbulence through the interface on the surfactant-free system. However for the case of added surfactant, the droplets formed a more coherent and homogeneous layer near the interface, as was also found by Davies and Haydon (1957). Davies and Wiggill also analyzed the acetic acid/water/toluene system and observed spontaneous emulsification of water droplets principally on the toluene side. A similar system (toluene over diluted butyric acid) was evaluated by Ward and Brooks (1952). They reported that if pure toluene was placed over the acid solution, strong mixing on the interface occurred and there was spontaneous emulsification of aqueous droplets on the toluene side.

Sterling and Scriven (1959) developed a hydrodynamic mathematical model to analyze the stability mechanisms of this phenomena. They considered two semi-infinite, static fluid phases in contact along a planar interphase in thermal equilibrium with a low concentration of a solute that transferred between the phases. They concluded that the presence or absence of a solute in a liquid-liquid system, the nature of this solute, and the direction through which it flowed (the turbulence is more intense if the solute transfers from the organic to the aqueous phase) strongly influenced the magnitude of the turbulence. This observation is consistent with experimental results from McBain and Woo (1937) who found that if a solution of 10% methanol in toluene was placed over

water, water droplets appeared spontaneously in the organic phase; however, no emulsification occurred if pure toluene was placed over water containing methanol.

However, interfacial turbulence does not explain all spontaneous emulsification above ultralow IFT. Wei (1955) examined a number of different liquids and observed spontaneous emulsification without turbulent activity at the interface when neither phase contained a solute. Similarly, Davies and Haydon (1957) showed that spontaneous emulsification of water in a 0.135 M solution of acetone in petroleum ether occurred even if a surfactant was added to the system to suppress interfacial turbulence. Davies and Haydon also showed that if a solution of ethanol/toluene is placed over water, strong interfacial turbulence and spontaneous emulsification occurred, and if a surfactant was added to the system to suppress the turbulence, emulsification still happened but water droplets formed closer to the interface and not as dispersed as the free-surfactant system. Spontaneous emulsification with surfactant suppressed turbulence has been confirmed by several researchers (Ostrovskii *et al*. , 1970; Sherwood and Wei, 1957; Olander and Reddy, 1964; Bakker *et al*., 1966, 1967; Davies and Wiggill, 1959; Ruckenstein and Berbente, 1963)

Diffusion and Stranding: Diffusion and stranding involves a chemical instability instead of a mechanical one. Davies and Rideal (1961) originally described this mechanism as regions of local supersaturation of the solute in one of the solvents produced by diffusion and emulsion droplets are formed due to phase transformation in these regions. This mechanism can explain spontaneous emulsification in the previously discussed systems with suppressed interfacial turbulence.

Ruschak and Miller (1972) derived a mathematical solution of the diffusion equations in a ternary system assuming semi-infinite phases (polar co-solvent/water/oil system). This theory assumes that the diffusivity coefficients are the same for all phases and the set of compositions in the system is independent of time. It predicts the occurrence or not of spontaneous emulsification and in which phase it occurs. Ruschak and Miller validated this theory with data from three different ternary mixtures: ethanol/toluene/water, propionic acid/toluene/water, and propanol/toluene/water. They demonstrated that spontaneous emulsification occurred when diffusion caused a supersaturated region near the interface. The authors proposed two possible mechanisms for the spontaneous formation of droplets: 1) phase transformation in a supersaturated region where new droplets are

created either by nucleation and growth or spinodal decomposition; 2) transport-induced breakup of the interface where small perturbations at the interface change the composition, fluxes, and velocity in the vicinity of the interface. If an increase in the amplitude of the perturbations satisfies the moving boundary condition and Fick's second law, it increases until the interface destabilizes and breaks up. The authors also noted that the emulsification rate increased considerably when there was diffusion of a solute from the phase in which it was less soluble into the phase in which it was more soluble. The validity of the diffusion path theory was tested successfully by Miller (2006) for water/alcohol/oil systems and also for systems containing surfactants. Note that when the diffusion and stranding mechanism is acting, any contribution of interfacial turbulence considerably increases the rate of emulsification by increasing rates of mass transfer near the interface (Davies and Rideal, 1962; Ruschak and Miller, 1972; Miller, 2006).

Friberg (2013) and Bozeya *et al*. (2013) analyzed water/ethanol/benzene systems. They found that when this solution was close to the plait point and was placed over water without mixing, spontaneous emulsification happened in both phases, principally in the aqueous phase, forming an emulsion layer. They found that Ruschak and Miller's model successfully predicted the occurrence of spontaneous emulsification for the first stage of the test (minutes), which is characterized by a fast emulsification rate that increases proportionally to the square root of time. The second stage (several days) was characterized by a very small additional emulsification and could not be modeled.

2.3.3 Spontaneous Emulsification in Crude Oil/Water Systems

Crude oils contain surface active species, most notably asphaltenes, that can stabilize emulsions and potentially contribute to spontaneous emulsification. Asphaltenes are fraction of the oil that is soluble in an aromatic solvent such as toluene but is insoluble in a paraffinic solvent such as *n*-heptane. Asphaltenes are a mixture of hundreds of thousands of species and are the densest, highest molecular weight, most aromatic, most polar, and most heteroatomic fraction of the oil. They have hydrophobic polynuclear aromatic structures containing hydrophilic heteroatomic functional groups. This combination makes them surface active. Asphaltenes are considered responsible for the high stability of water-in-crude oil emulsions, mainly because of their capacity to form a stable rigid film at the water droplet-oil interface (Alvarez *et al.*, 2009; Czarnecki *et al.*, 2013; Mclean

and Kilpatrick, 1997; Rane *et al.*, 2012; Tan *et al.*, 2009; Gafonova and Yarranton, 2001; Yarranton *et al*., 2000). Also, several studies have established the importance of other components of crude oils, such as resins, waxes, solids and naphthenic acids on the stability of emulsions (Alvarez *et al.*, 2009; Czarnecki, 2009; Czarnecki *et al.*, 2013; McLean and Kilpatrick, 1997; Varadaraj and Cornelius, 2012; Gafonova and Yarranton, 2001).

de Araujo *et al.* (2017) studied spontaneous emulsification in a water/asphaltene/toluene system using a spinning disk confocal microscope. They observed formation of micro-sized asphaltene-laden water droplets on the oil side of the interface with droplet radius 1 to 10 μm. Oil droplets on the water side were also observed, but in a considerably lower amount than the water droplets (99.7% were water droplets). The emulsification rate increased significantly with time as the droplets accumulated at the center of the meniscus of the oil/water interface due to gravitational settling, suggesting that these droplets were the denser phase. Some degree of coalescence occurred in this region. The droplets far from the center were not sufficiently close and avoided coalescence. The number of spontaneously emulsified droplets increased with higher asphaltene concentration (Araujo *et al*. 2017). They found that, in the early stages of the process, the time for coalescence to occur increased with aging. They attributed the aging effect to the formation of a strong viscoelastic network at the interface (see Figure 2.6).

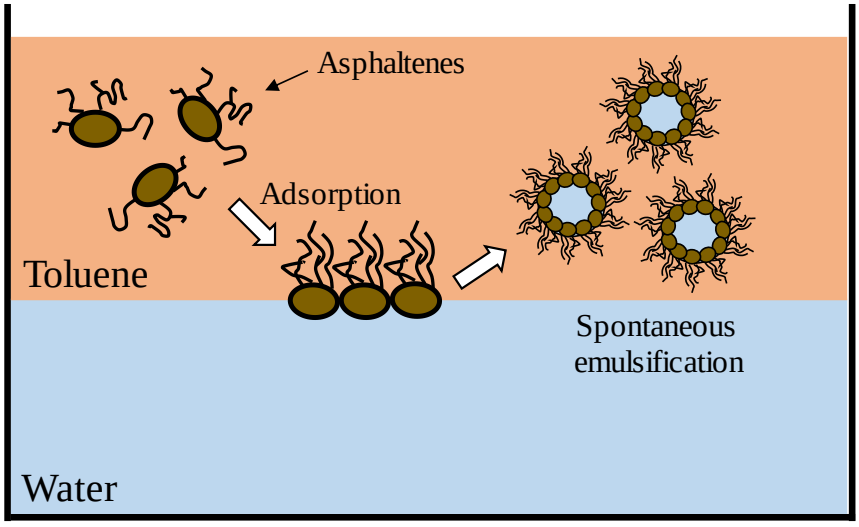

Figure 2.6. Schematic representation of the model by de Araujo *et al*., showing the spontaneous formation of water droplets at the oil side of the interface. Adapted from de Araujo *et al*. (2017).

Rudin and Wasan (1992) studied spontaneous emulsification on alkali-acidic oil systems with and without the presence of a petroleum sulfonate. They concluded that the addition of a surfactant created an interfacial resistance to mass transfer and made the interface more rigid. They also found that for these systems, interfacial turbulence was necessary but not a sufficient condition for spontaneous emulsification; it was also necessary to achieve low IFTs. However, spontaneous emulsification has been observed in diluted heavy oil/water systems at IFT values above 1 mN/m (Acevedo *et al*., 2001; Yeung *el al*., 1999; De Araujo *et al.*, 2017).

As mentioned previously, crude oil has natural components such as asphaltenes which are surface active and will tend to adsorb on the oil-water interface (Cyr *et al*. 1987). Acevedo *et al*. (2001) showed that natural surfactant concentrations in a Venezuelan bitumen were high enough to produce very low interfacial tension values (in the order of 10^{-2} mN/m) versus water. Spontaneous emulsification of water droplets was observed for this bitumen. However, for most water/bitumen systems, the interfacial tension is between 20 to 40 mN/m (Chaverot *et al*., 2008; Jafary *et al*., 2019) and ultralow interfacial tension is not a likely mechanism for spontaneous emulsification.

Yeung *el al*. (1999) observed spontaneous emulsification of water into bitumen at interfacial tensions below 10 mN/m. Here the IFT reduction and emulsification was due to area contraction. They used a micropipette technique to analyze the interfacial properties of micrometer-sized water droplets in various concentration of bitumen diluted in 1:1 heptol (1:1 *n*-heptane:toluene). They found that at high bitumen concentration (10 vol%), micrometer-sized droplets formed spontaneously from the surface of the original droplet and eventually detached irreversibly. They noticed that after several minutes the initially clear oil became full of 1 μm water droplets. Dabros (1999) proposed a "budding" mechanism hypothesizing that the compressed irreversibly adsorbed interfacial film crumpled and folded under compression, creating small pockets of water that became emulsion droplets.

2.4 Gravity Instability in Liquid-Liquid Systems

Several studies have shown the presence of instabilities in the form of viscous fingers at the edge of the steam chamber during the application of the SAGD method (Gotawala and Gates, 2008; Hejazi and Azaiez, 2012; Irani *et al.*, 2014; Ito and Ipek, 2005). Etminan *et al.* (2011) showed that

instabilities at the gas-bitumen interface enhance mass transfer between the solvent-carrying vapor and oil phase. Gatawala and Gates (2008) demonstrated using a numerical model that Rayleigh-Taylor instabilities (see Section 2.7.1) existed at the edge of the steam chamber when the steam quality was greater than a threshold value.

Instability occurs when a disturbance of the external or internal forces acting on a fluid or a system of fluids causes an unbounded change the fluid flow; that is, the fluid does not return to its original steady state after the disturbance (Friedlander and Yudovich, 1962). Instability in fluid dynamics and meteorology has been widely studied in the literature and several types exist depending on the physical phenomena involved (Benard, 1901; Lord Rayleigh, 1900; Taylor, 1950; Brouillette, 2002; Vujinovi and Kranj, 2015). For example, the Kelvin-Helmholtz instability occurs when there is a velocity difference across the interphase or when a shock wave accelerates the fluids (Richtmyer-Meshkov instability). The Rayleigh-Benard (confining plate on the top surface) and Benard-Marangoni convection (no confining plate) occur when there is a heating source from below and cooling source from above (Koschmieder, 1974; Benard, 1901; Brouillette 2002; Vujinovi and Kranj, 2015; Richtmyer, 1960; Meshkov, 1969; Lord Rayleigh, 1890). The instabilities relevant for this thesis is the Rayleigh-Taylor instability.

The Rayleigh-Taylor instability applies to the higher temperature diffusion experiments in this thesis where water is placed over bitumen with a lower density than the water. Rayleigh-Taylor instability is a fingering instability at an interface between two fluids of different densities. It occurs when the light fluid is pushing against the heavy fluid; for example, water placed on top of oil (Lord Rayleigh, 1900; G. Taylor, 1950; Baker *et al.*, 1993). If the binary fluid system is left completely undisturbed, a condition of an unstable equilibrium exists. However, if the interface is initially perturbed, the perturbation grows exponentially with time, giving rise to an instability.

Mathematical modeling of the Rayleigh-Taylor instability has been attempted by several authors (Weir Lawrie, 2009; Mailybaev, 2018; Popil, 1979; Waddell *et al.*, 2012). The growth rate of each instability can be determined with a linear stability analysis on a binary system of incompressible fluids initially separated by a planar interface. It is assumed that the fluids are initially stationary and that the pressures of both liquids are equal at the interface. The Laplace equation (which relates

surface energy to curvature and interfacial tension) is combined with Bernoulli's law (which governs fluid velocity) to derive the following expression for the growth rate of the instability (Baker *et al.*, 1993; Weir Lawrie, 2009):

$$\sigma = \sqrt{GAk - \frac{\gamma k^3}{\rho_1 + \rho_2}} \tag{2.26}$$

where σ is the growth rate, k is the wavenumber ($k = 2\pi/\lambda$), λ is the wavelength of the periodic instability, A is the Atwood number $\left(A = \frac{\rho_2 - \rho_1}{\rho_1 + \rho_2}\right)$, ρ_2 is the density of upper fluid, ρ_1 is the density of the lower fluid, γ is the interfacial tension, and G is the apparent gravity. If the fluids are miscible, Eq. 2.26 reduces to (Mailybaev, 2018; Waddell *et al.*, 2012):

$$\sigma = \sqrt{GAk} \tag{2.27}$$

For small amplitude perturbations of wavelength, A is the key factor governing the growth rate. For values of A close to 0 (such as bitumen and water), Rayleigh-Taylor instability flow takes the form of symmetric fingers of fluid (Waddell *et al.*, 2012). For A close to 1, the much lighter fluid "below" the heavier fluid takes the form of larger bubble-like plumes. Negative values of A indicate a stable interface. The system is unstable if the heavy fluid is above the lighter fluid (σ is real) and stable if the lighter fluid is above the heavy fluid (σ is imaginary) (Plesset and Whipple, 1974; Waddell *et al.*, 2012).

CHAPTER THREE: EXPERIMENTAL METHODS

This chapter summarizes the materials and experimental methods used in this thesis. The methodology for setting up the hydrocarbon/water/bitumen diffusion tests is described, as well as the procedure for processing and analyzing the data from which the solvent mass transfer rate and the water content in bitumen can be determined.

3.1 Materials

Two different Western Canadian bitumen samples were used in this thesis. The first, WC-B-A3 bitumen, was provided by CNOOC International Ltd. and was obtained from a SAGD project. The second, WC-B-B5, was a well-head sample from a SAGD project. Both samples were dewatered prior to delivery. Properties from the WC-B-A3 sample were taken from Grimaldos (2018) and properties from WC-B-B5 were taken from Perez (2019). The viscosity, water content and the results of the SARA assay are provided in Table 3.1.

Table 3.1. Properties of WC-B-A3 and WC-B-B5 bitumen samples (Grimaldos, 2018; Perez, 2019; Baydak, 2019). nd refers to not done.

Property	WC-B-A3	WC-B-B5
Viscosity at 50°C and 0.1 MPa, cP	5540	7590
Distillables, wt%	27.1	19.5
Saturates, wt%	9.6	7.7
Aromatics, wt%	26.9	29.8
Resins, wt%	18.4	18.9
C5-asphaltenes, wt%	17.7	23.5
Water Content, wt%	1.8	2.6

The following hydrocarbons were used in the mass transfer experiments: cyclohexane (OmniSolv, >99.9% purity) purchased from VWR International LLC; toluene (>99.5% purity), *n*-pentane (Reagent grade >98% purity) and *n*-heptane (technical) all from Fisher Chemical and purchased from Fisher Scientific. The following hydrocarbons were used for the emulsion experiments: toluene (OmniSolv, purity >99.9%) and *n*-heptane (OmniSolv, purity >99.5%) both from VWR

International LLC. Reverse osmosis water was used in all cases and was provided by the University of Calgary physical plant.

A bitumen sample with a reduced content of natural surfactants was required for one of the mass transfer experiments. Surfactants were removed by emulsifying water into the bitumen and then separating out the water. Surfactants accumulate at the water/oil interface due to their surface active nature and the adsorbed surfactants are removed when the emulsified water is removed. The procedure does not necessarily remove all of the surface active material from the bitumen but will tend to remove the most surface active or most strongly adsorbed components. To prepare this sample, raw bitumen was diluted with high purity toluene and *n*-heptane and emulsified with reverse osmosis water using a CAT5 Homogenizer. The mixture of *n*-heptane and toluene formed emulsions that were sufficiently stable but settled easily to provide enough supernatant to recover the treated bitumen. The bitumen:water ratio selected for the emulsion preparation was 1:1. The hydrocarbon dilution level was selected by trial and error until an emulsion was formed that, after 1.5 hours of settling, yielded two distinct phases: supernatant and stable emulsion. Combinations where water settled were immediately rejected. The final combination of components for the emulsions was 10.8 g bitumen, 180 mL of 25/75 Heptol (45 mL *n*-heptane, 135 mL toluene), and 10.8 g water.

The supernatant was decanted and centrifuged in a Heraeus Megafuge equipped with a TX-200 rotor to remove any remaining emulsified water. The centrifuge conditions were 3000 rpm for 6 min for the WC-B-B5 bitumen and 3400 rpm for 6 min for the WC-B-A3 bitumen. The supernatant was viewed under the microscope to verify that all visible emulsion had been removed. The supernatant from several batches were accumulated in a jar and the solvents were evaporated off in a fume hood for 2 weeks. The residue was dried in a 60°C vacuum for several weeks until its mass was constant. These procedures were carried out by Baydak (2019).

3.2 Mass Transfer Experiments

A schematic of the mass transfer experiments is provided in Figure 3.1. Layers of solvent over water over bitumen (or water over bitumen) were prepared in a 30 mL glass vial (diameter = 22.2 mm) and the height of each layer was monitored over time using a Mitutoyo cathetometer with

±0.01 mm precision. The change in layer heights was used to determine the mass of solvent and water transferred to the bitumen layer, as will be discussed later. For experiments performed above room temperature, a VWR water bath was used to maintain a set temperature to within ±0.1°C.

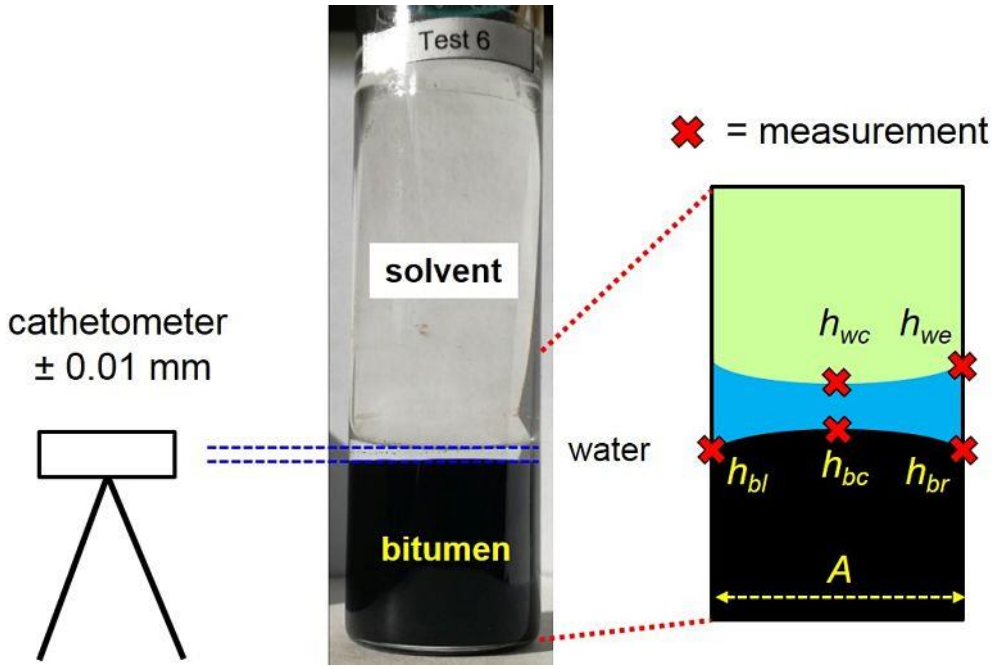

Figure 3.1. Schematic of a mass transfer experiment for a solvent/water bitumen system showing how the height of the interface is measured; toluene/water/WC-B-A3 bitumen, 0.35 cm water layer, 20°C.

To prepare a vial for a solvent/water/bitumen mass transfer experiment, the bitumen, water, and hydrocarbon were added sequentially as follows:

- 7.5 g of bitumen was weighed exactly into the bottom of a vial using a 5 mL syringe, being careful not to get bitumen on the glass walls.
- The vial was placed in a 60°C oven for 24 h and then in an ultrasonic bath for 1 hour to remove any bubbles present in the bitumen.
- The vial was placed in a freezer for 1 h in order to create a stable flat bitumen surface. The decrease in the bitumen temperature reduced its viscosity so that the interface did not deform when water was added to the vial.
- Immediately after taking the sample from the freezer, the desired mass of water (1 to 8 g) was weighed exactly and added gently on the top of the bitumen using a plastic pipette.

- An excess of hydrocarbon solvent was gently added above the water layer using a plastic pipette until the vial was nearly full.
- The vial was fitted with a Teflon seal to prevent evaporation.

The water phase was prepared in two ways: either unsaturated or presaturated. Unsaturated water was simply degassed reverse osmosis water whereas presaturated water was degassed reverse osmosis water that had been exposed to the hydrocarbon of interest for 24 hours.

Once the three phases were placed in the vial, the time of day was recorded and an initial measurement (t = 0) of the water and bitumen heights was taken with the cathetometer. The vial was either left to sit at room temperature or was placed into a water bath controlled at either 60 or 80°C. The height of each layer was measured periodically (weekly for the room temperature tests and daily for those at 60 and 80°C). For the above room temperature experiments, the vial was taken out of the bath for approximately 5 minutes for each height measurement. Photographs of the vials were taken every time a measurement was done immediately after taking out the sample from the bath. The experiment was terminated after a designated time or if the bitumen became unstable and connected with the solvent.

The procedure for a water/bitumen mass transfer experiment was exactly the same as above except that no solvent was added. In addition, at the end of the experiment, the bitumen layer was isolated for further analysis. To isolate the bitumen layer from the water, the water layer was gently and slowly removed with a pipette and then with a syringe/needle if there was encapsulation of visible droplets by the bitumen. Any droplets of water adhering to the glass walls were also removed. Samples of the bitumen were collected with a pipette and placed on a microscope slide were taken to observe any emulsified water. Photomicrographs were taken using a Zeiss Axiovert S100 inverted optical microscope equipped with an Axiocam CRT camera. Images were captured used AxioVision SE64 software. A Karl Fischer titration was performed on the whole of the remaining bitumen to determine a water content. The sampling and analysis was performed by Baydak (2019).

3.3 Processing of Data from Mass Transfer Experiment

3.3.1 Calculation of Water and Bitumen Volumes

The volumes of the water and bitumen are determined from the heights of the top of the bitumen and the top of the water and the known cross-sectional area of the vial. Since the interfaces are curved, both the edge and midpoint heights were measured, as shown in Figure 3.1. The edge height of the bitumen was not the same at all points on the perimeter and therefore the left and right edge heights were measured. The edge height of the water was uniform and only one point was measured. A reference point on the bottom of the vial was also measured and all heights were determined relative to this reference.

Flat Water/Bitumen Interface

At room temperature, particularly at early times, the bitumen/water interface tended to be flat or slightly curved downwards (concave) at the center. The average thickness of the bitumen layer was calculated as follows:

Flat interface

$$\Delta h_{b,avg} = \frac{h_{bl} + h_{br} + h_{bc}}{3} \tag{3.1}$$

Concave interface

$$\Delta h_{b,avg} = \frac{(h_{bl} + h_{br})/_2 + h_{bc}}{2} \tag{3.2}$$

where h_{bl}, h_{br}, and h_{bc} are the uncorrected, left, right and center heights, respectively, of the top of the bitumen layer and $\Delta h_{b,avg}$ is the average thickness of the bitumen layer. The bitumen layer volume at each time is simply given by:

$$V_{b,avg} = A\Delta h_{b,avg} \tag{3.3}$$

where $V_{b,avg}$ is the bitumen layer volume based on the uncorrected average height and A is the cross-sectional area of the vial.

The bitumen layer volumes were corrected based on the difference between the volume from the initial measured height and the volume based on the known mass of bitumen as follows:

$$V_b = V_{b,avg} + E_b \tag{3.4}$$

where V_b is the corrected average bitumen layer volume and the correction factor E_b is given by:

$$E_b = V_{b,t=0} - V_b^0 \tag{3.5}$$

and $V_{b,t=0}$ is the initial bitumen layer volume and V_b^0 is the mass-based bitumen layer volume given by:

$$V_b^0 = \frac{m_b}{\rho_b} \tag{3.6}$$

where m_b is the measured mass of bitumen and is ρ_b the density of the bitumen. At room temperature, the bitumen correction factor was typically within ±0.05 cm³ (±0.7%) of the bitumen layer volume.

The upper water interface was flat at all conditions except for the meniscus. The thicknesses of the edge and center of the water layer were determined from the difference between the height of the upper water interface and the height of the bitumen layer as follows.

$$\Delta h_{wc} = h_{wc} - h_{bc} \tag{3.7}$$

$$\Delta h_{we} = h_{we} - \frac{h_{br} + h_{bl}}{2} \tag{3.8}$$

where h_{wc} and h_{we} are, respectively, the edge, and center heights of the top of the water layer, and Δh_{wc} *and* Δh_{we} are, respectively, the edge, and center thicknesses of the water layer. The average thickness of the water layer was calculated as follows:

$$\Delta h_{w,avg} = \frac{\Delta h_{we} + \Delta h_{wc}}{2} \tag{3.9}$$

where $\Delta h_{w,avg}$ is the average thickness of the water layer. The water layer volume at each time is simply given by:

$$V_{w,avg} = A\Delta h_{w,avg} \tag{3.10}$$

where $V_{w,avg}$ is the water layer volume based on the uncorrected average height.

The water layer volumes were corrected based on the difference between the volume from the initial measured height and the volume based on the known mass of water as follows:

$$V_w = V_{w,avg} + E_w \tag{3.11}$$

where V_w is the corrected average water layer volume and the correction factor E_w is given by:

$$E_w = V_{w,t=0} - V_w^0 \tag{3.12}$$

and $V_{w,t=0}$ is the initial water layer volume and V_w^0 is the mass-based water layer volume given by:

$$V_w^0 = \frac{m_w}{\rho_w} \tag{3.13}$$

where m_w is the measured mass of water and ρ_w is the density of the water. At room temperature, the water correction factor was typically within ±0.07 cm³ (±5%) of the water layer volume.

Initial Interface Height above Room Temperature

The height (and volume) measurements at t=0 for the tests at 60 and 80°C were taken at room temperature. After the sample was placed in the water bath the system reached thermal equilibrium and all subsequent volume measurements were at the experimental temperature. Hence, the initial bitumen density was higher (lower volume) than the subsequent densities and the volumes could not be corrected based on the initial volume measurement. Instead, the measured volumes were linearly extrapolated to time zero to determine the expected initial volume at the experimental temperature, as shown in Figure 3.2. Then, the extrapolated volumes were used in Eqs. 3.5 and 3.12 instead of the initial measured volumes. Above room temperature, the bitumen and water correction factors were typically within ±0.4 cm³ (±5.2%) and ±0.2 cm³ (±4%) of the bitumen and water layer volumes, respectively.

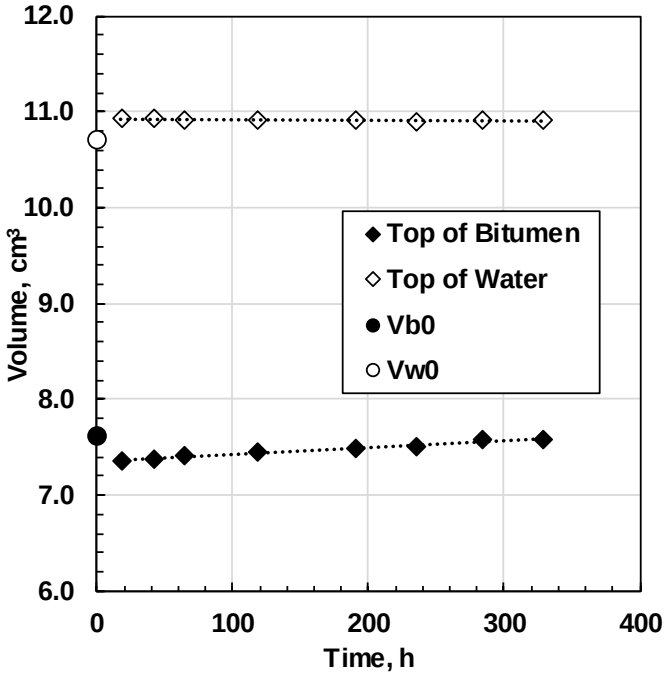

Figure 3.2. Extrapolation of uncorrected average bitumen layer height and top water height over time to determine initial heights (cyclohexane/water/WC-B-A3 bitumen, 1 cm water layer, 60°C). Note that the initial bitumen volume was higher than the later values because the temperature had not yet reached 60°C.

Domed Bitumen Interface

A dome (convex interface) formed at the bitumen/water interface for some mass transfer tests performed at room temperature and for all experiments performed at 60 and 80°C, as shown in Figure 3.3. In this case, the volume of the bitumen at each time is given by:

$$V_b = V_{b.avg} + E_b + V_{dome} \tag{3.14}$$

where $V_{b.avg}+E_b$ is the volume of the bitumen column below the dome and V_{dome} is the volume of the dome. The volume of the water layer is given by:

$$V_w = V_{w.avg} + E_w - V_{dome} \tag{3.15}$$

where $V_{w.avg}+E_w$ is the volume of the water column excluding the dome.

The dome volume was determined using a numerical approach. A photograph of the dome profile was taken and digitized using GetData Graph Digitalizer™ software. An example of a photo of a dome with its axes and mapped coordinates is shown in Figure 3.4. The coordinates were exported to Curve Expert Professional™ software for analysis. This software was used to find a mathematical equation that best fit the contour coordinates. It was found that the following function (Eq. 3.16) fit the dome profiles for all of the mass transfer tests done in this thesis (see Appendix B):

$$r = a + br^y + cy \tag{3.16}$$

where r is the radial location, y is the height of the curved segment, and a, b, and c are fitting parameters.

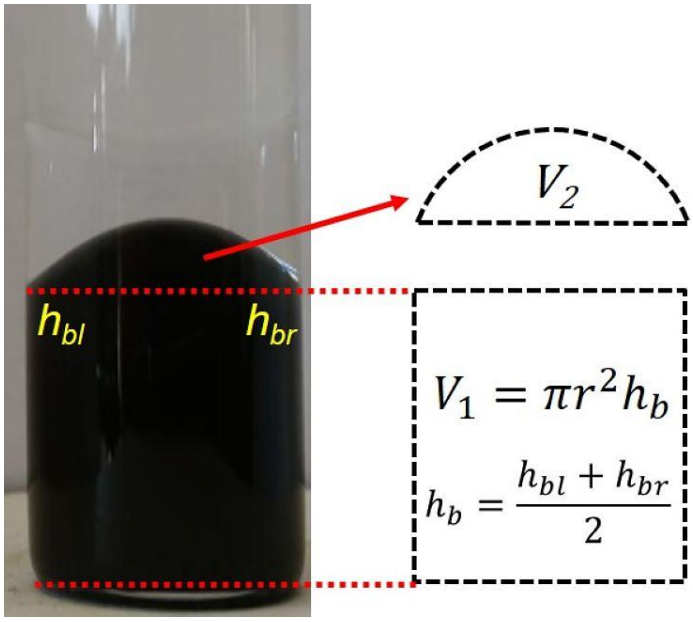

Figure 3.3. Photograph of a dome on a toluene/1.5 cm water/bitumen test at t=72 h.

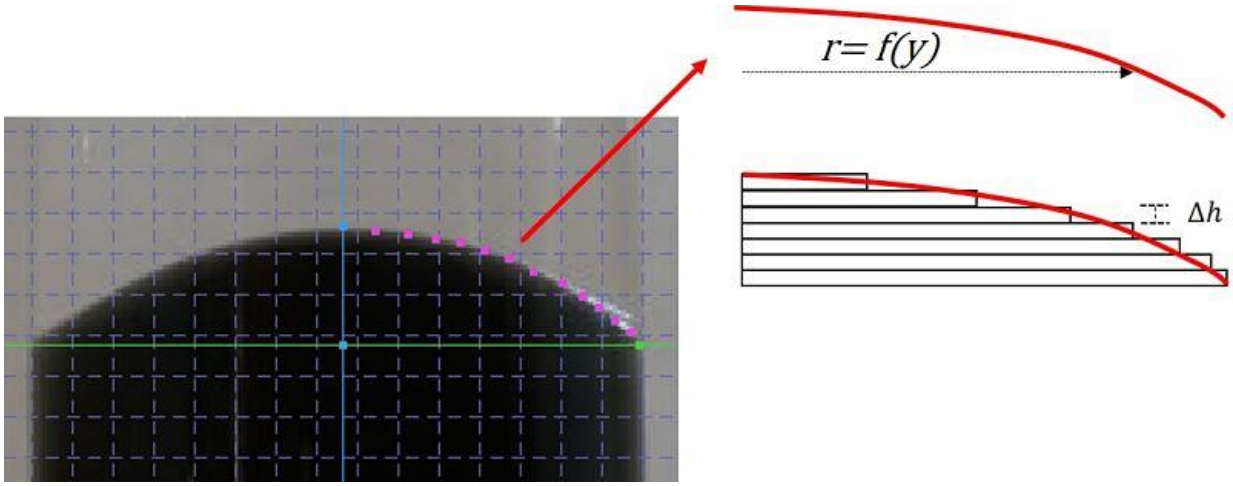

Figure 3.4. Photograph of a dome on a toluene/1.5 cm water/bitumen test at t=48 h.

The fitted profile equation was discretized into layers each with a fixed thickness of Δh and a radius equal to the value of the function evaluated at different each value of y (see Figure 3.4). Each layer is a disc and the volume of the dome is equal to the summation of the disc volumes given by:

$$V_{dome} = \pi \sum_{i=1}^{n} [f(y)]^2 \, \Delta h \qquad (3.17)$$

This method for calculating the volume of the bitumen assumes that the dome is symmetrical with respect to the y-axis. In fact, the domes were not perfectly symmetrical likely due to wettability variations at the glass surface. The uncertainty in the volumes from a lack of symmetry ranged from 5 to 15%, as discussed in Appendix A. The highest uncertainty from asymmetry was with toluene (highest solubility in water), possibly because the interfacial tension of bitumen and toluene is lower than with bitumen and the other solvents (Tsamantakis *et al*. 2005). A lower interfacial tension provides less resistance to the increase of surface area caused by the asymmetry.

The bitumen dome was formed immediately (t=0) for a few of the water/bitumen and solvent/water/bitumen tests. These tests were used to determine the deviation of the bitumen volume calculated using Eq. 3.14 versus the more accurate volume determined from the initial mass of the bitumen. The average deviation of the bitumen volume at t=0 ranged from ±0.1 to 0.3 cm^3 (±1-3 %). Similarly, the average deviation of the water volume at t=0 ranged between ±0.4 to 0.6 cm^3 (±6-9 %). The higher errors on the water volume are most likely due to the shape of the solvent/water interface which is slightly concave whereas this methodology assumes a horizontal interface.

The calculated bitumen and bitumen+water volumes for repeat runs were consistent until gravity instability occurred, as shown in Figure 3.5. The gravity instability manifested as a single bitumen finger that elongated through the water layer and eventually connected with the solvent above. The repeatability of the bitumen and total volume measurements before the instability is summarized in Table 3.2 and details are provided in Appendix B. The repeatabilities were 5% or less in all cases. The repeatability is less than the uncertainty due to asymmetry suggesting that asymmetry is the main source of error in the volume measurements.

Table 3.2. Average uncertainty of the bitumen and total volumes at 60°C for the evaluated systems.

System	**Bitumen Volume cm^3 (%)**	**Total Volume cm^3 (%)**
Toluene/water/bitumen	±0.06 (±6.0)	±0.004 (±0.4)
Cyclohexane/water/bitumen	±0.04 (±4.0)	±0.007 (±0.7)
n-Heptane/water/bitumen	±0.003 (±0.3)	±0.002 (±0.2)

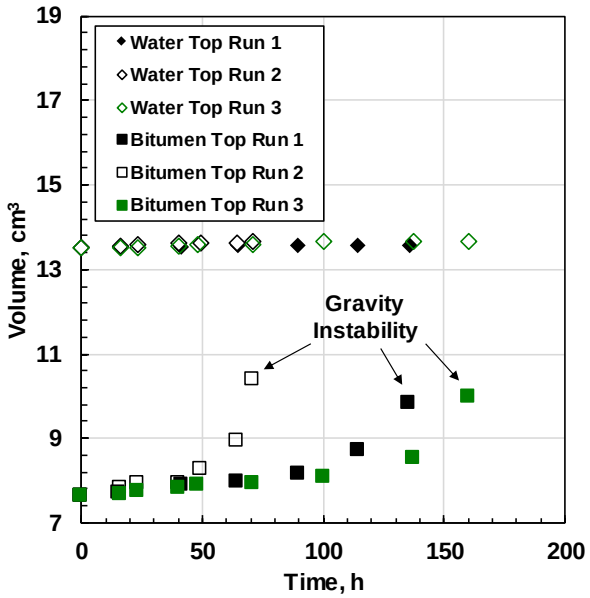

Figure 3.5. Change in bitumen and bitumen+water volumes for three runs of toluene/saturated water/WC-B-A3 bitumen experiment with a water layer thickness of 1.5 cm at 60°C.

3.2.3 Water Content in Bitumen

Changes in the water layer volume could be caused by mass transfer of the solvent or bitumen into the water, mass transfer of water into the bitumen and solvent layers, and evaporation of the water. The solubility of bitumen in water is very low (10^{-4} to 10^{-5} g/cm³, Chapter 4) and the solvent and bitumen masses in the water layer were negligible compared to the observed change in volume. The solubility of water in solvent is also very low, on the order of 10^{-4} to 10^{-5} g/cm³ (IUPAC-NIST solubility data series) and the amount of water lost to diffusion into the solvent layer was assumed to be negligible compared to the observed change in volume. The vials were sealed and therefore evaporation into air was also assumed to be negligible. It was further assumed that at the excess volumes of mixing were negligible at these very dilute conditions. Therefore, any change in the volume of the water layer was attributed solely to the transfer of water to the bitumen, as shown in Figure 3.6. As will be discussed later, the solubility of water in bitumen is very low and this mass is transferred via spontaneous emulsification.

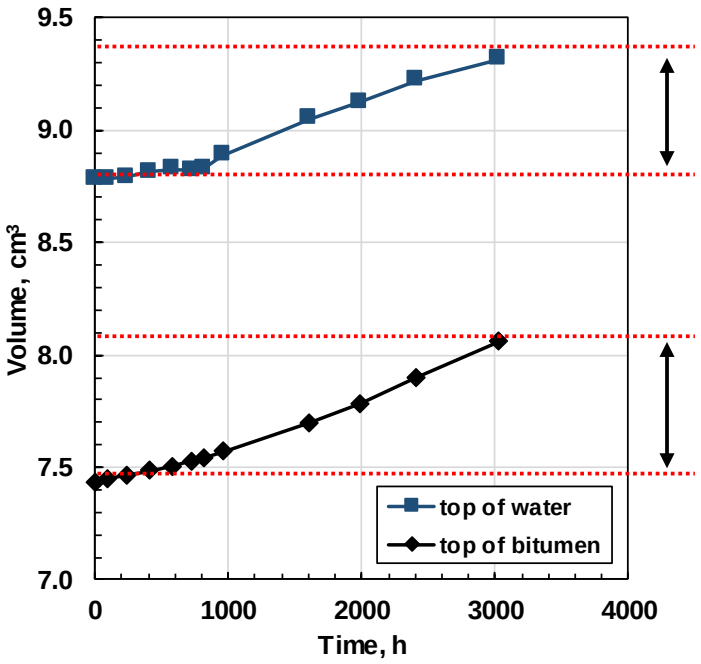

Rise indicates amount of solvent entering bitumen. (negligible solubility in water)

Rise indicates amount of solvent and water entering bitumen.

Solvent diffusion rate
Water content of bitumen

Figure 3.6. Interpretation of change in bitumen and total volume versus time; toluene/water/WC-B-A3 bitumen with a 0.35 cm water layer at 20°C.

The change in the water layer volume is given by:

$$\Delta V_w = V_w - V_{w,t=0} \tag{3.18}$$

The increase in the bitumen layer volume due to water transfer is then $-\Delta V_w$ and the water content in bitumen is given by:

$$w_w = \frac{-\Delta V_w \rho_w}{(V_b + \Delta V_w)\rho_b - \Delta V_w \rho_w} \tag{3.19}$$

where w_w is the mass fraction of water in the bitumen layer. Note that V_b is the volume of the bitumen layer and includes the water and solvent volumes within the layer. The solvent volumes are assumed to be negligible prior to gravity instability.

For the water/bitumen systems, the repeatability of the water contents was ±0.15 and ±0.52 wt% at 20 and 60°C, respectively, based on a 90% confidence interval. Some possible sources of error that affect the repeatability of the measurements are:

- the bitumen dome is not perfectly symmetrical around the y-axis.
- the inside edge of the bottom of the vials is curved so that they are not perfect cylinders.

- there were small variations on the time to make the measurements for the tests at high temperature (between 5-7 minutes).
- the system is disturbed every time the vial is moved to take a measurement. Since the vial could not be seen inside the bath this movement was unavoidable.

For the solvent/water/bitumen systems, the repeatability of the water contents was ±0.55 wt% and between ±0.05 to 2.3 wt% at 20 and 60°C, respectively. The higher uncertainty for the systems with solvent may be linked to the variation in the time to gravity instability, as shown in Figure 3.7. The water content increases more rapidly when the system becomes gravity stable more rapidly. The variation in the time to instability is discussed later. The repeatability analysis is provided in Appendix B.

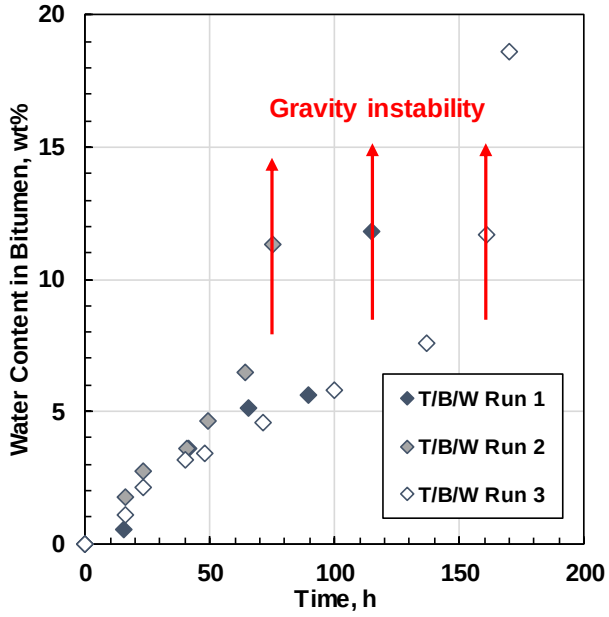

Figure 3.7. Water content in bitumen versus time for three runs of toluene/saturated water/WC-B-A3 bitumen experiment with a water layer thickness of 1 cm at 60°C.

3.2.4 Solvent Content in Bitumen

Changes in the combined volume of the bitumen and water layers volume could be caused by mass transfer of the solvent into the water or bitumen layers and mass transfer of bitumen into the solvent layers. As noted above, the solubility of solvent in water is very low and the mass of solvent transferred to the water was assumed to be negligible. Mass transfer of bitumen through the water

to the solvent is expected to be very slow and there was no discoloration of the solvent layer in the experiments. Therefore, the mass transfer of bitumen through the water into the solvent layer was also assumed to be negligible. Hence, the change in the combined bitumen and water layer volumes was attributed solely to the mass transfer of solvent into the bitumen layer, as shown in Figure 3.5. It was again assumed that there was no excess volume of mixing.

The volume change of the combined bitumen and water layers is given by:

$$V_s = V_t - V_{t,t=0} \tag{3.20}$$

where $V_{t,t=0}$ is the volume of the total column at t=0. The mass of solvent in bitumen at each time was calculated as follows:

$$m_s = \rho_s V_s \tag{3.21}$$

where ρ_s is the solvent density. The mass transfer rate is determined from the slope of the mass of diffused solvent versus time.

The repeatability of the solvent mass transfer measurements is summarized in Table 3.3. At 20°C, the uncertainty arises from the sources of error mentioned previously and is approximately ±0.02 cm³. The percentage error is higher for the *n*-pentane and cyclohexane systems because the solubility is lower; that is, the absolute error is divided by a smaller number. At 60°C, the percentage error in toluene is higher and may be linked to the elapsed time to gravity instability; the mass transfer rate is higher when the instability occurs sooner as shown in Figure 3.8. It is not obvious if the instability causes the increases in mass transfer or *vice versa*. The reason for the higher variations in the time to instability at 60°C is not known but could be caused by disturbances when taking measurements as discussed in the next section. Note, the gravity instability occurred much later in the other solvents and did not significantly impact their measurements; the error for these solvents is comparable to the error at 20°C. The repeatability analysis is provided in Appendix B.

Table 3.3. Average uncertainty of the solvent transferred to the bitumen layer at 20 and 60°C for the evaluated systems.

System	**Solvent Transfer cm³ (%)**
Toluene/water/bitumen at 20°C	±0.038 (±22)

n-Pentane/water/bitumen at 20°C	±0.067 (±34)
Toluene/water/bitumen at 60°C	±0.057 (±35)
Cyclohexane/water/bitumen at 60°C	±0.022 (±30)
n-Heptane/water/bitumen at 60°C	±0.015 (±3.4)

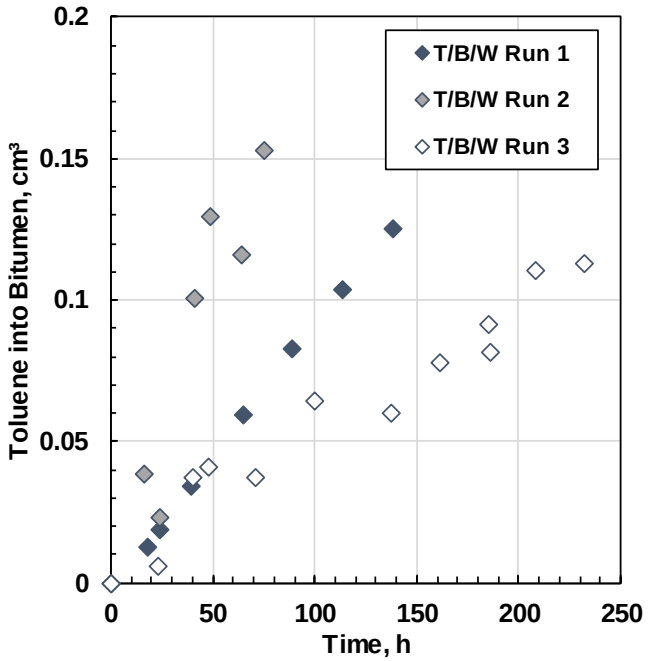

Figure 3.8. Toluene into bitumen versus time for three runs of toluene/saturated water/WC-B-A3 bitumen experiment with a water layer thickness of 1 cm at 60°C.

3.3 Convection Test

One of the possible sources of error during the height measurements at 60 and 80°C was that the vials have to be moved from the warm water bath to the room temperature cathetometer. Although the vials were moved very gently, it was possible that this motion accelerated the emulsification rate and/or the solvent mass transfer rate. In addition, the temperature gradients from the transient temperature changes during this measurement could cause convection.

To investigate this effect, a set of six identical tests of the toluene/water/WC-B-A3 bitumen system with a 1.5 cm unsaturated water layer thickness were performed at 60°C. Each test was performed for a different time and the layer heights were measured only once at the end of the test. The results

were compared to three repetitions performed with the same fluids using the standard procedure (multiple layer height measurements during the test).

Figures 3.9a and 3.9b show that the toluene content and water content in the bitumen, respectively, for the convection test are within the scatter of the three repeats with the conventional method. The toluene content was at the high end of the range of scatter while the water content was at the low end. Hence, it appears that the transfer of vials for the height measurements was not the main source of the scatter prior to gravity instability. Interestingly, no gravity instability was observed in the duration of the convection test. It is possible that the transfer of the vials contributed to the uncertainty in the time to gravity instability.

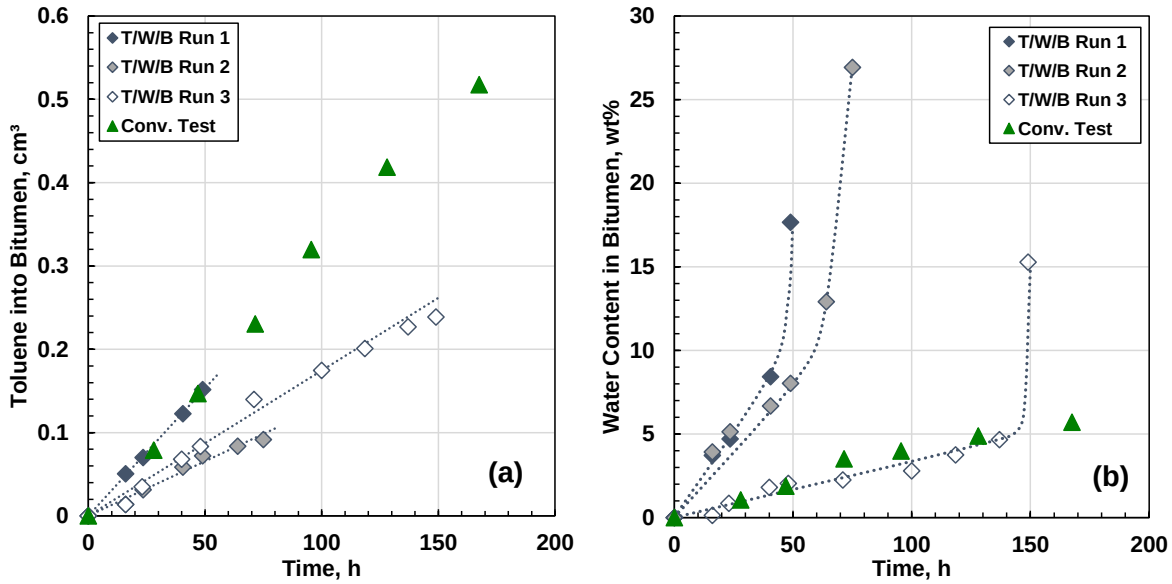

Figure 3.9. Results of the convection tests and three identical runs did with toluene/1.5 cm of unsaturated water/ WC-B-A3 bitumen: a) toluene into bitumen versus time; b) water content in bitumen versus time.

CHAPTER FOUR: RESULTS AND DISCUSSION

This chapter presents the results from the liquid-liquid solvent/water/bitumen diffusion experiments and the water/bitumen diffusion tests. First, the fluid properties required to interpret the diffusion experiments are presented. Then, the results of water/bitumen tests are discussed. Next, the steady state diffusion model used to model the experimental results for the solvent diffusion rate is explained and the results for the solvent/water/bitumen diffusion tests are discussed. Finally, some correlations for the emulsification rate, solvent transfer rate, time to instability and water height are presented.

4.1 Fluid Properties

The fluid properties required to interpret the diffusion experiments are the densities of the bitumen, water, and solvent, the solubility and diffusivity of the solvent in water, and the solubility of water in bitumen, all at the temperatures of interest (20 to 80°C).

4.1.1 Fluid Densities

Densities of solvent and water at 0.1 MPa were taken from the NIST Chemistry Book (2018). Experimentally measured densities of WC-B-A3 and WC-B-B5 bitumen at 50, 75 and 100°C were taken from Grimaldos (2018) and Perez (2019), respectively, and are provided in Table 4.1. The experimental data for density was extrapolated to lower temperatures using the following empirical correlation fitted to the higher temperature data (Saryazdi *et al*., 2013):

$$\rho_b = (A^* - B^*T)\exp\{[F^*\exp(D^*T)](P - 0.1)\} \quad (4.1)$$

where ρ_b is the density of the bitumen in kg/m³, P is the pressure in MPa, T is the temperature in K, and A^*, B^* F^* and $D^*$are fitting parameters. The fitted parameters are provided in Table 4.2 and the fitted densities used in this study are provided in Table 4.3. Eq. 4.1 fit the density of bitumen with a maximum absolute deviation of $1.2\cdot10^{-4}$ g/cm³.

The fitted bitumen densities and the water and solvent density values are provided in Table 4.3. Figure 4.1 compares the density of the two bitumens and water at different temperatures. There is

a neutral buoyancy point between water and WC-B-A3 bitumen at 60°C. The WC-B-B5 bitumen is approximately 0.01 g/cm^3 denser than water over the range of temperatures of interest. Hence, a layer of WC-B-B5 bitumen under water will be gravity stable. The WC-B-A3 bitumen is denser than water up to approximately 60°C but then becomes slightly denser than water at higher temperatures. A layer of WC-B-A3 bitumen under water may be gravity unstable above 60°C.

Table 4.1. Measured densities of WC-B-A3 and WC-B-B5 bitumen at 0.1 MPa and 50, 75 and 100°C; data from Grimaldos (2018) and Perez (2019).

Fluid	**Density at 50°C, g/cm^3**	**Density at 75°C, g/cm^3**	**Density at 100°C, g/cm^3**
WC-B-A3	0.9902	0.9744	0.9584
WC-B-B5	1.0010	0.9851	0.9694

Table 4.2. Parameters for the bitumen density equation.

Component	A^* **kg/m^3**	B^* **kg/(m^{3}K)**	F^* **1/MPa**	D^* **1/K**
WC-B-A3	1196.2	0.63743	0.00014	0.00433
WC-B-B5	1211.3	0.65085	0.00018	0.00455

Table 4.3. Fitted densities of WC-B-A3, WC-B-B5, reverse osmosis water, toluene, cyclohexane, *n*-heptane and n-pentane at 0.1 MPa and 20, 60 and 80°C.

Fluid	**Density at 20°C, g/cm^3**	**Density at 60°C, g/cm^3**	**Density at 80°C, g/cm^3**
WC-B-A3	1.0094	0.9838	0.9711
WC-B-B5	1.0207	0.9944	0.9814
Water	0.9982	0.9832	0.9718
Toluene	0.8669	0.8292	0.8098
Cyclohexane	0.7786	0.7402	0.7202
n-Heptane	0.6838	0.6494	0.6314
n-Pentane	0.6257	-	-

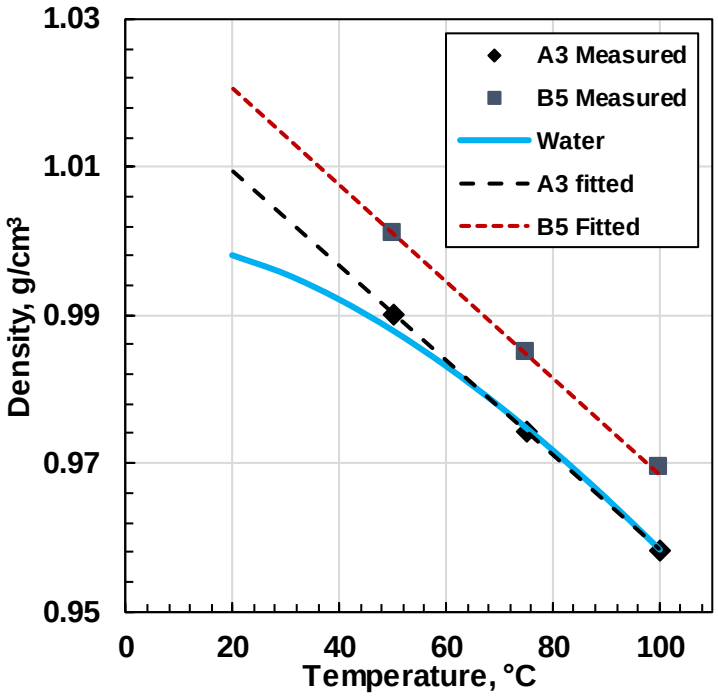

Figure 4.1. Densities of water, WC-B-B5 and WC-B-A3 bitumen versus temperature. Bitumen data from Grimaldos (2018) and Perez (2019).

4.1.2 Solubility and Diffusivity of Solvents in Water

Values for the diffusivity coefficient and solubility of the evaluated solvents in water were found in the literature and are listed in Table 4.4.

Table 4.4. Solubility and diffusivity coefficients of toluene, cyclohexane, *n*-heptane and *n*-pentane in water at 0.1 MPa and 20, 60 and 80oC. Diffusivity data taken from: a) Bonoli and Witherspoon, (1969), b) Landolt-Börnstein (1990); c) Zou *et al*. (2007). Solubility data taken from NIST solubility database (2008).

Solvent	Temperature °C	Solubility in Water g/cm³	Diffusivity in Water cm²/h
Toluene	20 [a]	0.00059	0.0306
	60 [a]	0.00086	0.0774
	80 [b]	0.00317	0.1037
Cyclohexane	20 [a]	0.000085	0.0335
	60 [a]	0.00017	0.0785
	80 [b]	0.00026	0.1010
n-Heptane	60 [c]	0.0000033	0.0613
	80 [b]	0.000004	0.0855
n-Pentane	20 [a]	0.00004	0.0302

4.1.3 Solubility of Water in Bitumen

The solubility of water in WC-B-A3 and WC-B-B5 bitumen at temperatures between 20 and 80°C was determined using a correlation (Satyro *et al.*, 2013). Details are provided in Appendix C. The solubilities are provided in Table 4.5. The solubility of water in both bitumen samples at 80°C is less than 0.06 wt%.

Table 4.5. Solubility of water in WC-B-A3 and WC-B-B5 bitumen samples versus temperature; calculated from Satyro *et al*. (2013) correlation.

Temperature °C	Water in WC-B-A3 wt%	Water in WC-B-B5 wt%
20	0.013	0.014
40	0.021	0.022
60	0.034	0.036
80	0.055	0.057

4.2 Water/Bitumen Systems

Before considering the mass transfer of solvent through water into bitumen, the behavior of water of bitumen was examined at the same conditions (20, 60, and 80°C) to determine if there were any interactions between the bitumen and water that could affect the mass transfer measurements with solvent. Both the WC-B-A3 and WC-B-A5 bitumens initially contained some emulsified water: 1.8 wt% in WC-B-A3 and 2.6 wt% in WC-B-B5, as measured Elaine Baydak using the Karl Fischer method. Figure 4.2 shows that the water was dispersed as water droplets with diameters less than 1 μm and 3 μm diameter, respectively.

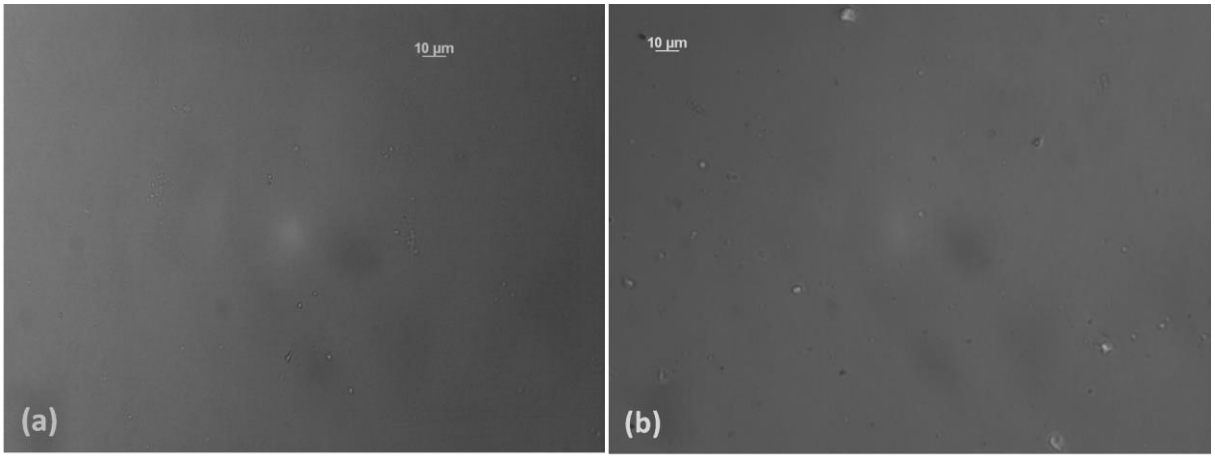

Figure 4.2. Micrographs of bitumen before contact with water layer: a) WC-B-A3 (initially 1.8 wt% water content); b) WC-B-B5 bitumen (initially 2.6 wt% water content).

4.2.1 Water/WC-B-A3 Bitumen

Figure 4.3 shows photographs of a typical water/WC-B-A3 bitumen experiment at 20 and 60°C. The bitumen density was initial lower than that of water at 80°C and therefore 80°C was not examined. At 60°C, the bitumen layer formed a dome, consistent with a meniscus between two similar density fluids confined by a water-wet surface. The dome increased over time. As noted below, a significant amount of water was emulsified into the bitumen at 60°C and this water must lower the local density of the bitumen and reduce the density difference between the bitumen and water, leading to a larger meniscus height (larger dome). At 20°C, the dome only appeared after 1000 h when the water content in bitumen became significant (discussed below). It is not clear why no dome formed initially. The water phase remained clear and colorless for the duration of

the experiments, suggesting that no oil-in-water (O/W) emulsification occurred, this was confirmed with a micrograph to the water phase for a test at 60°C as shown in figure 4.4.

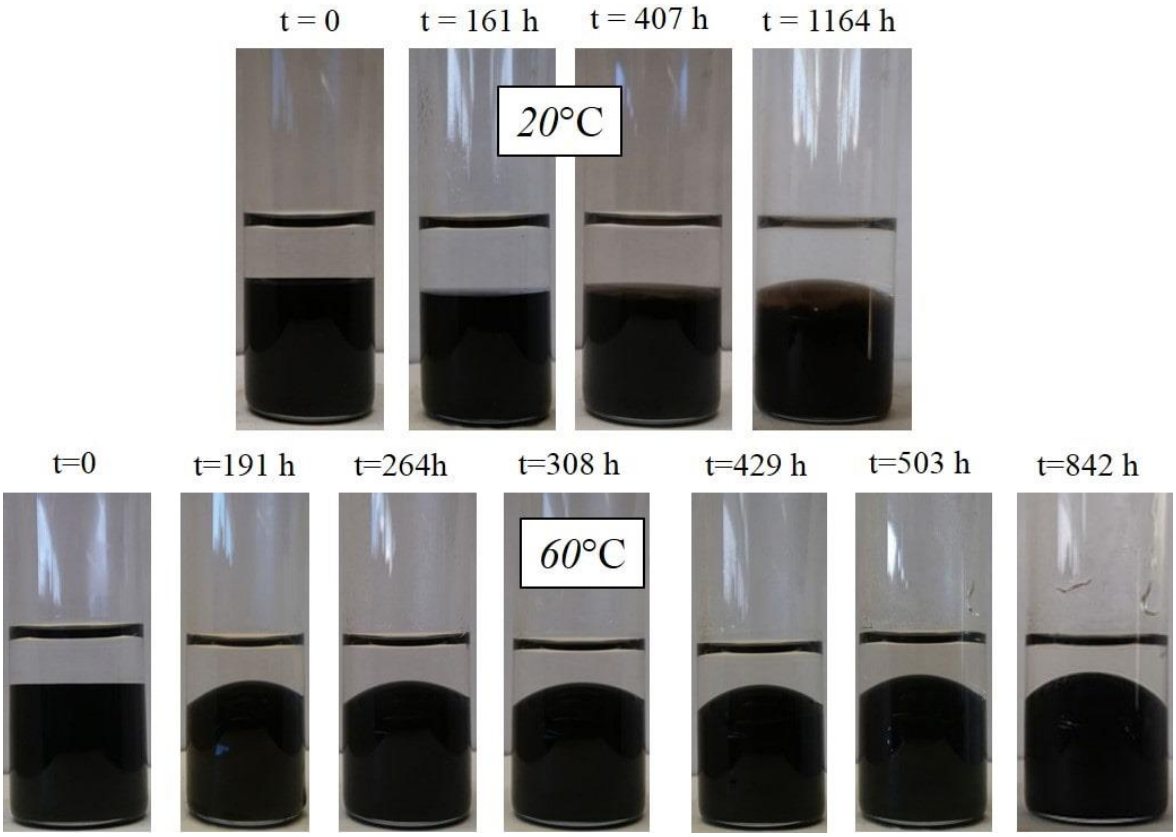

Figure 4.3. Photographs of water/WC-B-A3 bitumen with 1 cm of unsaturated water at 20 and 60°C.

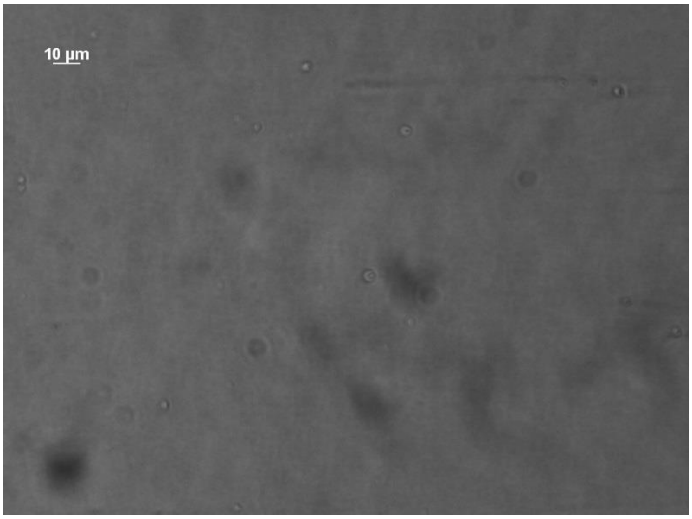

Figure 4.4. Micrograph of the water phase of a water/WC-B-A3 bitumen test at 60°C after 842 hours.

The volume of the bitumen layer increased, indicating that water was entering the bitumen. Figure 4.5 shows the change in water content over time in WC-B-A3 bitumen at 20 and 60°C for water layer heights of 1, 1.5 and 2 cm. The initial water content was subtracted from the actual measured water content. The open symbols are the water contents determined from the volume change of the bitumen layer in the images provided in Appendix B. For this binary system, any increase in the bitumen volume is equal to the volume of water entering into the bitumen. These water contents were within experimental error (±0.6 wt%) of all but one of the water contents measured with the Karl Fischer method at 60°C (solid symbols). The water content increased significantly over time, reaching a plateau value of approximately 5 wt%. The emulsification rate was higher at higher temperature. The water contents are far above the solubility of water in bitumen (< 0.06 wt%, Table 4.5) and suggest that water had become emulsified into the bitumen over time.

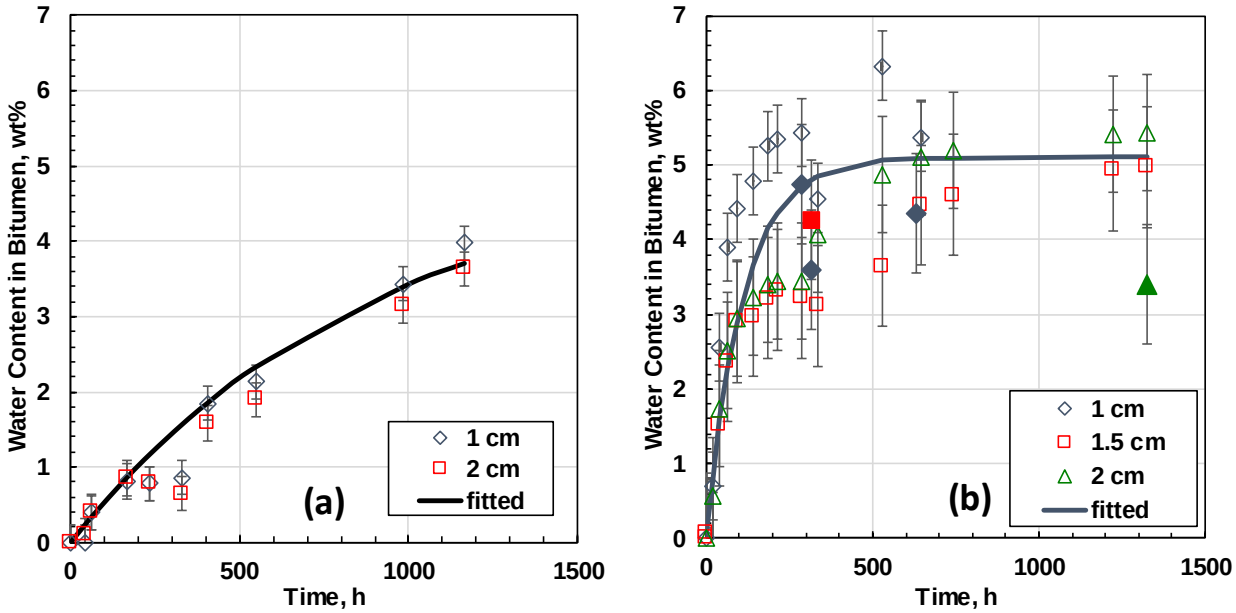

Figure 4.5. Incremental water content in WC-B-A3 bitumen over time for different water layer heights at: a) 20°C; b) 60°C. Open symbols from volume change method; closed symbols from Karl Fischer.

Figures 4.6a and 4.6b are micrographs of the very top of the bitumen layer and the approximate middle of the layer of a water/bitumen test at 20°C and 1200 hours. The size and number of droplets is significantly higher than in the bitumen at the start of the experiment, confirming emulsification. Most of the water droplets are concentrated on the top of the bitumen layer and

mainly have diameters between 1 and 3 μm with a few droplets with diameters up 8 μm. In the middle layer water droplets are considerably less frequent and range from 1 to 5 μm in diameter. This water droplet diameter range is characteristic of water in oil macroemulsions (Tadros 2009; Schramm, 1992; Shaw, 1981; Lake, 1989; Becher, 1966; Summer, 1954). The results are consistent with a spontaneous emulsification study by De Araujo *et al*., (2017). They observed spontaneously formed water droplets of 2 μm of diameter in a toluene/asphaltene solution at 20°C and noted that the water droplets were considerably more concentrated in the center of the meniscus.

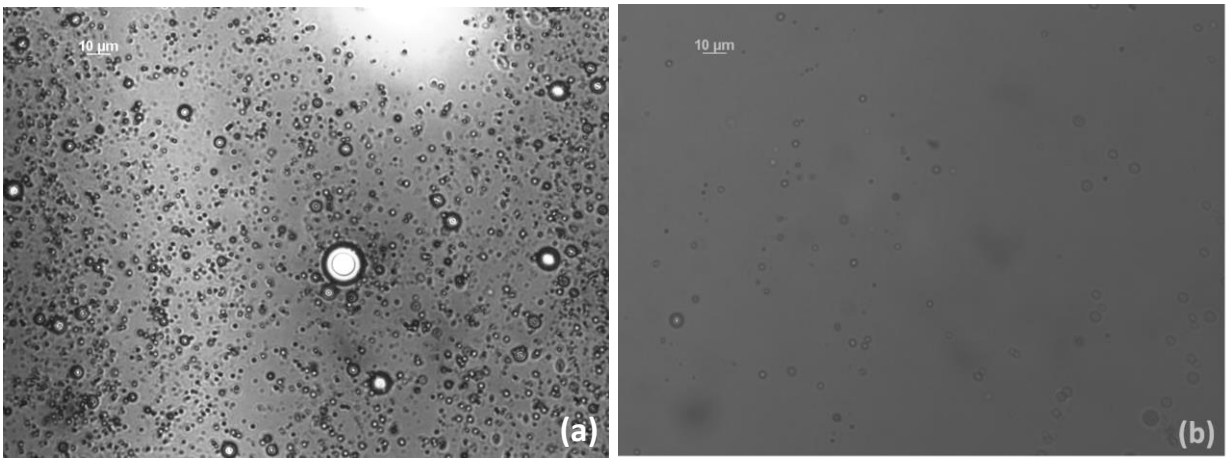

Figure 4.6. Micrographs of bitumen (1 cm unsaturated water/WC-B-A3 bitumen at 20°C) after 1200 hours: a) top of the bitumen layer; b) middle of the bitumen layer.

Figures 4.7a and 4.7b show two micrographs of the top of the bitumen layer and the middle of the bitumen layer of a water/bitumen test at 60°C after 650 hours. At this temperature water droplets (1 to 5 μm diameter) are not concentrated on the top as they were at 20°C; the movement to lower into the bitumen phase might be due to bitumen having lower viscosity at 60°C which facilitates the settling of the water droplets.

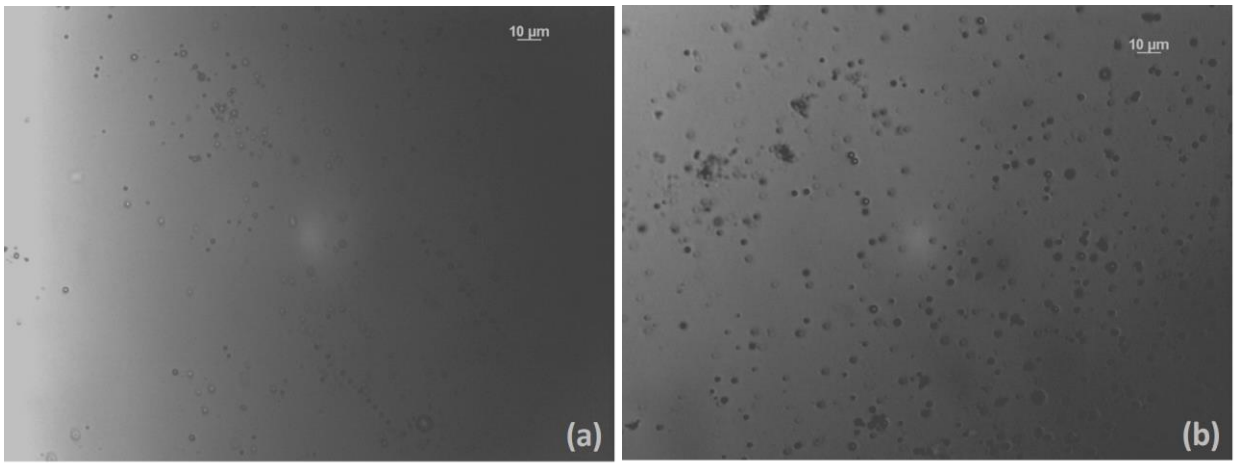

Figure 4.7. Micrographs of bitumen (1 cm unsaturated water/WC-B-A3 bitumen at 60°C) after 650 hours: a) top of the bitumen layer; b) middle of the bitumen layer.

The emulsification rate was required to aid in the interpretation of the solvent/water/bitumen mass transfer experiments. The water content data in Figure 4.5 were fitted with the following correlation:

$$w_w = w_{w,max}(1 - \exp(-kt)) \qquad (4.1)$$

where $w_{w,max}$ is the maximum value of the water content in bitumen, *t* is time in hours, and *k* is a fitting parameter in *1/h* which depends on the temperature and type of bitumen. The fitted equation is shown in Figure 4.5 and the fitted parameters are listed in Table 4.6. Equation 4.1 fit the data with an average deviation of 0.17 and 0.35 wt% for the tests at 20 and 60°C, respectively, less than the experimental error of 0.24 and 0.68 wt%.

Table 4.6. Fitting parameters of the water content in bitumen equation.

System	$w_{w,max}$, **wt %**	***K, 1/h***
WC-B-A3/water at 20°C	4.9	0.0011
WC-B-A3/water at 60°C	5.1	0.0090
WC-B-B5/water at 60°C	5.1	0.0006
WC-B-B5/water at 80°C	6.1	0.0050

4.2.2 Water/WC-B-B5 Bitumen

Figure 4.8 shows photographs of a typical water/WC-B-B5 bitumen experiment at 20, 60 and 80°C. In this case, the bitumen layer formed a dome even at 20°C, consistent with the formation of a meniscus. At 20°C, the water phase remained clear and there was no evidence of O/W emulsification. However, at 60 and 80°C, the water developed a brownish tinge and micrographs indicated the presence of emulsified oil. Figure 4.9 is a micrograph of the brown colored water phase for water/WC-B-B5 bitumen at 60°C and shows the presence of an oil-in-water emulsion with oil droplets of 1 to 5 μm in diameter.

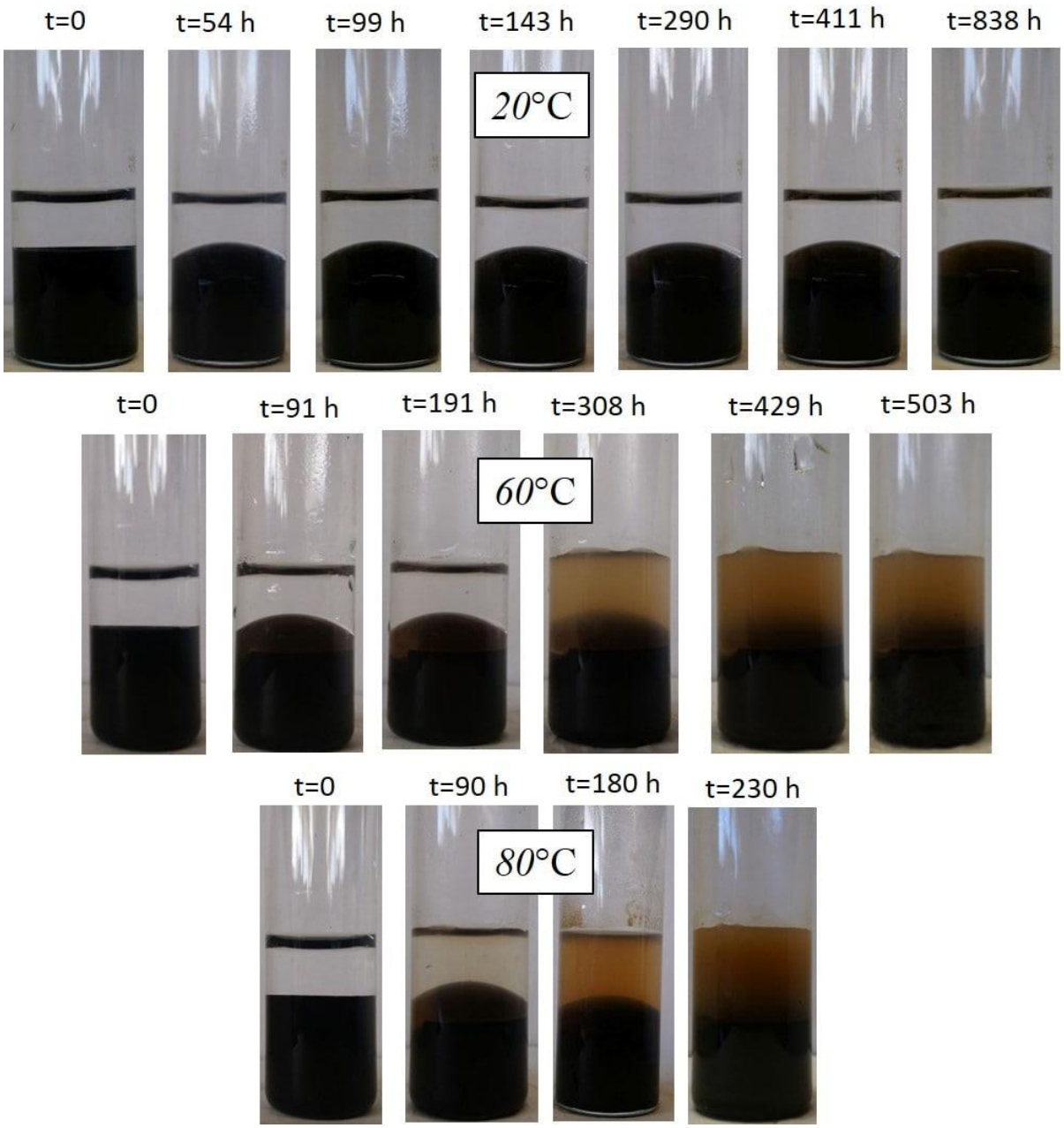

Figure 4.8. Photographs of water/WC-B-B5 bitumen with 1 cm of unsaturated water at 20, 60 and 80°C.

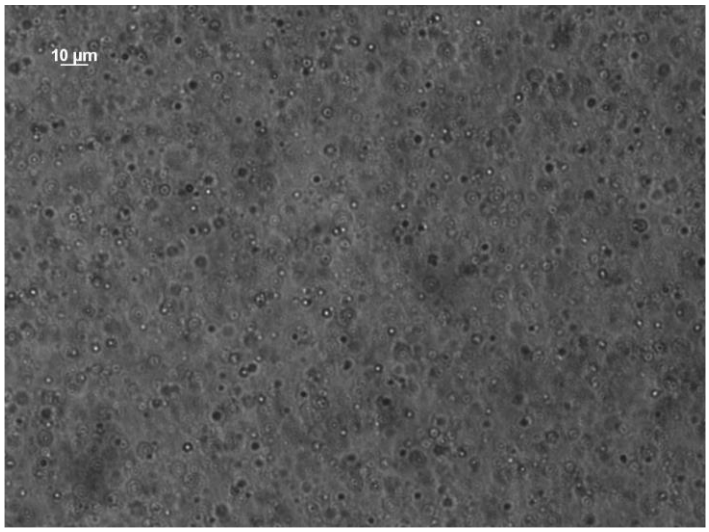

Figure 4.9. Micrograph of the water phase of a water/WC-B-B5 bitumen test at 60°C after 503 hours.

As observed with the water/WC-B-A3 system, the volume of bitumen layer increased over time indicating that water was entering the bitumen. Figure 4.10 shows micrographs of the top and middle of the bitumen phase for water/WC-B-B5 bitumen at 60°C where the water droplets in the bitumen were 1 to 10 µm in diameter, indicating presence of a macroemulsion. Figure 4.11 shows the water content in bitumen for both WC-B-A3 and WC-B-B5 bitumen samples at 20 and 60°C and for WC-B-B5 bitumen at 80°C. The water layer height was 1 cm for the three temperatures and both bitumen samples. In general, the rate of W/O emulsification for the WC-B-B5 bitumen was less than for WC-B-A3 bitumen. Possible explanations are that: 1) the WC-B-B5 bitumen contains less surface active components capable of stabilizing emulsions; 2) the formation of an O/W emulsion may have depleted the available surface active components in the WC-B-B5 bitumen; 3) the formation of the O/W emulsion mechanically interfered with the formation of the W/O emulsion.

At 60 and 80°C, water was emulsified into the bitumen and bitumen was emulsified into the water. The transfer of bitumen to the water in not accounted for so the volume based water contents may be too high. At 60°C the Karl Fischer titration measurement for the water in WC-B-B5 bitumen matched the volumetric calculation, indicating that the mass of oil transferred to the water at this temperature after 400 hours was not significant. However, at 80°C, the Karl Fischer titration

measurements are 2 to 3 wt% lower than the volumetric measurements, suggesting there a significant amount of bitumen emulsifying into the water.

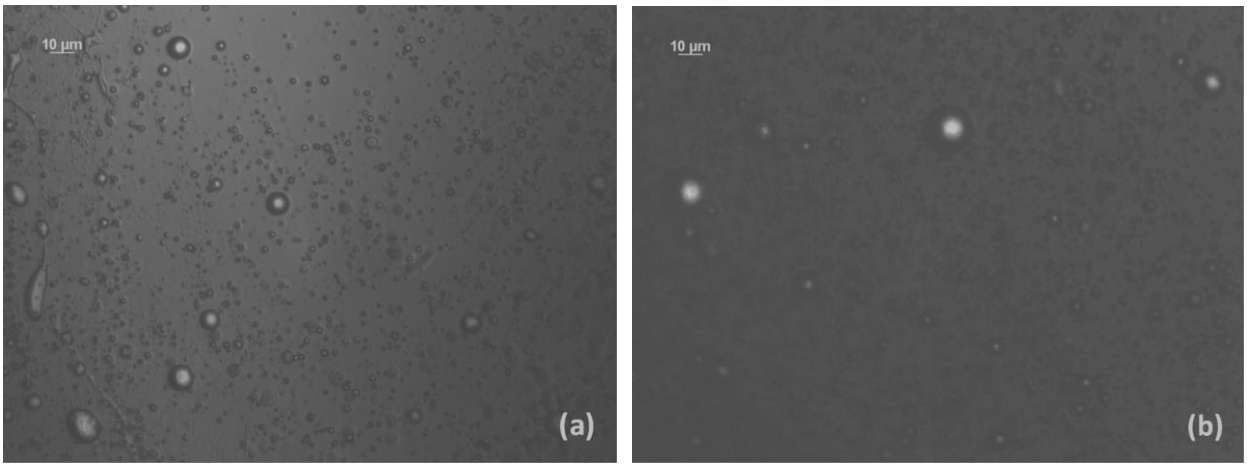

Figure 4.10. Micrographs of bitumen (1 cm unsaturated water/WC-B-B5 bitumen at 60°C) after 842 hours: a) top of the bitumen layer; b) middle of the bitumen layer.

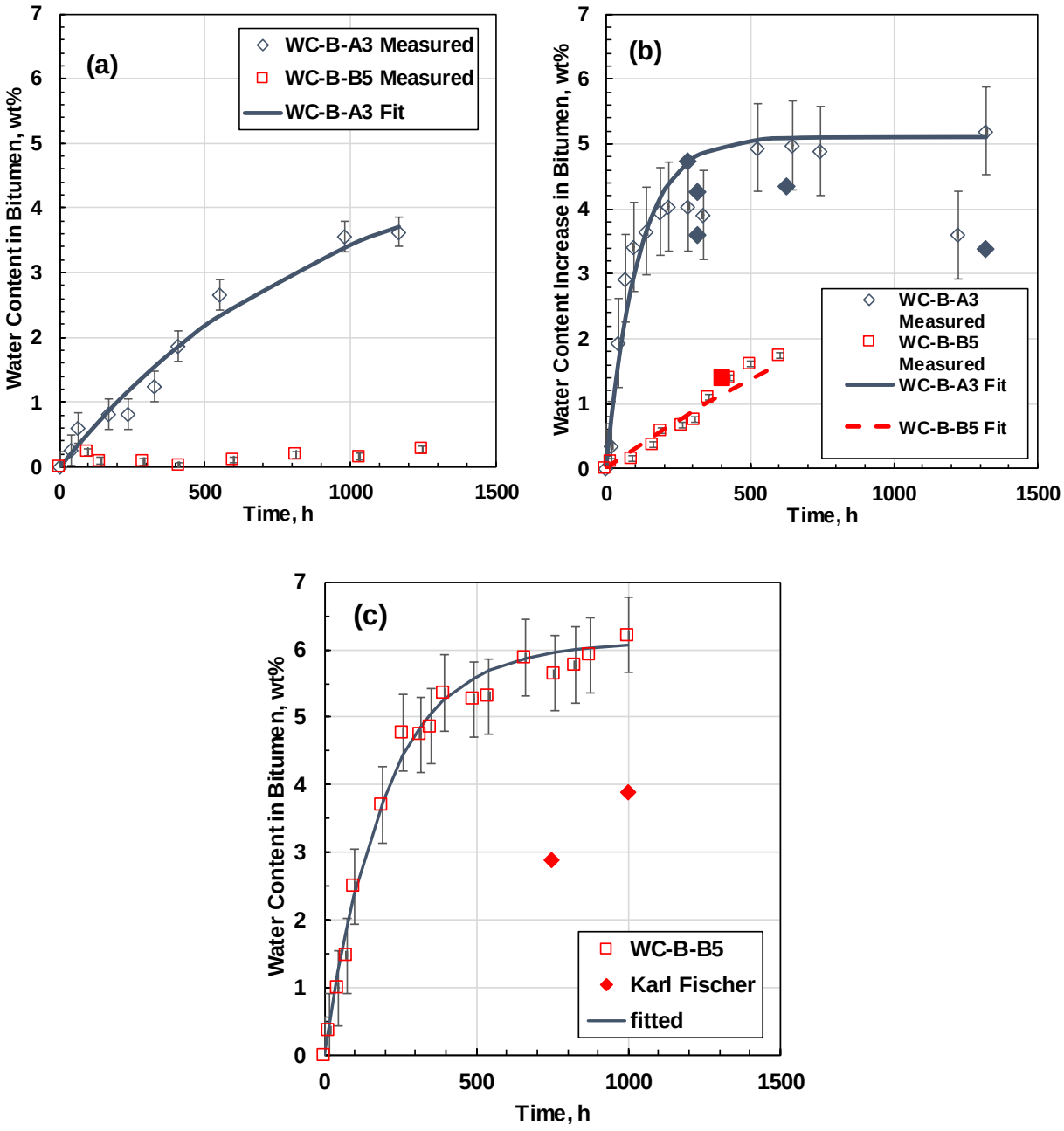

Figure 4.11. Incremental water content in WC-B-A3 and WC-B-B5 bitumen for a 1 cm water layer height at: a) 20°C; b) 60°C; c) 80°C. Open symbols from volume change method; closed symbols from Karl Fischer.

4.2.3 Effect of Removing Natural Surfactants

There is spontaneous emulsification of water into bitumen for both WC-B-B5 and WC-B-A3 bitumen samples and there is also spontaneous emulsification of bitumen into water for WC-B-B5

bitumen. As discussed in Section 2.3.2, spontaneous emulsification is likely attributable to naturally present surface active agents in the bitumen. These can reduce the interfacial tension enough (although not necessarily to the ultralow IFT values) that water droplets will form spontaneously on the bitumen and/or *vice versa* (Yeung *el al*., 1999). Other mechanisms such as interfacial turbulence and diffusion and stranding likely contribute to emulsification. To prove that natural surfactants were responsible for the spontaneous emulsification, both bitumen samples were partially stripped of natural surfactants (see Section 3.1). Then the water/bitumen tests were repeated with the stripped bitumen at 20 and 60°C and compared with the original water/bitumen tests.

Water/WC-B-A3 Bitumen

Photographs of the water/bitumen tests at 20 and 60°C for the original and stripped WC-B-A3 bitumen are provided in Appendix D. Figure 4.12 shows the water content in the original and stripped WC-B-A3 bitumen at 20 and 60°C. The water content in the stripped WC-B-A3 was below 0.4 wt% at both temperatures, in contrast to the 3.7 and 5.2 wt% water in the original bitumen at 20 and 60°C, respectively. Figure 4.13 shows micrographs of the top and middle layer of the stripped WC-B-A3 bitumen at 60°C after 1000 hours. Similar to the original bitumen, the water droplet diameters ranged from 1 to 5 μm (macroemulsion) but the concentration of water droplets was considerably lower than in the original bitumen (see Figure 4.7). It appears that the stripping procedure removed most of the surface active components responsible for spontaneous emulsification and that without these components spontaneous emulsification does not occur.

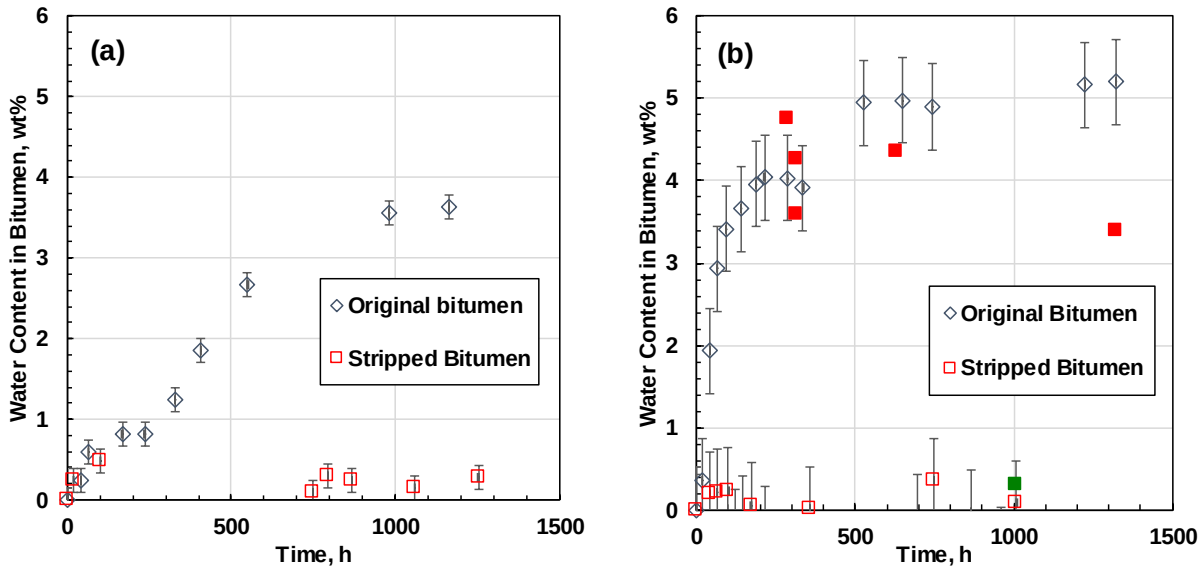

Figure 4.12. Incremental water content in WC-B-A3 bitumen for the original and stripped bitumen samples at: a) 20°C; b) 60°C. Open symbols from volume change method; closed symbols from Karl Fischer.

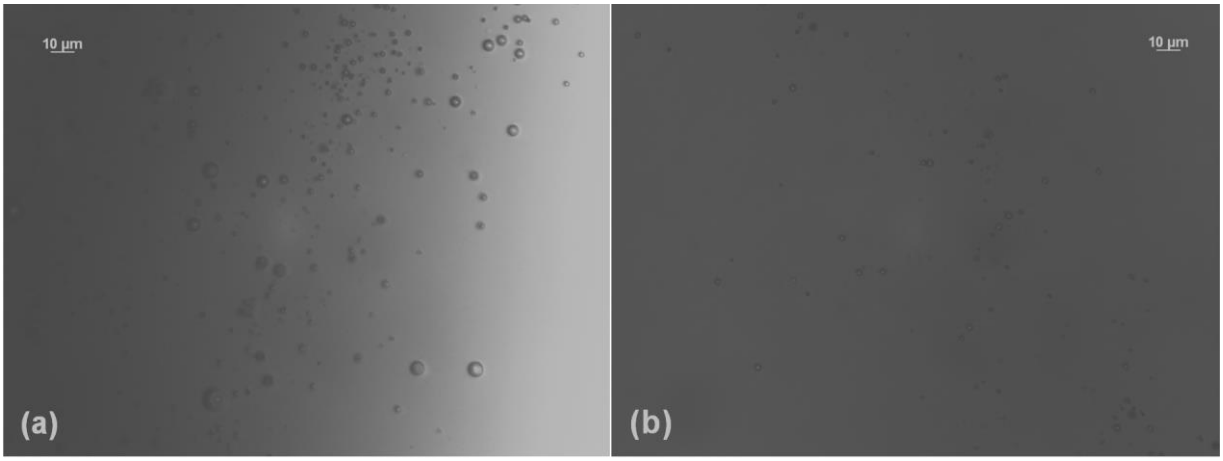

Figure 4.13. Micrographs of stripped bitumen (1 cm unsaturated water/WC-B-A3 bitumen at 60°C) after 1000 hours: a) top of the bitumen layer; b) middle of the bitumen layer.

Water/WC-B-B5 Bitumen

Photographs of the water/bitumen tests at 20 and 60°C for the original and stripped WC-B-B5 bitumen are provided in Appendix D. No discoloration was observed in the stripped bitumen tests indicating that no O/W emulsion formed. Figure 4.14 shows the water content in the original and stripped WC-B-B5 bitumen at 20 and 60°C. The water content in the stripped WC-B-B5 was below

0.6 wt% at both temperatures. There is no significant difference from the water content of the original bitumen test at 20°C because negligible emulsion formed in either case. However, the water content of the stripped bitumen is lower than that the 1.7 wt% the original bitumen at 60°C. Figure 4.15 shows micrographs of the top and middle layer of the stripped WC-B-A3 bitumen at 60°C after 1000 hours. The water droplet diameters for the top and middle of the bitumen layer ranged from 1 to 2 μm and 0.5 to 1 μm, respectively, indicating the presence of a macroemulsion. However this range of diameters is lower than that of the original bitumen (1 – 10 μm) and the concentration of water droplets in the SR middle bitumen layer is less than that of the original bitumen. It again appears that the stripping procedure removed most of the surface active components responsible for spontaneous emulsification and that without these components neither spontaneous W/O or O/W emulsification occurred.

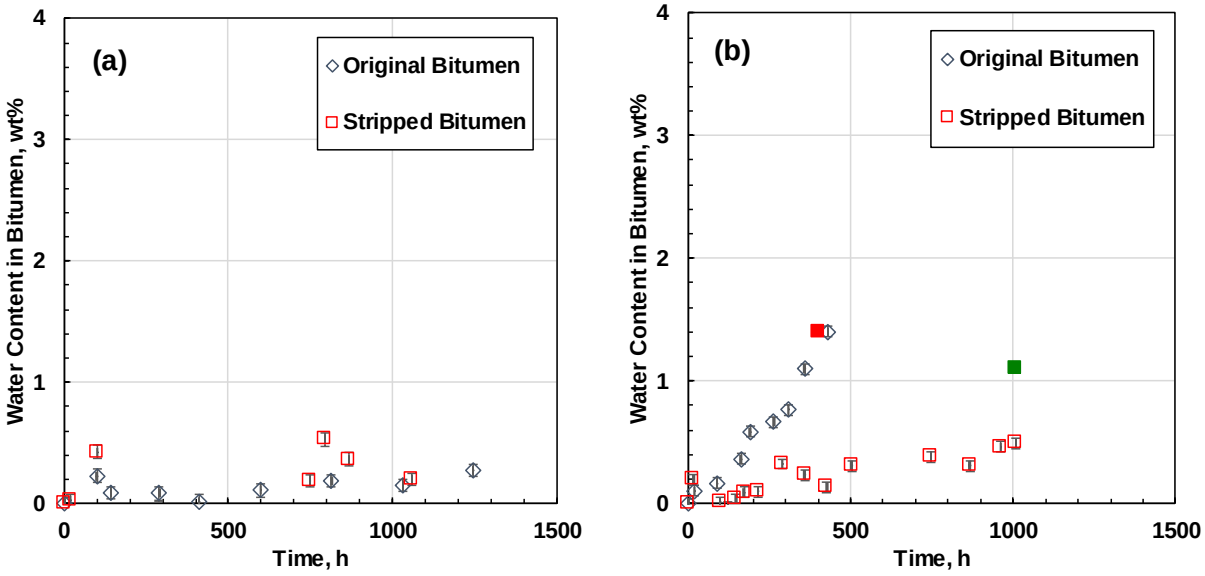

Figure 4.14. Incremental water content in WC-B-B5 bitumen for the original and stripped bitumen samples at: a) 20°C; b) 60°C. Open symbols from volume change method; closed symbols from Karl Fischer.

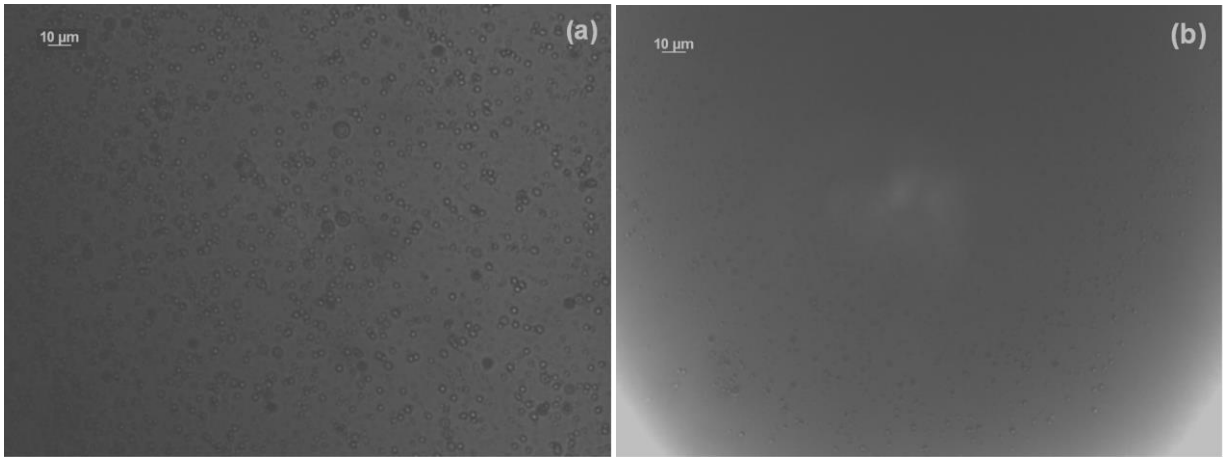

Figure 4.15. Micrographs of stripped bitumen (1 cm unsaturated water/WC-B-B5 bitumen at 60°C) after 1000 hours: a) top of the bitumen layer; b) middle of the bitumen layer.

4.3 Solvent/Water/Bitumen Systems

The expected effect of a layer of water on the mass transfer of solvent to bitumen is illustrated in Figure 4.16. The solvent has a low solubility in water and establishes that solubility at the interface between the solvent and water. The solvent is miscible in the bitumen and is expected to rapidly diffuse into the bitumen leaving a very low concentration in the water immediately above the bitumen layer. Since the solubility of the solvent in the water is low, the concentration gradient is low, and the solvent mass transfer rate through the water is expected to be low. The steady state solution for the mass transfer of solvent through the water layer is presented below. Then the experimental results at 20°C, where this mass transfer model was found to apply, are discussed. Finally, the results at higher temperatures, where other factors altered the mass transfer rate, are discussed.

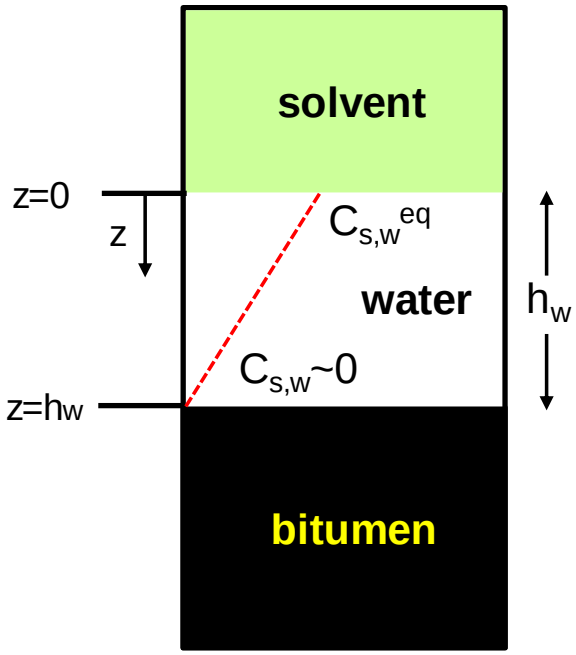

Figure 4.16. Schematic of the solvent mass transfer into bitumen through a water layer.

4.3.1 Solvent Mass Transfer Model

Solvent mass transfer on the solvent/water/bitumen tests was modeled using Fick's first law. Only mass transfer through the water layer was evaluated; the mass transfer into and through the bitumen was not modeled. The following assumptions are made to obtain a solution:

One Dimensional Diffusion: The vials used in the experiments have a diameter of 2.2 cm, far greater than the path length for diffusion. Therefore, it was assumed that wall effects were negligible. The solvent/water interface was flat in all experiments. The water/bitumen interface was initially flat at 20°C but formed domes after sufficient mass transfer of solvent into the bitumen and at higher temperatures. With a flat interface, there is no radial concentration gradient and mass transfer is expected to be one dimensional in the axial direction. When a dome forms, radial diffusion can occur but in most experiments would only affect a fraction of the axial diffusion profile and was neglected. In general, the dome was less than 13% of the thickness of the water layer before reaching instability.

Isothermal System: The experiments at room temperature were placed in a fume hood at a temperature of 20 ±0.1°C. The tests at 60 and 80°C were placed in a water bath with temperature

variation ±0.1°C. Therefore the system was considered to be isothermal. However, small temperature gradients may exist in the temperature bath causing convection as will be discussed later.

No Chemical Reactions: The solvents used in this thesis do not react with water and bitumen at the evaluated temperatures. Reactions may occur above 250°C (Gray 2015). Hence, chemical reactions were not included in the model.

No Natural Convection: The experiments were set up such that there was no density driven convection in the system from the beginning of the test because the solvent density was less than the water density which in turn was less than the bitumen density. At higher temperatures, the bitumen density exceeded the water density but interfacial forces held the bitumen in place. Therefore, it was assumed that there was no natural convection. Eventually, when sufficient solvent diffuses into the bitumen, the bitumen density was reduced enough to cause convection. The model was only applied to gravity stable data.

No Forced Convection: Two potential sources of forced convection were identified: 1) moving the vials to the cathetometer; 2) temperature gradients in the water bath. The convection test (see Section 3.3) showed that the transfer of vials for the height measurements did not accelerate the mass transfer rate and therefore was not considered to be a convection source. As will be discussed later, the mass transfer rates at higher temperatures were faster than expected from steady state mass transfer and it is possible that some natural convection occurred. For modeling purposes, natural convection was neglected.

Constant Diffusivity: A constant diffusivity of solvent in water was assumed because the concentrations of the solvents evaluated in water are extremely low (see Table 4.4) and approach the infinite dilution condition.

Negligible Solvent Concentration Above Water/Bitumen Interface: It was assumed that the solvent partitioned highly to the bitumen at the water/bitumen interface such that the concentration of solvent in the water above the interface was near zero. The solvent partitions strongly to the

bitumen because it is far more soluble in the bitumen than in water. Toluene is completely miscible in bitumen at the conditions evaluated in this thesis, 80°C and 0.1 MPa (Forte and Taylor, 2015; Motahhari *et al*. 2011; Yarranton et al., 2010). *n*-Pentane and *n*-heptane are partially miscible in bitumen. They are miscible until reaching a solvent concentration in the bitumen between 40 and 50 wt% where the onset of asphaltene precipitation occurs (Akbarzadeh *et al*., 2003; Johnston *et al*., 2017). They remain miscible with the light phase and simply reject more asphaltenes at higher solvent contents.

Steady State: The mass transfer was assumed to be at a steady state condition; that is, the time to establish a steady state was assumed to be negligible compared with the duration of the experiments. The time for a solvent molecule to reach the bitumen phase (*i.e.*, penetration time) was calculated using the infinite acting solution for dilute systems (see Eq. 2.21). This solution assumes a semi-infinite water layer so it is valid until the solvent reaches the bitumen. Concentration profiles of the solvent in water for the systems evaluated in this thesis are shown in Appendix E. Results of the penetration time for the minimum and maximum water layer heights and the time scale duration of the corresponding systems are shown in Table 4.7. Experimental time scales for the tests at 20 and 60°C were on average 5000 and 150 times greater than the penetration time, respectively. Therefore, the penetration time was neglected and the steady state solution was applied from the beginning of the experiment.

Table 4.7. Solvent penetration time of the solvent/water/bitumen systems evaluated in this thesis.

System	Penetration Time h	Experiment Duration h
Toluene/water/bitumen at 20°C $h_{w,\,min}$ = 0.45 cm, $h_{w,\,max}$ = 0.85 cm	0.18 – 2.2	2000 – 4000
Cyclohexane/water/bitumen at 20°C $h_{w,\,min}$ = 0.25 cm, $h_{w,\,max}$ = 0.45 cm	0.2 – 0.7	1000 – 4000
n-Pentane/water/bitumen at 20°C $h_{w,\,min}$ = 0.25 cm, $h_{w,\,max}$ = 0.45 cm	0.2 – 0.7	3000 - 4000
Toluene/water/bitumen at 60°C $h_{w,\,min}$ = 1 cm, $h_{w,\,max}$ = 2 cm	1.2 – 6	80 – 200
Cyclohexane/water/bitumen at 60°C $h_{w,\,min}$ = 1 cm, $h_{w,\,max}$ = 2 cm	1.5 – 15.8	200 – 500

n-Heptane/water/bitumen at 60°C $h_{w,\,min}$ = 0.5 cm, $h_{w,\,max}$ = 1 cm	0.4 – 1.7	1000 – 1300

The general solution of Fick's first law for steady state, non-reaction, one-dimensional isothermal diffusion was provided in Chapter 2 (Eq. 2.10) and is repeated here for convenience:

$$m_A = \frac{AtD_{AB}}{L}(c_{1A} - c_{2A}) \tag{2.10}$$

where m is the mass of component A diffused through Component B, A is the cross sectional area, t is time, D_{AB} is the diffusivity of Component A in B, L is the film thickness, and C_{1A} and C_{2A} are the concentrations of A at the boundaries. The boundary conditions for the experiments in this thesis were shown in Figure 4.16. The vertical coordinate, z, ranges from 0 at the water interface to h_w at the water/bitumen interface, where h_w is the thickness of the water layer. At the solvent/water interface (z=0), the concentration of solvent is equal to the solubility of solvent in water (a Dirichlet equilibrium boundary condition) given by:

$$c_s(z = 0, t) = C_{s,w}^{eq} \tag{4.2}$$

where $C_{s,w}^{eq}$ is the solubility of solvent in water. At the water/bitumen interface ($z=h_w$), the concentration at the water side of the water/bitumen interface is negligible compared to $C_{s,w}^{eq}$ and is approximated by:

$$c_s(z = h_w, t) = 0 \tag{4.3}$$

After applying these boundary conditions, Eq 2.10 can be written as follows:

$$m_s = AtD_{sw}\frac{C_{s,w}^{eq}}{h_w} \tag{4.4}$$

where m_s is the mass of solvent diffused to the bitumen, D_{sw} is the diffusivity coefficient of solvent in water, and A is the surface area of the bitumen. The volume of solvent diffused to the bitumen is given by:

$$V_s = \frac{AtD_{sw}C_{s,w}^{eq}}{\rho_S h_w} \tag{4.5}$$

where ρ_S is the solvent density. At steady state, the flux of solvent through the water and entering the bitumen is constant; that is, the mass and volume of the bitumen layer are expected to increase linearly over time assuming negligible excess volume of mixing. Since the solubility of the solvent in the water is very low, the water volume remains nearly constant; hence, the increase in the water+bitumen volume is expected to equal the increase in the bitumen volume.

4.3.2 Solvent/Water/Bitumen Systems at 20°C

Experiments were performed with initially pure water and water pre-saturated with solvent. The observed solvent mass transfer and water content in bitumen varied considerably for some cases from experiment to experiment and the variations did not correlate to the water saturation condition (see Appendix F). In addition, pre-saturation would only affect the initial non-steady state mass transfer which was already established to be negligible compared with the duration of the experiment. Therefore, the saturation condition is not discussed further.

4.3.2.1 Toluene/Water/WC-B-A3 Bitumen

Figure 4.17 shows photographs of typical toluene/water/bitumen diffusion experiments for the WC-B-A3 bitumen. Two distinct and seemingly random behaviors were observed: flat interfaces throughout the experiment and domed interfaces that formed gradually over time. The domed interfaces corresponded to experiments where spontaneous emulsification was observed, as shown in Figure 4.18. It is possible that the emulsified water accumulated under the water/bitumen interface, increasing the local density closer to that of water, causing a meniscus to grow. It is not known why emulsification occurred in some experiments and not others. It is possible that the content of surface active components is not consistent between the bitumen samples.

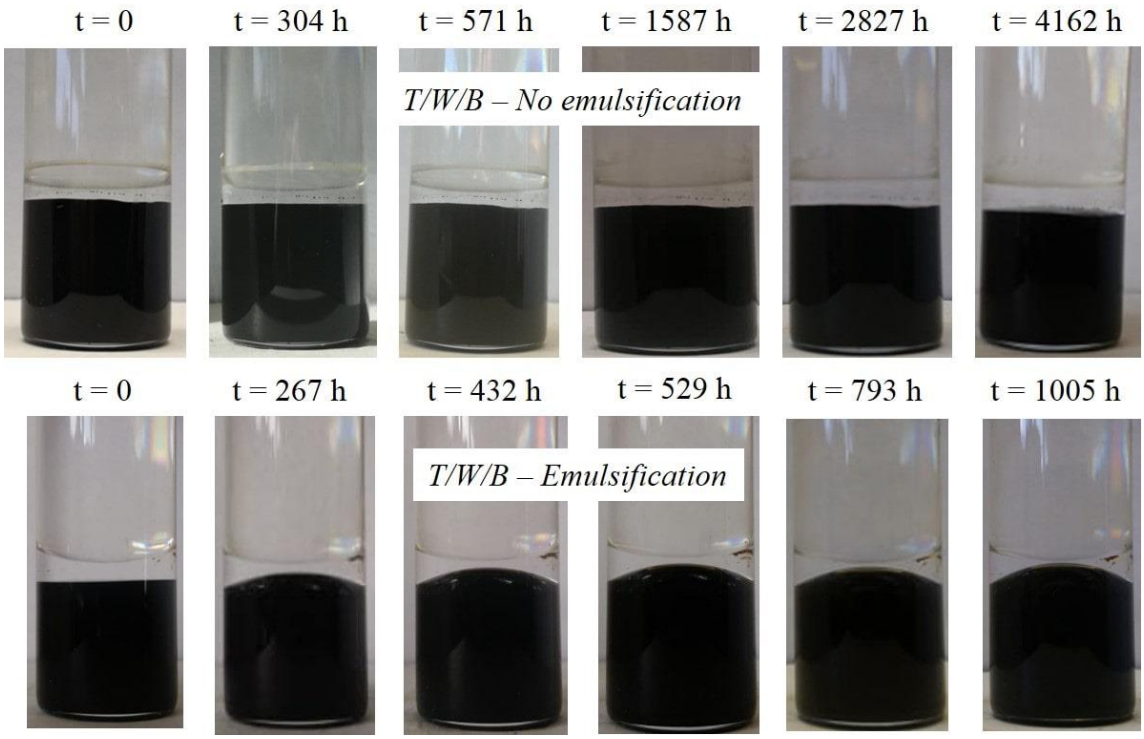

Figure 4.17. Photographs of two experiments performed with same procedure for toluene/water/WC-B-A3 bitumen with a 0.45 cm water layer at 20°C: top) no emulsion observed; bottom) spontaneous emulsification observed.

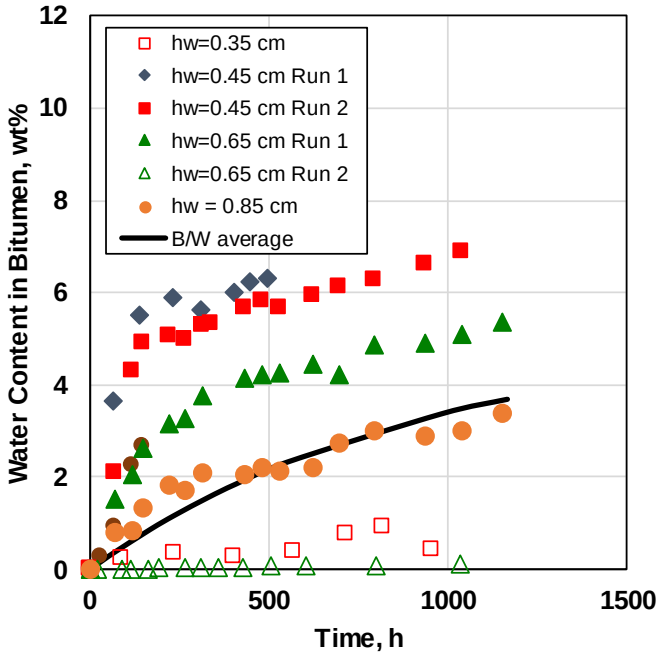

Figure 4.18. Incremental water content in bitumen layer over time for toluene/water/WC-B-A3 bitumen systems at 20°C. Solid symbols indicated a domed interface formed and open symbols indicate a flat interface persisted.

Mass Transfer without Spontaneous Emulsification

First consider the experiments where no spontaneous emulsification occurred. Figures 4.19a and 4.19b show the volume of toluene entering the bitumen over time for a toluene/water/WC-B-A3 bitumen system at 20°C with water layer thicknesses of 0.25 and 0.35 cm, respectively. After a lag time of approximately 250 hours, the toluene volume increases linearly over time as predicted by the steady state diffusion model. The predicted slope (volume transfer rate for a 0.25 cm of water layer height) of 2.8 x 10^{-4} cm^3/h was within 7.5% of the measured slope of 2.6 x 10^{-4} cm^3/h.

The reason for the lag time is unknown but it is possible that asphaltenes adsorb at the water/bitumen interface and create a barrier to mass transfer. Interfacial barriers have been proposed as a potential factor for delaying mass transfer of a solute through the interface of a binary and partially miscible liquid – liquid system, *e.g.*, alcohol/water/oil (Hutchinson, 1947; Blocker, 1957; Hennenberg *et al*., 1979). It is not clear why the barrier would disappear or be overcome after the lag time. It is possible that the solvent gradually penetrates and alters the structure of the barrier. Lag times varied considerably and will be discussed in more detail later.

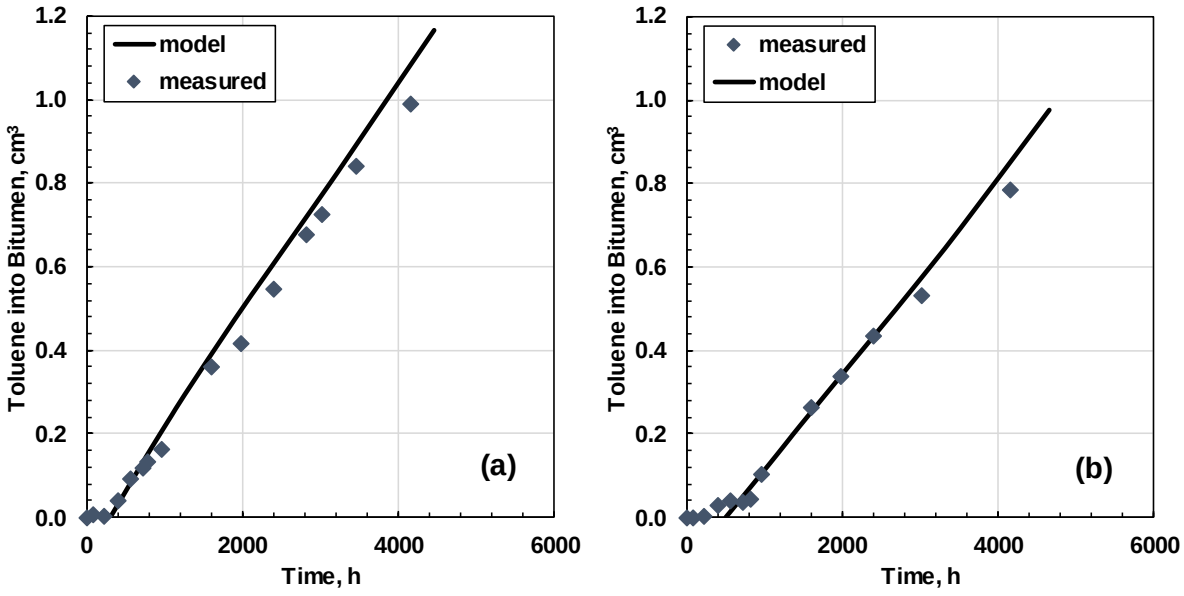

Figure 4.19. Measured and modeled volume of toluene entering bitumen layer for a toluene/water/WC-B-A3 bitumen system at 20°C for water layer heights of: a) 0.25 cm; b) 0.35 cm. Note, there was some experimental error for the 0.25 cm case and the measured height was slightly higher than 0.25 cm.

Figure 4.20a shows the volume of toluene entering the bitumen over time at three different water layer thicknesses. The data were adjusted (shifted left) to remove the lag time. Lag times ranged from 250 to 400 hours for the toluene systems with no emulsification. The volume transfer rate decreased as the layer thickness increased (giving a lower concentration gradient) as predicted by the steady state mass transfer model. Hence, in the absence of spontaneous emulsification, steady state, one-dimensional mass transfer of solvent through the water layer was established after a lag time.

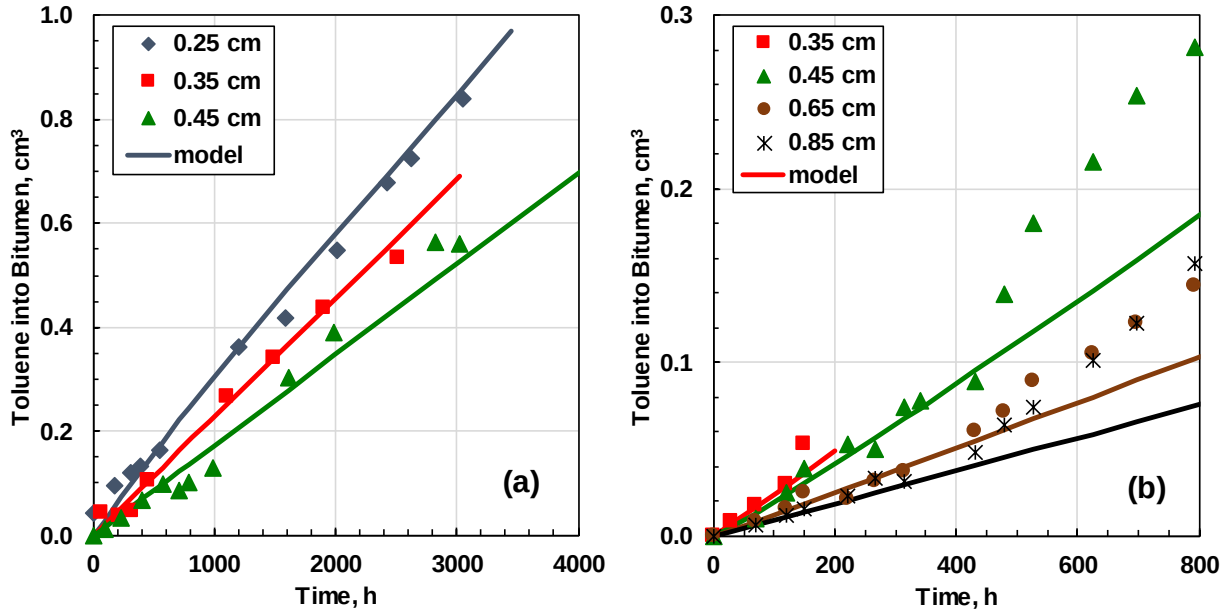

Figure 4.20. Effect of water layer thickness on volume of toluene entering bitumen layer over time for a toluene/water/WC-B-A3 bitumen system at 20°C: a) no spontaneous emulsification and lag time removed; b) with spontaneous emulsification and no lag time adjustment.

Mass Transfer with Spontaneous Emulsification

Figures 4.21a and 4.21b show the volume of toluene entering the bitumen over time and the change in water content in the bitumen layer over time, respectively, for three runs with a water layer height of 0.45 cm. Run 1 did not exhibit any emulsification and the toluene volume transfer rate was as predicted. Runs 2 and 3 exhibited high emulsification rates and reached a water content in bitumen between 6 and 7 wt%. There was no lag in the commencement of mass transfer when spontaneous emulsification occurred suggesting that either the emulsification process prevented the formation of a mass transfer barrier or the mass transfer barrier prevented emulsification.

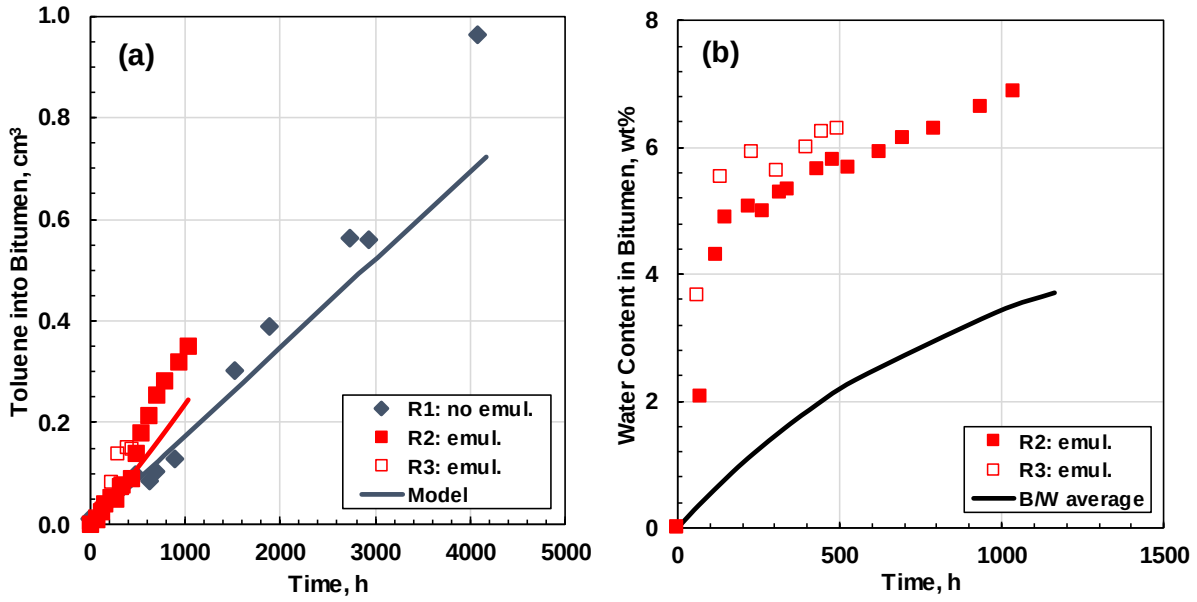

Figure 4.21. Comparison of three toluene/water/WC-B-A3 bitumen runs at 20°C with a water layer height of 0.45 cm: a) toluene volume entering bitumen layer; b) and incremental water content in the bitumen layer. The times for Run 1 (R1) were adjusted to remove the lag time.

Figure 4.21a shows that the toluene volume transfer rate was higher than predicted for the runs with spontaneous emulsification for a 0.45 cm water layer thickness. Figure 4.20b shows the same effect at other water layer thicknesses. The reason for the enhanced mass transfer rate is not known. One hypothesis is that the dome shaped interface that occurs when emulsion form accelerates mass transfer. A dome shaped interface gives shorter distances for mass transfer distance and creates two-dimensional diffusion pathways. Both factors would increase the mass transfer rate. The problem with this hypothesis is that the dome effect is localized to the region near the dome and, therefore, should be more significant for thinner water layers. In fact, the dome effect is independent of the water layer thickness. An alternative hypothesis is that some of the light oil components diffuse into water layer and form an O/W emulsion. Perhaps water emulsification creates a disturbance at the interface that promotes light component diffusion. The emulsified oil droplets could create gravity convection and enhance mass transfer. A problem with this hypothesis is that no evidence of oil emulsification was observed for the WC-B-A3 bitumen and the toluene volume transfer rate was lower for the WC-B-B5 bitumen which formed both a W/O and an O/W emulsion at 60°C (discussed later). Note that in all cases only some of the water and

bitumen emulsified and the three phases (bitumen, water, solvent) persisted throughout the experients unless gravity instability occurred.

Figure 4.21b shows that the extent of spontaneous emulsification was greater than observed in the water/bitumen systems at 20°C. It is possible that the presence of solvent reduced the interfacial viscosity allowing for more rapid emulsification. Another possibility is that the enhanced solvent mass transfer rate reduced the bitumen viscosity faster than mass transfer that follows a steady state model, allowing the natural surfactants in the bitumen to migrate to the water/bitumen interface more rapidly.

4.3.2.2 Cyclohexane/Water/WC-B-A3 Bitumen

Figure 4.22 shows that, as with toluene, in some experiments no emulsification occurred and the interface remained flat while in other experiments, spontaneous emulsification occurred and a domed interface formed gradually over time. Similarly, lag times were observed when there was no emulsification but did not occur when there was emulsification. The reason for these differences is not known but it is possible that different bitumen samples contained different amounts of surface active components leading to the differences in emulsification.

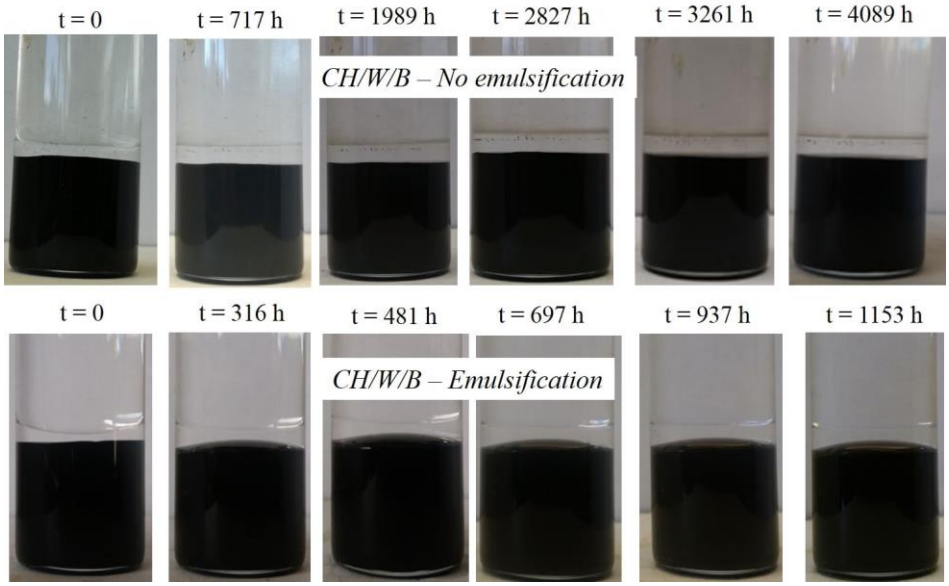

Figure 4.22. Photographs of two experiments performed with same procedure for cyclohexane/water/WC-B-A3 bitumen with a 0.35 cm water layer at 20°C: top) no emulsion observed; bottom) spontaneous emulsification observed.

Mass Transfer Without Spontaneous Emulsification

Figure 4.23a shows the volume of cyclohexane transferred to the bitumen over time in a cyclohexane/water/WC-B-A3 bitumen system at 20°C for different water layer heights. Figure 4.23b shows the same data adjusted to remove the lag time. The measured volume transfer rates after the lag time range from 2.1 x 10^{-5} to 4.0 x 10^{-5} cm³/h depending on the water layer thickness. The predicted volume transfer rates are within 28% of the measured rates. The volume transfer rate is much lower in cyclohexane than in toluene (3.5 x 10^{-5} cm³/h cyclohexane versus 2.6 x 10^{-4} cm³/h toluene for a 0.25 cm water layer thickness) because the solubility of cyclohexane in water is lower.

The lag times ranged from 1000 to 2000 hours, considerably greater than the 250 hours for toluene/water/bitumen. The longer lag times can be attributed to the slower mass transfer rate such that more time is needed to accumulate enough solvent to penetrate and disrupt the interfacial barrier and begin solvent mass transfer to the bitumen.

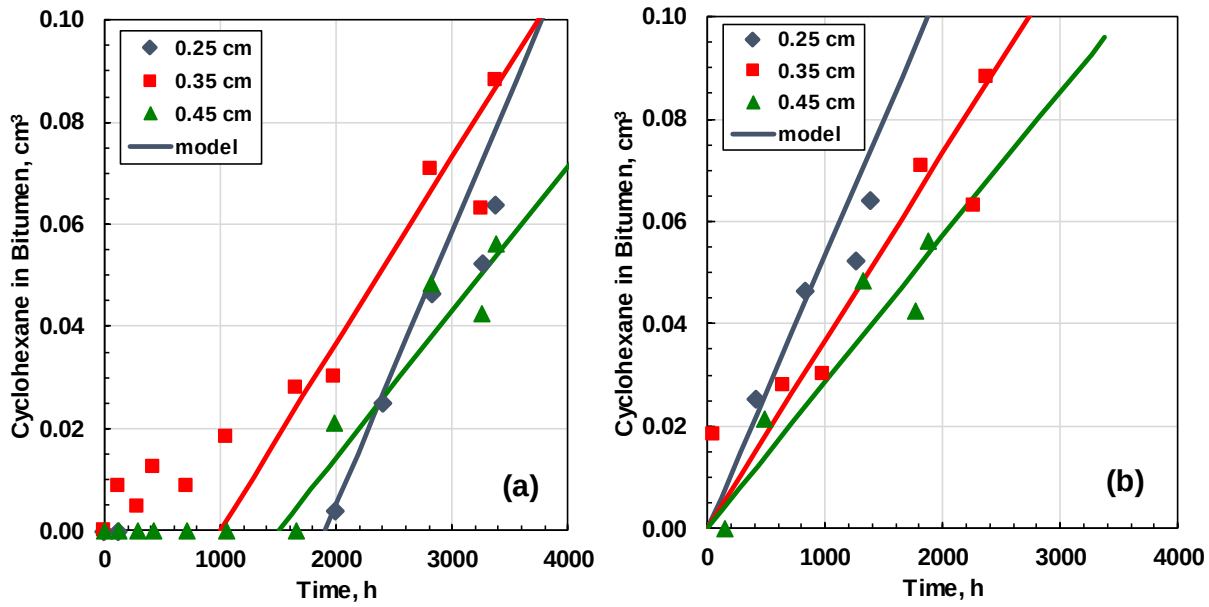

Figure 4.23. Volume of cyclohexane entering bitumen layer over time for a cyclohexane/water/WC-B-A3 bitumen systems at 20°C with no spontaneous emulsification: a) as measured; b) data shifted to remove lag time.

Mass Transfer With Spontaneous Emulsification

Figures 4.24a and 4.24b show the volume of cyclohexane entering the bitumen layer and the change in water content in the bitumen layer over time, respectively, for cyclohexane/water/WC-B-A3 bitumen systems. The maximum amount of emulsified water is approximately 2.5 wt%, less than the maximum of approximately 6 wt% observed in toluene. It is not clear why the maximum values differ. Similar to the toluene systems, the lag time was negligible in the cyclohexane systems when spontaneous emulsification occurred and the emulsification correlated to an enhanced cyclohexane mass transfer rate.

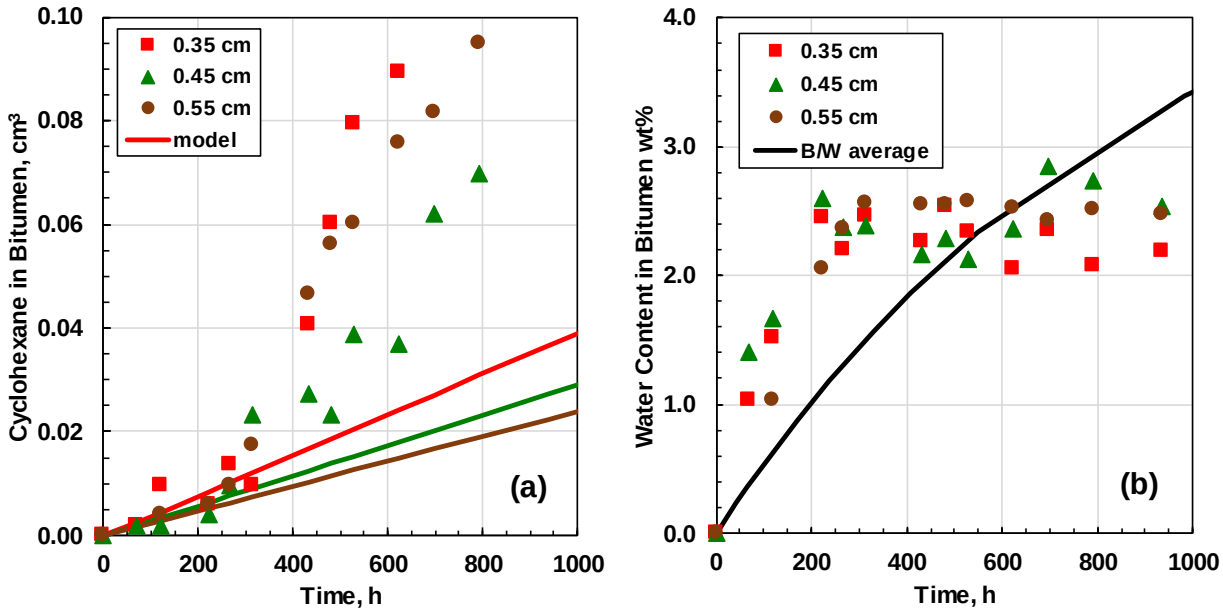

Figure 4.24. Effect of water layer thickness for a cyclohexane/water/WC-B-A3 bitumen system at 20°C with spontaneous emulsification: a) volume of cyclohexane entering bitumen layer; b) incremental water content of bitumen layer.

4.3.2.3 *n*-Pentane/Water/Bitumen

A small number of mass transfer experiments were performed with *n*-pentane sufficient to compare with the other solvents. Photographs of the *n*-pentane/water/bitumen experiments were similar to the cyclohexane/water/bitumen photographs and are provided in Appendix B. Figures 4.25a and 4.25b show the volume of *n*-pentane entering bitumen layer and the change in water content over time for two *n*-pentane/water/WC-B-A3 bitumen systems. The first system was with a 0.25 cm layer, the interface remained flat, and there was a no spontaneous emulsification. The lag time was

negligible; the only experiment with no emulsification where this was the case. The reason for this discrepancy is unknown. The predicted volume transfer rate was within 15% of the measured rate of 2.6 x 10^{-5} cm³/h. The volume transfer rate is lower in *n*-pentane than in cyclohexane (2.6 x 10^{-5} cm³/h *n*-pentane versus 3.5 x 10^{-5} cm³/h cm³/h cyclohexane for a 0.25 cm water layer thickness) because the solubility of *n*-pentane in water is lower. The second system was with a 0.30 cm layer and spontaneous emulsification did occur. Again, there was a correlation between enhanced solvent mass transfer and the emulsification of water into the bitumen.

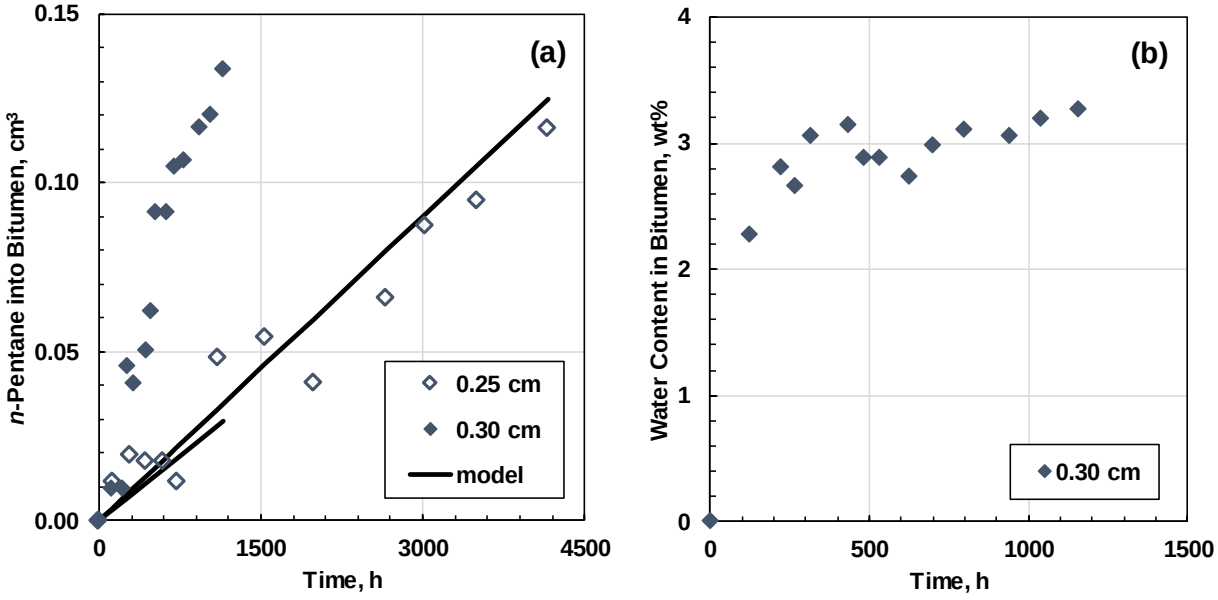

Figure 4.25. Comparison of two mass transfer experiments (0.25 cm and 0.30 cm water layer thickness) with *n*-pentane/water/WC-B-A3 bitumen at 20°C: a) volume of *n*-pentane entering the bitumen layer; b) incremental water content in the bitumen layer. Spontaneous emulsification occurred in the 0.30 cm experiment but not in the 0.25 cm experiment. There was negligible lag time in both cases.

4.3.2.4 Toluene/Water/WC-B-B5 Bitumen

Figures 4.26a and 4.26b compare the volume of toluene entering the bitumen layer and the change in water content in the bitumen layer over time, respectively, for toluene/water/WC-B-A3 bitumen and toluene/water/WC-B-B5 bitumen, both at 20°C with a water layer height of 0.65 cm. In both cases, a domed interface was formed and spontaneous emulsification of water into the bitumen occurred. There was no O/W emulsification at 20°C.

The emulsification rate was significantly lower for the WC-B-B5 bitumen than the WC-B-A3 bitumen suggesting that the WC-B-B5 bitumen contains less surface active components capable of stabilizing emulsions. Unlike the WC-B-A3 bitumen, spontaneous emulsification in the WC-B-B5 bitumen had little impact on the toluene mass transfer rate likely because the emulsification rate was low. The WC-B-A3 tests with low emulsification rates also had little enhancement of the mass transfer rate.

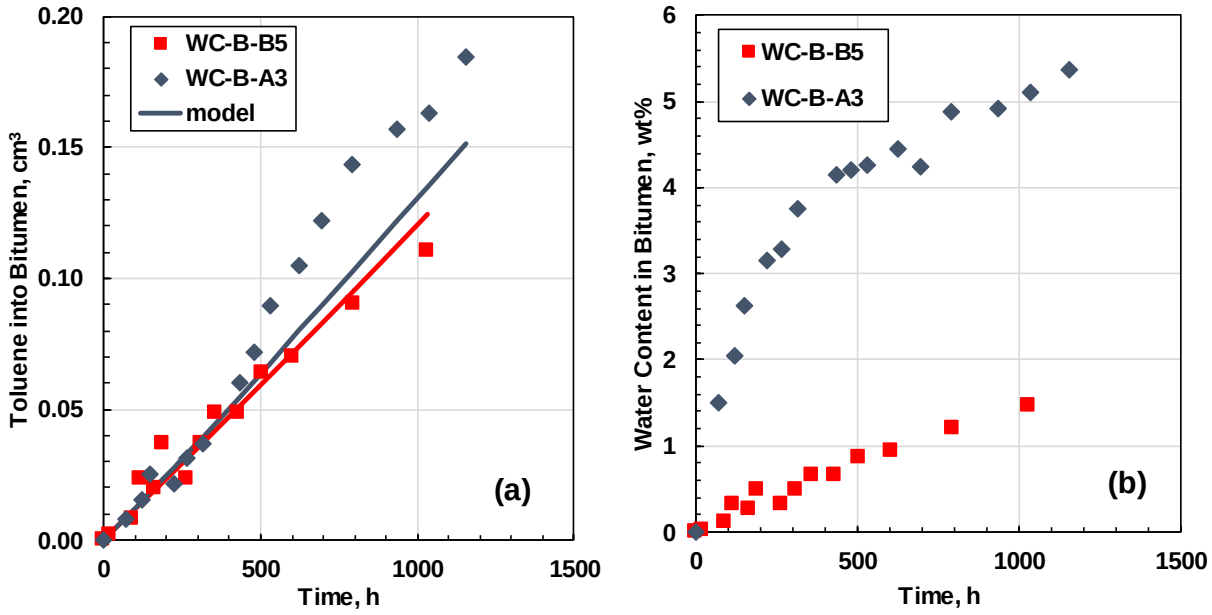

Figure 4.26. Comparison of mass transfer experiment with WC-B-B5 and WC-B-A3 bitumen for toluene/water/bitumen system at 20°C with a 0.65 cm water layer: a) volume of toluene entering bitumen layer; b) incremental water content in bitumen layer.

4.3.2.5 Summary for Solvent/Water/Bitumen Systems at 20°C

The following observations were made for the solvent/water/bitumen systems at 20°C:

- Spontaneous emulsification occurred in some runs and not in others; the occurrence of emulsification appeared random and may indicate that the natural surfactants in the bitumen varied from sample to sample
- When no spontaneous emulsification occurred, there was a lag of hundreds to thousands of hours, depending on the solvent, before steady state mass transfer was established; the lag suggests that a barrier to mass transfer was established at the water/bitumen interface that

was penetrated/disrupted over time. Lag time appears to be inversely proportional to the solvent volume transfer rate but there is considerable scatter, as shown in Figure 4.27.

- A steady state mass transfer model predicted the mass transfer data after the lag time
- The mass transfer rate was proportion to the solubility of the solvent in water and therefore was fastest in toluene and lowest in *n*-pentane as shown in Figure 4.28.
- When spontaneous emulsification occurred, the water/bitumen interfaces became dome shaped, there was no lag time, and the mass transfer rate was enhanced; the enhanced mass transfer may arise because the dome shaped interface reduces the distance for mass transfer and allows for two-dimensional mass transfer.
- The solvent volume transfer rate and the emulsification rate may be correlated, as shown in Figure 4.29. The correlation is not clear at the low mass transfer rates where the scatter in the measured mass transfer rate is relatively high.

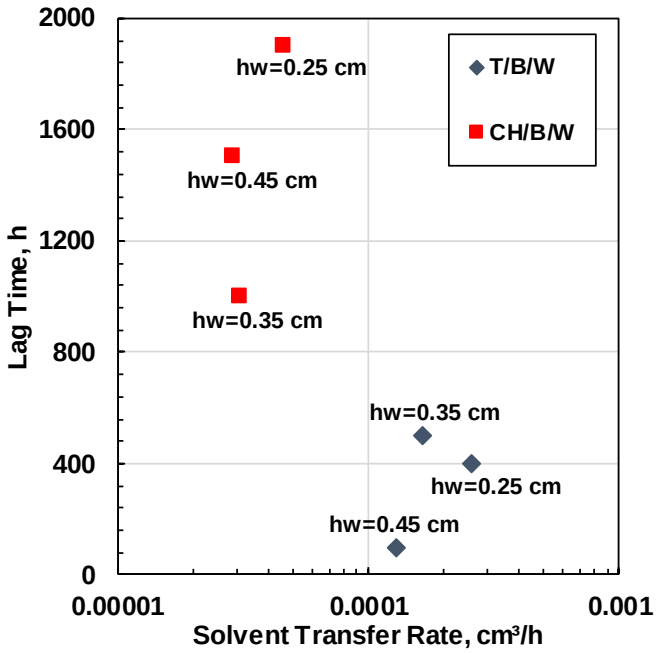

Figure 4.27. Cross plot of lag time versus solvent volume transfer rate for the solvent/water/WC-B-A3 bitumen systems at 20°C with different water layer thicknesses. T=toluene, CH=cyclohexane, B=bitumen, and W=water.

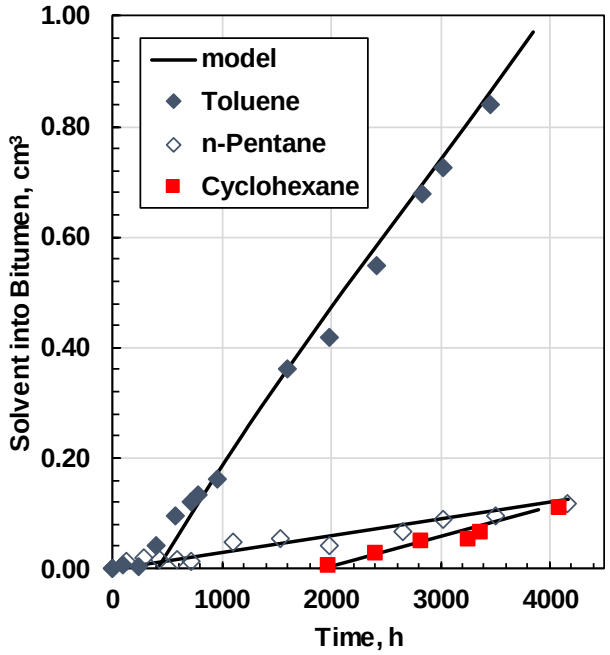

Figure 4.28. Comparison of mass transfer experiments with toluene, cyclohexane, and n-pentane for solvent/water/WC-B-A3 bitumen systems at 20°C with 0.25 cm water layer and no W/O emulsification.

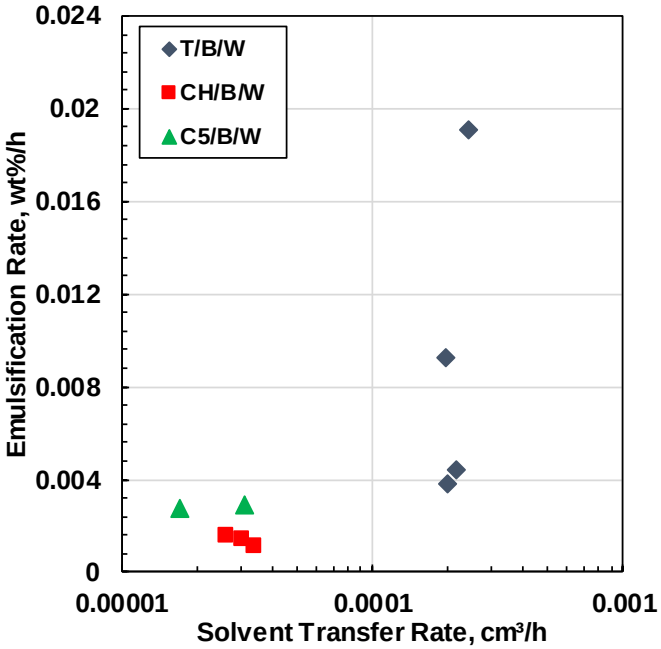

Figure 4.29. Correlation of emulsification rate to solvent volume transfer rate for the solvent/water/WC-B-A3 bitumen systems at 20°C with water layer heights of 0.35 cm. T=toluene, CH=cyclohexane, C5=n-pentane, B=bitumen, and W=water.

The mass transfer rate for each solvent was modeled for each layer thickness and the results are compared with the measured rates in Table 4.8. The experimental error for the measured rates was 12% based on three repetitions. For toluene and cyclohexane, the ARD ranges from 1 to 16% and *n*-pentane ARD goes up to 45%. This high deviation for the *n*-pentane results is attributed to a higher uncertainty in the measurements because the mass transfer rate was very low.

Table 4.8. Average relative deviations (ARD) for the measured and predicted solvent mass transfer rates at 20°C. Only data unaffected by spontaneous emulsification included.

System	Water Layer cm	Measured g/h	Predicted g/h	ARD %
T/W/B	0.25	0.00026	0.00028	8
	0.35	0.00021	0.00023	12
	0.45	0.00018	0.00021	15
	0.65	0.00013	0.00013	1
	0.85	0.00011	0.00009	16
CH/W/B	0.25	0.000046	0.000053	16
	0.35	0.000032	0.000037	15
	0.45	0.000030	0.000029	4
	0.55	0.000026	0.000023	12
C5/W/B	0.25	0.000021	0.000029	37
	0.30	0.000031	0.000029	6
	0.35	0.000045	0.000025	45

4.3.3 Solvent/Water/Bitumen Systems at 60°C

4.3.3.1 Toluene/Water/WC-B-A3 Bitumen

Figure 4.30 shows photographs of typical toluene/water/bitumen diffusion experiments for the WC-B-A3 bitumen at 60°C. Figures 4.31a and 4.31b show the volume of toluene entering the bitumen layer and the change in water content of the bitumen layer over time, respectively for three runs for toluene/water/WC-B-A3 bitumen systems at 60°C with a water layer thickness of 1.5 cm. The results for the other water layer thicknesses were similar (see Appendix B).

There were significant differences from the tests performed at 20°C. Dome shaped interfaces, spontaneous emulsification, and negligible lag times were observed in all cases. Gravity instability (pronounced elongation of water/bitumen interface and eventual contact with the solvent layer) occurred after 50 to 150 hours (see Figure 4.30). Once the bitumen bypassed the water and touched the solvent, some of the bitumen mixed with the solvent and then the water/bitumen interface returned approximately to its initial condition. The whole process repeated until all of the bitumen had mixed with the solvent.

The initial emulsification rate was initially similar to the water/bitumen average but increased as the system became gravity unstable. The volume of toluene in bitumen needed to decrease the density of the oil layer below the density of water is 0.05 cm^3. This toluene volume in bitumen was achieved at the time that coincided with the rapid increase in the water content in bitumen. The rapid increase may be related to increase in the interfacial area when the dome becomes unstable.

The W/O emulsification rate varied considerably from test to test. As discussed in Chapter 3, small differences in the wettability of the vials may cause local variations in the water/glass/bitumen contact angle. These variations may affect the growth rate and shape of the bitumen dome. These effects would be more noticeable for more rapidly growing domes; *i.e.*, at higher temperature. Gravity instability is closely related to the shape of the dome and the time to instability similarly varied considerably from test to test. The solvent mass transfer rate also varied considerably but in general was significantly enhanced, up to 10 times faster than predicted by the steady state model. This enhancement may be partly caused by the more prominent bitumen dome giving a greater surface area and shorter distance for mass transfer, and more potential for two-dimensional diffusion. However, the enhanced mass transfer rate did not correlated to the water layer thickness and the mass transfer rates tended to be high well before the dome became prominent, both suggesting that another mechanism is at play. It is possible that small temperature gradients within the temperature bath caused convection and accelerated the mass transfer. Since the rates were enhanced and varied considerably, the steady state model under-predicted the mass transfer as shown in Figure 4.32.

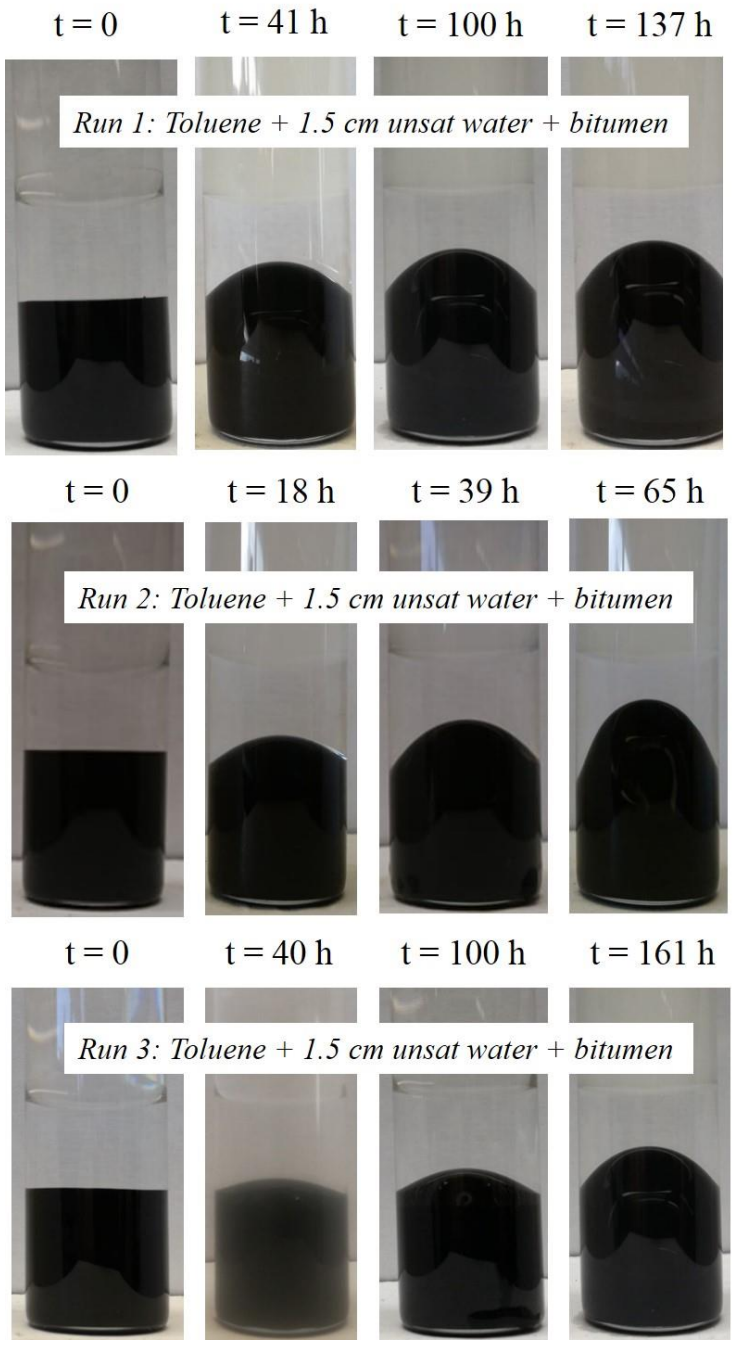

Figure 4.30. Photographs of three experiments performed with same procedure for toluene/water/WC-B-A3 bitumen with a 1.5 cm water layer at 60°C.

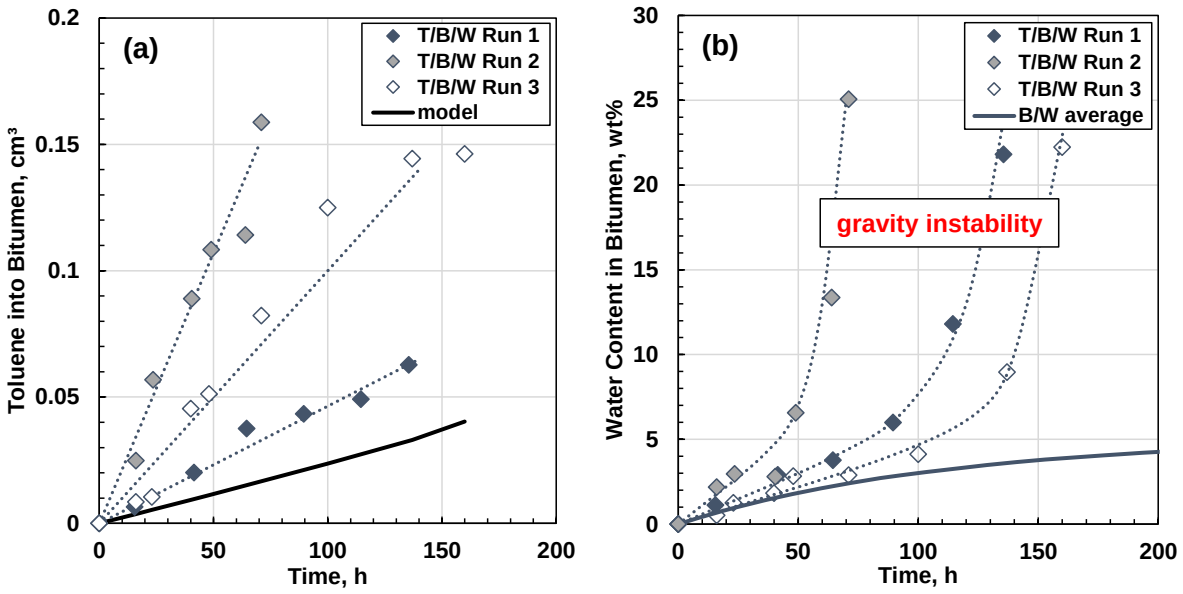

Figure 4.31. Comparison of three toluene/water/WC-B-A3 bitumen runs at 60°C with a water layer height of 1.5 cm: a) toluene volume entering bitumen layer; b) and incremental water content in the bitumen layer.

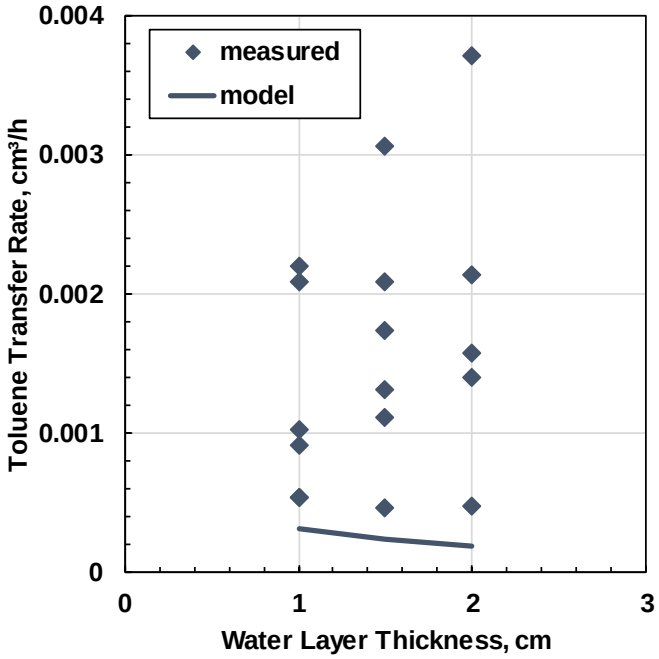

Figure 4.32. Toluene volume transfer rate versus water layer thickness for all of the experiments performed on toluene/water/WC-B-A3 bitumen systems at 60°C.

4.3.3.2 Cyclohexane/Water/Bitumen

Photographs of the cyclohexane/water/bitumen experiments were similar to the toluene/water/bitumen photographs and are provided in Appendix B. Figures 4.33a and 4.33b show the volume of cyclohexane entering the bitumen layer and the change in water content of the bitumen layer over time, respectively, for cyclohexane/water/WC-B-A3 bitumen systems at 60°C with a water layer height of 1.0 cm. The results for these tests are similar to the results for the toluene/water/bitumen systems.

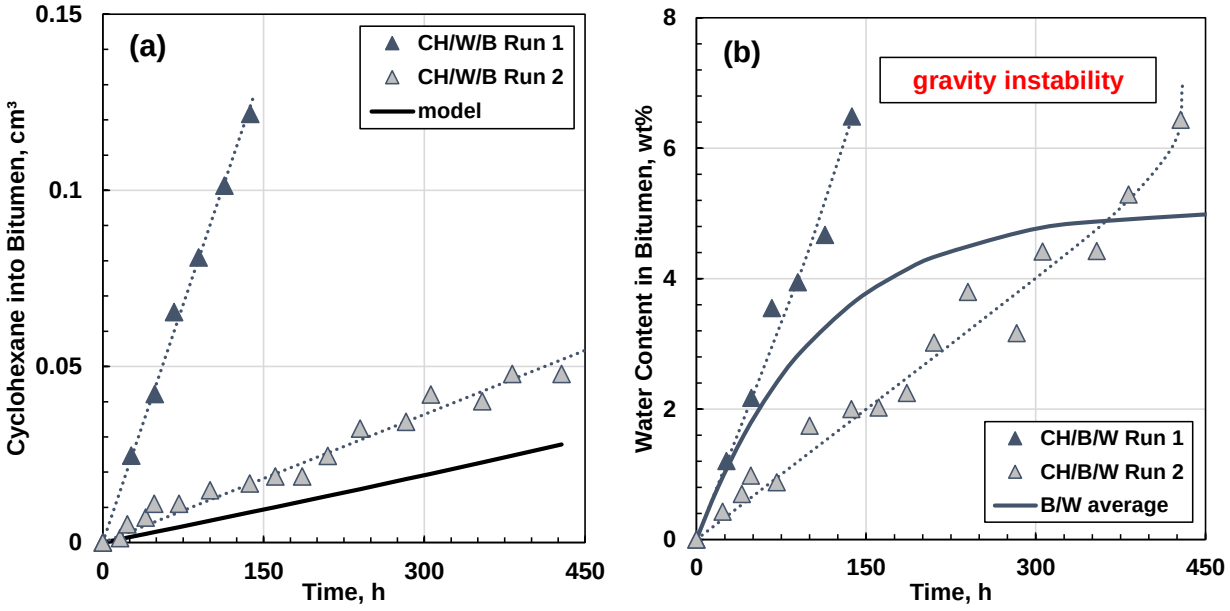

Figure 4.33. Comparison of two cyclohexane/water/WC-B-A3 bitumen runs at 60°C with a water layer height of 1.0 cm: a) cyclohexane volume entering bitumen layer; b) and incremental water content in the bitumen layer.

Some of the tests with cyclohexane exhibited a different behavior. For example, Figures 4.34a and 4.34b show the volume of cyclohexane entering the bitumen layer and the change in water content of the bitumen layer over time, respectively, for cyclohexane/water/WC-B-A3 bitumen systems at 60°C with a water layer height of 1.5 cm. In this case, the cyclohexane mass transfer rate is initially near the steady state model prediction but transitions to high mass transfer rates happened at approximately 200 hours. Similar results were observed for a layer thickness of 2.0 cm. The reason for the transition is unknown but it is possible that the temperature gradients in the bath changed due to unknown factors (i.e. change in room conditions) or that the location of the vial in the

temperature bath (and therefore the local temperature gradients) shifted after the layer heights were measured. A change in the temperature gradients could trigger convection.

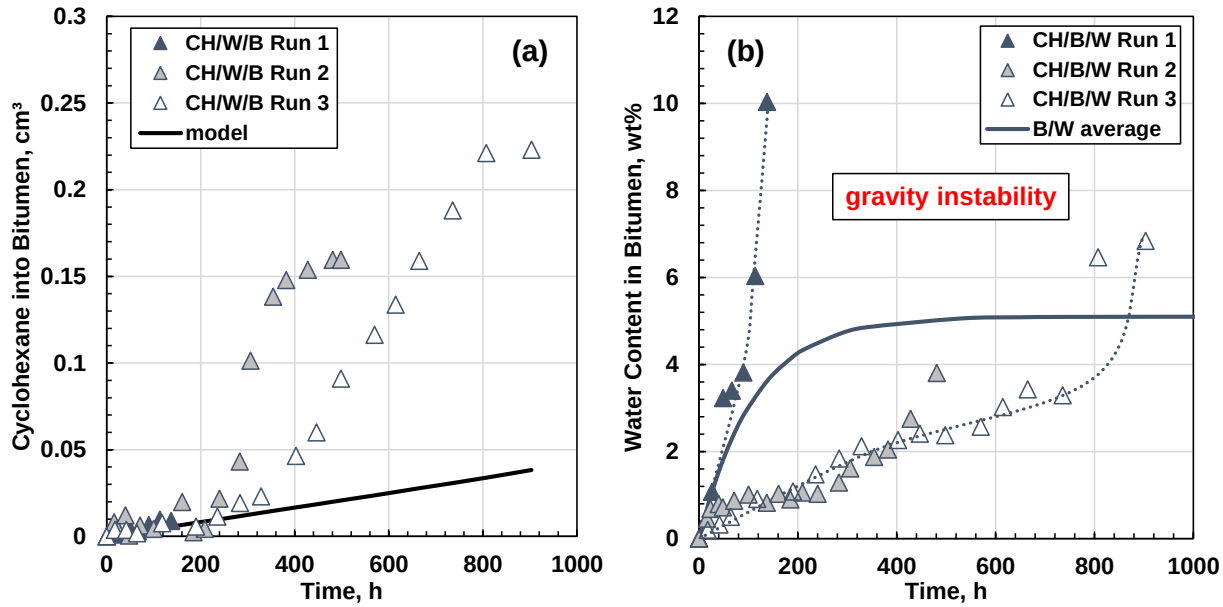

Figure 4.34. Comparison of two cyclohexane/water/WC-B-A3 bitumen runs at 60°C with a water layer height of 1.5 cm: a) cyclohexane volume entering bitumen layer; b) and incremental water content in the bitumen layer.

4.3.3.3 *n*-Heptane/Water/Bitumen

Photographs of the *n*-heptane/water/bitumen experiments were similar to the cyclohexane/water/bitumen photographs and are provided in Appendix B. Figures 4.35a and 4.35b show the volume of *n*-heptane entering the bitumen layer and the change in water content of the bitumen layer over time, respectively, for *n*-heptane/water/WC-B-A3 bitumen systems at 60°C with a water layer height of 0.5 cm. The results are qualitatively similar to the cyclohexane systems with the transition to higher mass transfer rates.

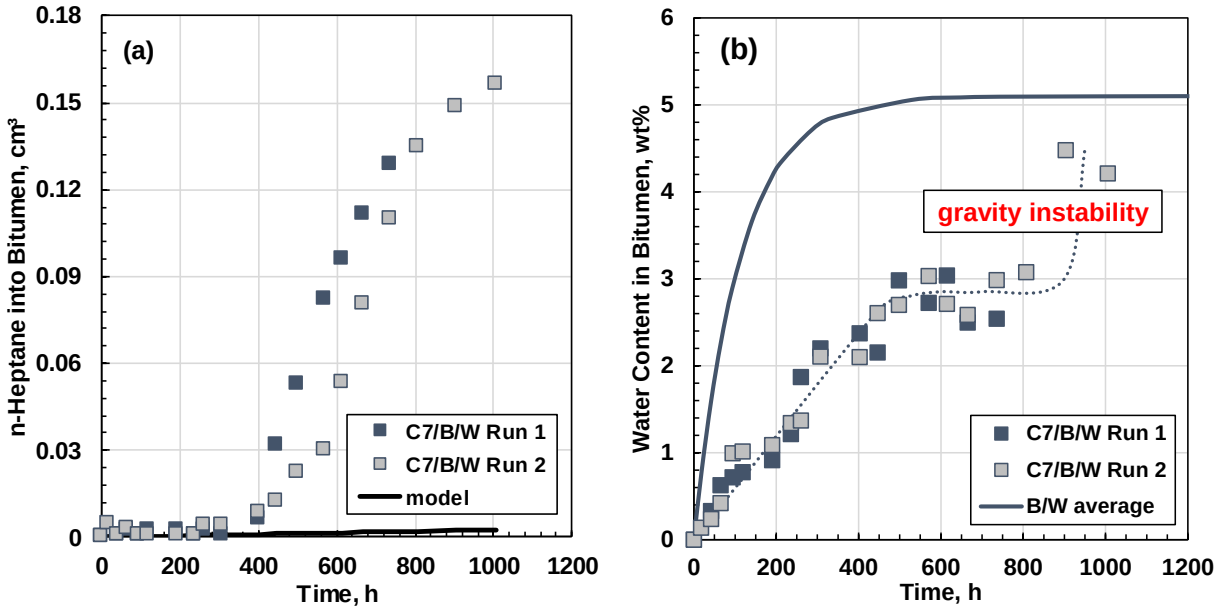

Figure 4.35. Comparison of two *n*-heptane/water/WC-B-A3 bitumen runs at 60°C with a water layer height of 0.5 cm: a) *n*-heptane volume entering bitumen layer; b) and incremental water content in the bitumen layer.

4.3.3.4 Toluene/Water/WC-B-B5 Bitumen

Figures 4.36a and 4.36b compare the volume of toluene entering the bitumen layer and the change in water content in the bitumen layer over time, respectively, for toluene/water/WC-B-A3 bitumen and toluene/water/WC-B-B5 bitumen, both at 60°C with a water layer height of 1.0 cm. In all cases, there was spontaneous W/O emulsification and enhancement mass transfer. There was no significant difference between the WC-B-A3 and WC-B-B5 bitumen results.

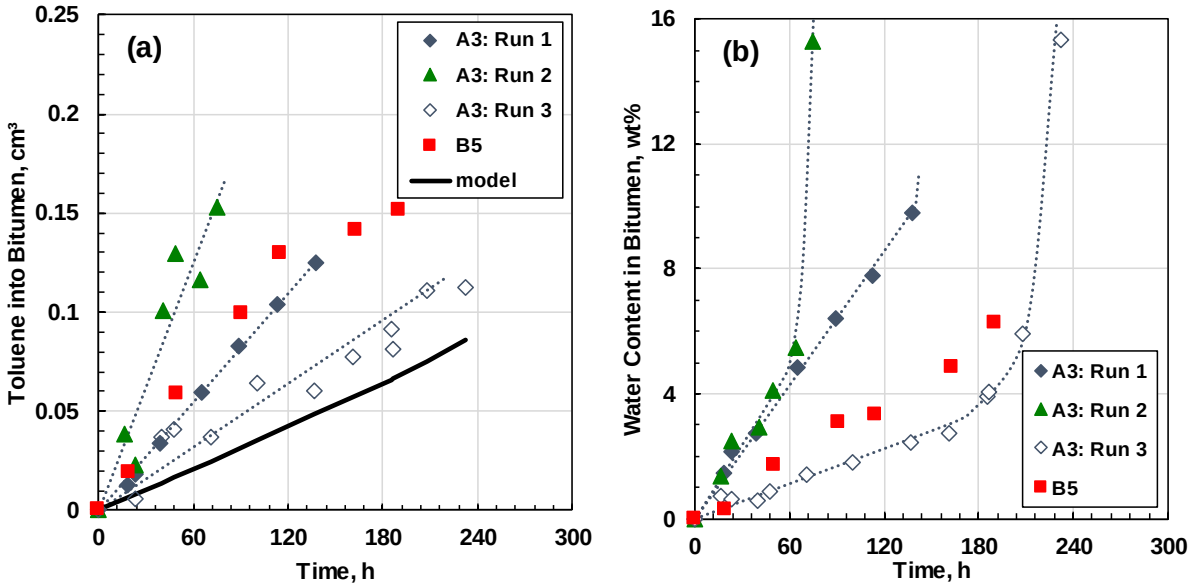

Figure 4.36. Comparison of mass transfer experiment with WC-B-B5 and WC-B-A3 bitumen for toluene/water/bitumen system at 60°C with a 1.0 cm water layer: a) volume of toluene entering bitumen layer; b) incremental water content in bitumen layer.

4.3.3.5 Effect of Removing Natural Surfactants

Figures 4.37a and 4.37b compare the volume of toluene entering the bitumen layer and the incremental water content of the bitumen layer, respectively, for toluene/water/bitumen systems (at 60°C with a water layer height of 1.5 cm) prepared with the original unmodified WC-B-A3 bitumen and the WC-B-A3 bitumen partially stripped of natural surfactants. Photographs of the experiments are provided in Appendix D. The stripped bitumen did not form a spontaneous emulsion (water content did not change) and the time to gravity instability increased substantially (500 hours compared with 75 to 150 hours for the original bitumen). The longer time to instability could reflect a change in interfacial tension after removing surface active material. Higher interfacial tension would provide more resistance to the gravity forces. Finally, the mass transfer rate is similar to that of the original bitumen. This similarity indicates that the emulsion does not enhance mass transfer. The most likely explanation for the enhanced mass transfer is convection from temperature gradients in the water bath.

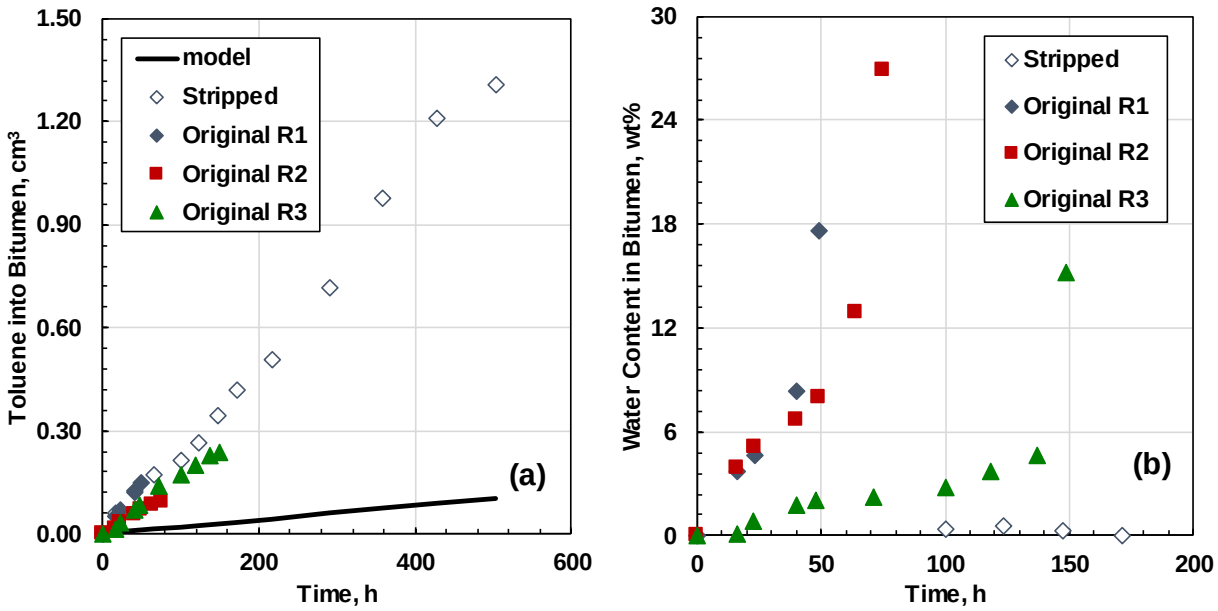

Figure 4.37. Comparison of mass transfer experiments with original and stripped WC-B-A3 bitumen for toluene/water/bitumen systems at 60°C with 1.5 cm water layer: a) volume of toluene entering bitumen layer; b) incremental water content of bitumen layer.

Figures 4.38 shows the same kind of data for toluene/water/bitumen systems (at 60°C with a water layer height of 1.5 cm) prepared with the original and stripped WC-B-B5 bitumen. In this case, the spontaneous emulsion still occurred albeit at a lower rate, indicating that not all of the natural surfactants had been removed. The water layer remained colorless (see Appendix D) suggesting that little or no O/W emulsion formed. As observed with the WC-B-A3 bitumen, the time to instability was relatively high (900 hours) and the mass transfer rate was significantly greater than the steady state prediction. Note that the experiment for the original bitumen stopped at 150 hours because the O/W made it impossible to take measurements. It is concluded that natural surfactants are responsible for spontaneous emulsification but neither they nor emulsion formation are responsible for enhanced mass transfer.

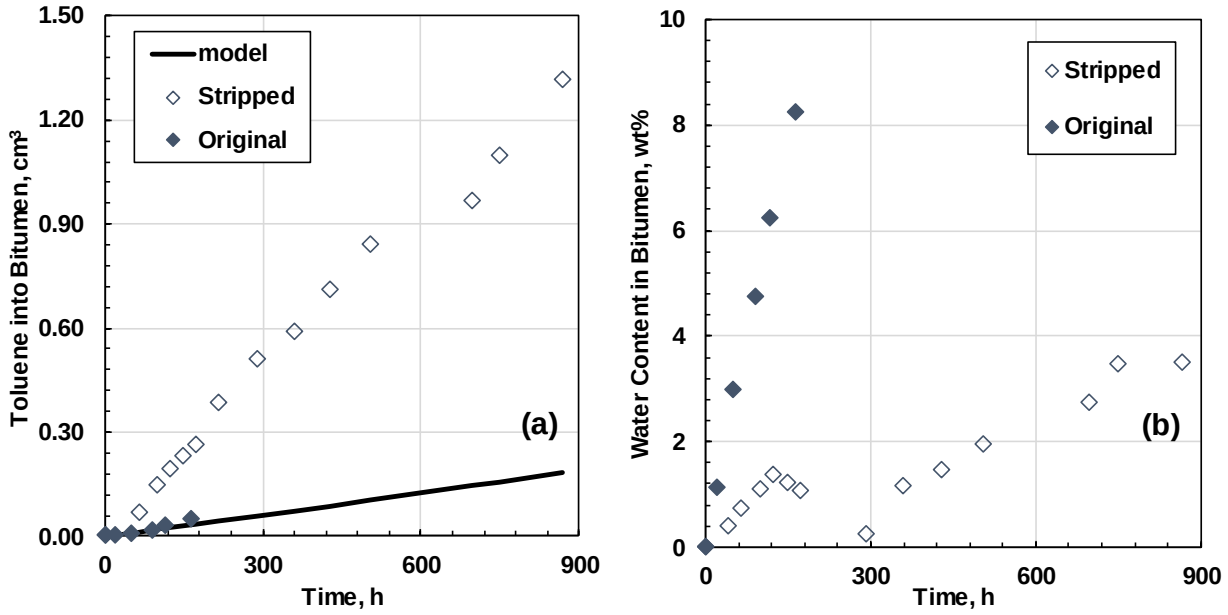

Figure 4.38. Comparison of mass transfer experiments with original and stripped WC-B-B5 bitumen for toluene/water/bitumen systems at 60°C with 1.5 cm water layer: a) volume of toluene entering bitumen layer; b) incremental water content of bitumen layer.

4.3.3.6 Summary for Solvent/Water/Bitumen Systems at 60°C

The following observations were made for the solvent/water/bitumen systems at 60°C:

- Spontaneous emulsification occurred in all runs with unmodified bitumen; stripping out natural surfactants eliminated the spontaneous emulsification
- There was no lag before mass transfer started.
- The interface was dome shaped and became gravity unstable over time in all cases.
- The mass transfer rates were higher than predicted from the steady state mass transfer model; it is hypothesized that the enhanced mass transfer is caused by convection induced by small temperature gradients in the water bath.
- The mass transfer rate was still approximately proportion to the solubility of the solvent in water and therefore was fastest in toluene and lowest in *n*-heptane as shown in Figure 4.39a.
- The emulsification rate was highest in the toluene systems (highest mass transfer rate) and lowest in the *n*-heptane systems as shown in Figure 4.39b; it appears that the emulsification rate correlates to the mass transfer rate as shown in Figure 4.40.

- The time to gravity instability also correlated to the mass transfer rate as shown in Figure 4.41; this correlation is expected because the instability depends on the density difference between the bitumen dome and water and the decrease in the density of the bitumen dome depends on the mass transfer rate.

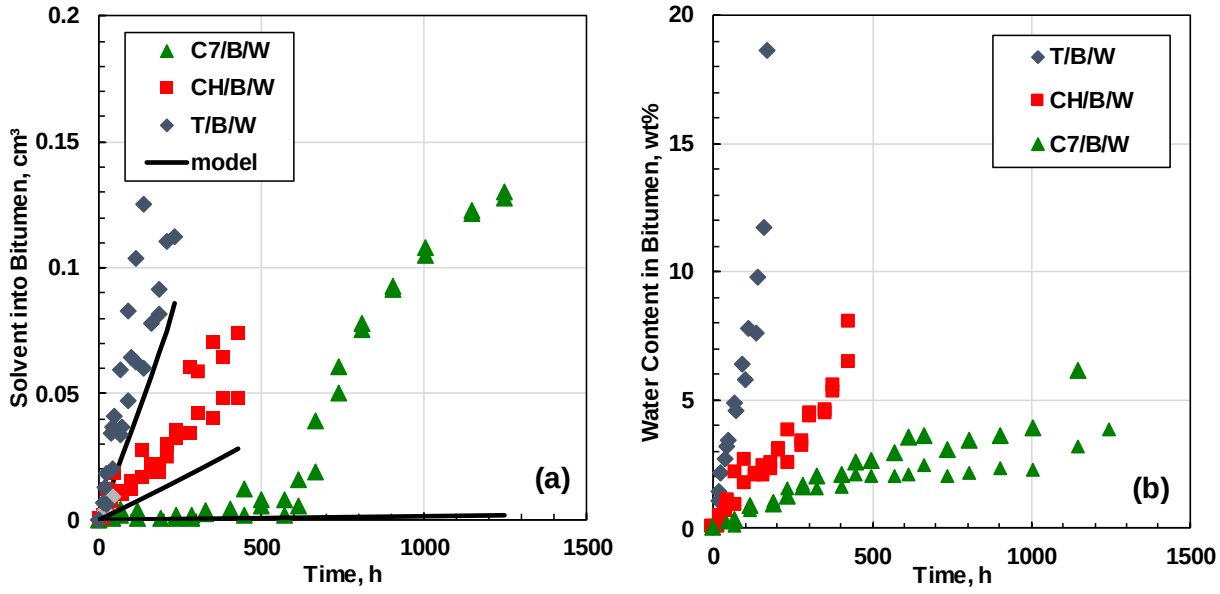

Figure 4.39. Comparison of mass transfer experiments with toluene, cyclohexane, and n-heptane for solvent/water/bitumen systems at 60°C with 1.0 cm water layer: a) volume of toluene entering bitumen layer; b) incremental water content of bitumen layer.T=toluene, CH=cyclohexane, C7=*n*-heptane, B=bitumen, and W=water.

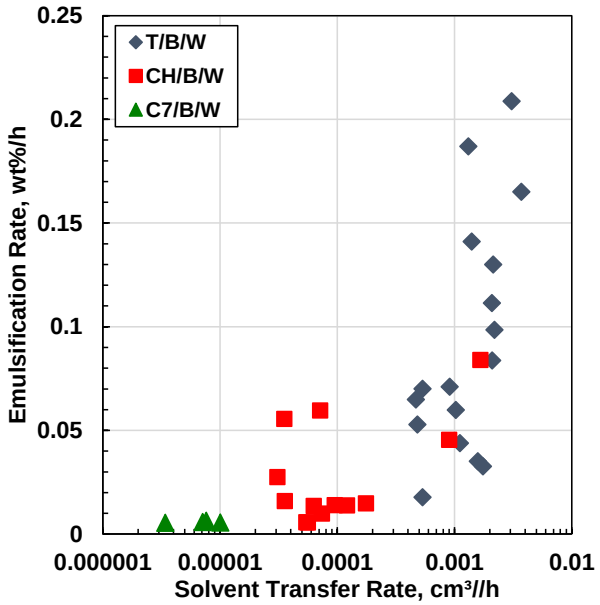

Figure 4.40. Correlation of emulsification rate to solvent volume transfer rate for the solvent/water/WC-B-A3 bitumen systems at 60°C with water layer heights of 1.0 cm. T=toluene, CH=cyclohexane, C7=*n*-heptane, B=bitumen, and W=water.

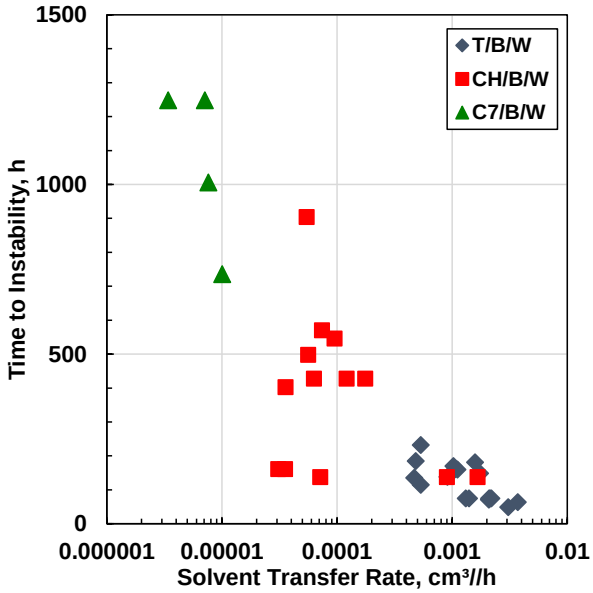

Figure 4.41. Correlation of time to instability to solvent volume transfer rate for the solvent/water/WC-B-A3 bitumen systems at 60°C with water layer heights of 1.0 cm. T=toluene, CH=cyclohexane, C7=*n*-heptane, B=bitumen, and W=water.

The mass transfer rates, water into bitumen (W/O) emulsification rates, and time to instability for the data collected at 60°C are summarized in Table 4.9. The average relative deviations (ARD) for the measured and predicted solvent mass transfer rates for the evaluated systems at 60°C are provided in Tables 4.10 to 4.12 for toluene, cyclohexane, and *n*-heptane, respectively.

Table 4.9. Average volume and mass transfer rates, W/O emulsification rates, and time to instability for solvent/water/WC-B-A3 bitumen systems at 60°C.

Solvent	Transfer Rate cm^3/h above, g/h below	W/O Emulsification Rate wt%/h	Time to Instability h
Toluene hw = 1.0, 1.5 and 2.0 cm	0.0009 ±0.0004 0.0008 ±0.0003	0.09 ±0.10	120 ±90
Cyclohexane h_w = 1.0 cm	0.00072 ±0.00073 0.00053 ±0.00054	0.04 ±0.03	280 ±170
Cyclohexane h_w = 1.5 and 2.0 cm	0.00006 ±0.00001 0.00004 ±0.00001	0.023 ±0.04	400 ±120
n-heptane h_w = 0.5 and 1.0 cm	0.000007 ±0.000003 0.00053 ±0.00054	0.04 ±0.03	1300 ± 100

Table 4.10. Measured and modeled mass transfer rates for the toluene/water/WC-B-A3 bitumen systems at 60°C.

Layer Thickness cm	Measured $x10^{-4}$ g/h	Predicted $x10^{-4}$ g/h	ARD %
1.0	10.1	2.5	75.2
1.5	13.5	1.7	87.4
2.0	15.5	1.3	91.6

Table 4.11. Measured and modeled mass transfer rates for the cyclohexane/water/WC-B-A3 bitumen systems at 60°C.

Layer Thickness cm	Measured $x10^{-4}$ g/h	Predicted $x10^{-4}$ g/h	ARD %
1.0	5.3	0.45	91.5
1.5	0.5	0.30	40.0
2.0	0.4	0.23	42.5

Table 4.12. Measured and modeled mass transfer rates for the *n*-heptane/water/WC-B-A3 bitumen systems at 60°C.

Layer Thickness Cm	Measured $x10^{-4}$ g/h	Predicted $x10^{-4}$ g/h	ARD %
0.5	0.057	0.017	70.1
1.0	0.034	0.008	76.4

4.3.3.7 Implications for *In Situ* Processes

The results obtained in this thesis suggest that while a water layer creates a barrier to mass transfer at low temperatures (below 60°C), the barrier may break down at higher temperatures due to gravity instability and spontaneous emulsification. Gravity instability causes the bitumen to elongate, finger, and bypass the water layer, allowing early contact between bitumen and solvent, promoting mass transfer and dilution. Spontaneous emulsification may enhance the mass transfer rate. Thermal gradients which are likely in solvent-assisted steam processes also enhance the mass transfer rate.

Gravity instability will be enhanced at higher temperatures and for solvents with higher solubility in water. Highly water soluble solvents such as aromatics will likely achieve connection times between solvent and bitumen of hours or even minutes at typical SA-SAGD operating conditions. Alkanes, which are more commonly implemented, have very low solubilities in water however at the expected bitumen/vapor interface temperatures (100 to 150°C) can also achieve connection times of hours or minutes. These processes will likely be accompanied by W/O and/or O/W spontaneous emulsification and the emulsification degree will increase with the temperature and the solvent solubility in water. Hence, solvent-assisted *in situ* recovery processes are not likely to be significantly impacted by a water-layer barrier and emulsion formation may occur in the reservoir.

CHAPTER FIVE: CONCLUSIONS AND RECOMMENDATIOS

This thesis aimed to: 1) measure solvent mass transfer rates into bitumen through a water layer at different temperatures, water layer heights, types of bitumen and solvent, 2) model the solvent mass transfer data with a liquid-liquid diffusion model and 3) measure and investigate spontaneous emulsification of water into bitumen and bitumen into water. The results are intended to provide a better understanding of the physical phenomena during the application of an SA-SAGD method. This chapter lists the main contributions and conclusions of this thesis and the recommendations for future work in the same area.

5.1 Contributions

The main contributions from this thesis are:

1. The development of a new practical methodology to measure solvent mass transfer and emulsification rates in a liquid-liquid solvent/water/bitumen system up to 80°C and 0.1 MPa.
2. Measurements of solvent mass transfer rates and emulsification rates for three families of solvents (aromatic, *n*-alkanes and a cyclic alkane), different water layer heights, two Western Canadian Bitumen and three temperatures (20, 60 and 80°C).
3. Confirmation that at 20°C in the absence of water-in-oil emulsification, the mass transfer of solvent through the water layer followed one dimension steady state model diffusion.
4. Experimental evidence of gravity instability of bitumen in a solvent/water/bitumen system. Gravity instability occurred faster at higher temperatures and for solvents with higher solubility in water, leading to earlier bitumen/solvent mixing.
5. Experimental evidence of spontaneous emulsification of water into bitumen and bitumen into water for two different Western Canadian Bitumen by volumetric measurements, Karl Fischer titrations and micrography of the bitumen while performing water/bitumen tests at temperatures up to 80°C.
6. Confirmation that natural surfactants are responsible for spontaneous emulsification of water into bitumen and bitumen into water for both Western Canadian Bitumen samples used in this thesis.

7. Experimental evidence that gravity instability and likely convection enhanced the solvent mass transfer at 60°C. The emulsification rate and time to gravity instability were found to correlate to the mass transfer rate. These results strongly suggest that water will provide little barrier to mass transfer at steam temperature due to gravity instability and convection. The results also suggest that spontaneous emulsification in the reservoir is likely.

5.2 Conclusions

5.2.1 Experimental Methodology

The experimental methodology developed to measure solvent mass transfer and emulsification rates consisted of layering a solvent/water/bitumen system in a glass vial and measuring the water and bitumen volume changes using a cathetometer. Tests performed at temperatures higher than 20°C were performed in a water bath. Data before the system started destabilizing via gravity instability was used for the analysis. Volumetric measurements of the water content in bitumen for water/bitumen tests (no solvent) using this methodology were validated by Karl Fischer titrations. The difference between the two results was within experimental error.

The main source of error in the experiments is likely convection which will increase the mass transfer from diffusion alone. The effect of convection while transferring the vial from the water bath to the cathetometer shown to be negligible. However, there are likely small local thermal gradients within the temperature bath which could enhance mass transfer and reduce the repeatability of the measurements.

5.2.2 Water/Bitumen Results

Spontaneous emulsification of water bitumen was observed for both WC-B-A3 and WC-B-B5 bitumen. The emulsification was validated by Karl Fischer titrations and micrography. The drop sizes ranged from 1 to 10 μm. Spontaneous emulsification of bitumen into the water was observed only for the WC-B-B5 bitumen. The bitumen-in-water emulsion gradually turned the water brown and its presence was confirmed with micrographs.

The W/O emulsification rate increased with increasing temperature. The amount of emulsified water eventually reached a plateau suggesting that the emulsification depended on a limited supply of natural surfactants. No emulsification was observed in bitumen partially stripped of surface active components confirming that natural surfactants were responsible for the spontaneous emulsification. The extent of emulsification was lower in the WC-B-B5 bitumen likely because the bitumen had less natural surfactants or because some of the natural surfactants partitioned to the O/W limiting the supply available for the W/O emulsions.

5.2.3 Solvent/Water/Bitumen Results

In all cases, there was no significant difference in the mass transfer rates and emulsification rates measured with unsaturated and water pre-saturated with solvent. The reason is that the solvent penetrates the water layer and establishes a steady state conditions within hours while the duration of the mass transfer experiment is hundreds of hours. Hence, the unsaturated and pre-saturated experimental conditions are the same for the majority of the measurement time.

The following conclusions were drawn for the solvent/water/bitumen systems at 20°C:

- The occurrence of spontaneous emulsification appeared to be random suggesting that the natural surfactants in the bitumen varied from sample to sample
- When no spontaneous emulsification occurred, there was a lag of hundreds to thousands of hours, depending on the solvent, before steady state mass transfer was established. The lag suggests that a barrier to mass transfer was established at the water/bitumen interface that was penetrated/disrupted over time
- The mass transfer after the lag time was diffusion controlled and followed the predicted one-dimension steady state diffusive mass transfer rate.
- The mass transfer rate was proportion to the solubility of the solvent in water and therefore was fastest in toluene and lowest in *n*-heptane.
- When spontaneous emulsification occurred, the water/bitumen interfaces became dome shaped, there was no lag time, and the mass transfer rate was enhanced. The enhanced mass transfer may arise because the dome shaped interface reduces the distance for mass transfer and allows for two-dimensional mass transfer.

The following observations were made for the solvent/water/bitumen systems at 60°C:

- Spontaneous emulsification occurred in all runs with unmodified bitumen. Stripping out natural surfactants eliminated the spontaneous emulsification confirming that natural surfactants were required for spontaneous emulsification to occur.
- There was no lag before mass transfer started. It is possible that spontaneous emulsification prevented a mass transfer barrier from forming.
- The interface was dome shaped and became gravity unstable over time in all cases.
- The mass transfer rates were higher than predicted from the steady state mass transfer model. It is hypothesized that the enhanced mass transfer is caused by convection induced by small temperature gradients in the water bath.
- The mass transfer rate was still approximately proportion to the solubility of the solvent in water and therefore was fastest in toluene and lowest in *n*-heptane.
- The emulsification rate was highest in the toluene systems (highest mass transfer rate) and lowest in the *n*-heptane systems. The emulsification rate correlates to the mass transfer rate.
- The time to gravity instability also correlated to the mass transfer rate. This correlation is expected because the instability depends on the density difference between the bitumen dome and water and the decrease in the density of the bitumen dome depends on the mass transfer rate.

5.3 Recommendations

Recommendations for future studies are provided below.

1. Evaluate mass transfer through the water layer using different diameter vials to assess the impact of wall effects and capillary forces.
2. Use a larger temperature bath in the experimental methodology developed in this thesis to create more exact isothermal conditions in order to minimize forced thermal convection.
3. Modify the proposed steady state mass transfer model to include 2D diffusion for the experiments with domed interfaces.
4. Perform gravity drainage experiments in a Hele-Shaw cell for a layered solvent/water/bitumen system at ambient conditions with inclined interfaces and measure the bitumen production rate for different types of solvent, types of bitumen and water layer

thicknesses. Study quantitatively the emulsification rates by measuring the water content in bitumen with the Karl Fischer titration test and qualitatively by taking micrographs to the bitumen phase. Take photographs to the interfaces to study any gravity instability that can accelerate the solvent/bitumen mixing.

5. Perform the experiments outlined in Point 3 at higher temperatures and pressures. To do so, it will be necessary to design a Hele-Shaw set up that: 1) allows photographs of the interface to be taken inside the oven used to control the temperature; 2) minimizes temperature gradients in the Hele-Shaw cell; 3) has a transparent wall to observe the bitumen profiles that can withstand the experimental pressure.

REFERENCES

Acevedo, S., Gutierrez, X. and Rivas, H. (2001). Bitumen-in-Water Emulsions Stabilized with Natural Surfactants. *J. Colloid Interface Sci.* 242: 230–238.

Akbarzadeh, K., Alboudwarej, H., Beck, J., Svrcek, W. Y. and Yarranton, H. W. (2003). Regular Solution Model for Asphaltene Precipitation from Bitumens and Solvents. *AIChE J*. 49 (11): 2948 – 2956.

Aleksandar, V. and Rakovec, J. (2015). Kelvin-Helmholtz Instability. *Liubliana University Seminar*.

Alvarez, G., Poteau S., Langevin D., Argillier, J-F and Salager, J-L. (2009). Heavy Oil - Water Interfacial Properties and Emulsion Stability : Influence of Dilution. *Energy & Fuels*. 15 (23): 294 – 299.

Aoki, K., Li, M., Chen, J. and Nishiumi, T. (2009). Spontaneous Emulsification at Oil - Water Interface by Tetraalkylammonium Chloride. *Electro. Chem. Community*. 11: 239-241.

Baker, G., Caflisch, R and Siegel, M. (1993). Singularity Formation during Rayleigh - Taylor Instability. *J. Fluid. Mech*. 252: 51 - 78.

Bakker, C. A. P., Van Buytenen, P. M. and Beek, W. J. (1966). Interfacial Phenomena and Mass Transfer. *Chem. Eng. Sci*. 21: 1039 – 1046.

Bayestehparvin, B., Ali, S. M. F. and Abedi, J. (2018). Solvent Based and Solvent Assisted Processes : State of the Art. *SPE EOR Conference at Oil and Gas West Asia*, Muscat, Oman. March 1–21.

Becher, P. (1966). *Emulsions: Theory and Practice*. 2nd Ed., ACS Monograph Series 162. *Amer Chem Soc*: Washington D.C, USA.

Bénard, H. (1901). Les tourbillons cellulaires dans une nappe liquide. *Revue Générale des Sciences Pures et Appliquées*. 11: 1261–1271 and 1309–1328.

Bijeljic. B., Muggeridge, A. H, and Blunt M.J. (2003). Multicomponent Mass Transfer across Water Films during Hydrocarbon Gas Injection. *Chem. Eng. Sci*. 58(11): 2377–88.

Bird, R.B., Stewart, W.E., Lightfoot, E. N. (2002). *Transport Phenomena*, 2nd Ed., Jon Wiley & Sons, New York, USA.

Bonoli, L and Witherspoon, P. A. (1968). Diffusion of Aromatic and Cycloparaffin Hydrocarbons in Water from 2 to 60°. *J. Phys. Chem*. 72(7): 2532 – 2534.

Bozeya, A., Al-Bawab, A., Friberg, S. E., Ge, L. and Rong, G. (2013). Spontaneous Emulsification between Incompatible Aqueous Solutions in the Water/Ethanol/Benzene System. *J. Colloid Interface Sci*. 395: 161–65.

Brouillette, M. (2002). The Richtmyer - Meshkov Instability. *Ann. Rev. Fluid Mech*. 34: 445 - 468.

Butler, R. M. (1987). Rise of Interfering Steam Chambers. *J. Can. Petr. Technol*. 26(3): 70–75.

Butler, R. M. (1998). SAGD Comes of Age! *J. Can. Petr. Technol*. 37(7): 9–12.

Butler, R. M., Mcnab, G. S. and Lo, H. Y. (1981). Theoretical Studies on the Gravity Drainage of Heavy Oil during In Situ Steam Heating. *Can. J. Chem. Eng*. 59(4): 455–460.

Campbell, B. T., and Orr Jr, F.M. (1985). Flow Visualization for CO_2/Crude-Oil Displacements. *SPE J*. 25(05): 665–78.

Cash, R. L., Cayias, J. L., Hayes, M., MacAllister, D. J., Schares, T., Schechter, R. S and Wade, W. H. (1975). Spontaneous Emulsification-A Possible Mechanism for Enhanced Oil Recovery. *Conf. SPE of AIME*. Dallas, Texas. 28 September-1 October.

Castor, T. P and Somerton, W. H. (1977). Interfacial Instabilities in Porous Media. *47th Annual California Regional Meeting of SPE of AIME*. Bakersfield, California. 13 – 15 April.

Chaverot, P., Cagna, A., Glita, S and Rondelez, F. (2008). Interfacial Tension of Bitumen - Water Interfaces. Part 1 : Influence of Endogenous Surfactants at Acidic PH. *Energy & Fuels*. 22 (9): 790 – 798.

Crank, J. (1975). *The mathematics of Diffusion*, 2nd edition, Oxford University Press, London, Britain.

Cussler, E.L. (2009). *Diffusion: Mass Transfer in Fluid Systems*, 3rd edition, Cambridge, New York, USA.

Cyr, N., Mclntyre, D. D., Toth, G and Strausz, O. P. (1987). Hydrocarbon Structural Group Analysis of Athabasca Asphaltene and its g.p.c Fractions by C n.m.r. *Fuel*. 66: 1709 - 1714.

Czarnecki, J. (2009). Stabilization of Water in Crude Oil Emulsions. Part 2. *Energy & Fuels*. 77 (7): 1253 – 1257.

Czarnecki, J., Tchoukov, P., Dabros, T and Xu, Z. (2013). Role of Asphaltenes in Stabilization of Water in Crude Oil Emulsions. *The Canad. Journ. Chem. Eng*. 91: 1365 – 1371.

Dabros, T.,Yeung, A., Masliyah, J and Czarnecki, J. (1999). Emulsification through area contraction. *J. Colloid Interface Sci*. 210: 222–224.

Davies, J. T and Haydon D. A. (1957). *Proc. Second Intern. Congr. Surface Activity*. 1: 417 – 476.

Davies, J. T and Rideal, E. K. (1961). Interfacial Phenomena. *Academic Press*, New York, USA.

Davies, J. T and Wigill, J. B. (1959). Diffusion across the Oil/Water Interface. *Proc. Royal. Soc. Lond*. 255: 277 – 291.

Dawe, E. O and Egbogah R. A. (1981). Oil Recovery Spontaneous Emulsification Aspect. *32nd Annual Tech. Meeting of the Pet. Soc. of CIM*. 81-32-40.

De Araujo, S. B., Merola, M., Vlassopoulos, D and Fuller, G. G. (2017). Droplet Coalescence and Spontaneous Emulsification in the Presence of Asphaltene Adsorption. *Langmuir*. *Amer. Chem. Soc.* 33: 10501 – 10510.

Dehghanpour, H., Li, G and Mojarad, M. (2014). Emulsion Flow at the Edge of a Steam Chamber. *SPE Heavy Oil Conf*, Calgary, Alberta, Canada, 10 - 12 June 2014.

Do, H D, and Pinczewski W. V. (1993). Diffusion-Controlled Swelling of Reservoir Oil by Indirect Contact with Injection Gas. *Chem. Eng. Sci*. 1993; 48(18): 3243 - 3252.

Dong, L. (2011). Effect of Vapor–liquid Phase Behavior of Steam–light Hydrocarbon Systems on Steam Assisted Gravity Drainage Process for Bitumen Recovery. *Fuel*. 95: 159–168.

E. Friberg, Stig. (2013). Potential Correlation between Spontaneous Emulsification and the Plait Point in the System Water/Benzene/Ethanol: A Phase Diagram Approach. *Soft*. 02(01): 1–6.

Etminan, S. R. (2014). Improved Experimental and Mathematical Techniques for Measurement of Solvent Gas Diffusivity in Heavy Oils. Ph.D. Dissertation, University of Calgary, Calgary, Canada.

Etminan, S. R., Haghighat, P., Maini, B. B and Chen, Z. H. (2011). Molecular Diffusion and Dispersion Coefficient in a Propane-Bitumen System: Case of Vapor Extraction (VAPEX) Process. *SPE EUROPEC/EAGE Annual Conf. and Exhib*. Vienna, Austria. May 23 - 26.

Euzeko, C. C., Wang, J and Gates, I. D. (2012). Investigation of Emulsion Flow in Steam-Assisted Gravity Drainage. *SPE J*. 18: 440 – 447.

Faradonbeh, M. R., Harding, T. G and Abedi, J. (2016). Semianalytical Modeling of Steam/Solvent Gravity Drainage of Heavy Oil and Bitumen: Unsteady-State Model with Curved Interface. *Fuel*. 183: 568 - 582.

Fayazi, A, and Kantzas, A. (2018). Modeling of CO_2 Diffusion into Water-Shielded Oil at Pore Scale Using Moving Mesh Technique. *Chem. Eng. Sci*. 179: 64–72.

Fingas, M., Fieldhouse, B., Bobra, M and Tennyson, E. (1993). The Physics and Chemistry of Emulsions. *Workshop Emul*. Washington D.C, USA.

Fortre, E and Taylor, S. E. (2015). Thermodynamic Modelling of Asphaltene Precipitation and Related Phenomena. *Adv. in Colloid and Interface Sci*. 217: 1 - 12.

Friedlander, S and Yudovich, V. (1962). Instabilities in Fluid Motion. *Notices of the Amer. Math. Soc*. 45(11): 1358 - 1367.

Gafonova, O. V and Yarranton, H. W. (2001). The Stabilization of Water-in-Hydrocarbon Emulsions by Asphaltenes and Resins. *J. Colloid Interface Sci*. 241: 469–478.

Gates, I. D and Chakrabarty, N. (2008). Design of the Steam and Solvent Injection Strategy in Expanding Solvent Steam-Assisted Gravity Drainage. *J Can Pet Tech*. 47(9): 12–20.

Ghoroori, M. A., Shahrabadi, A, and Jamialahmadi, M. (2017). Prediction of Gas Diffusion Coefficient for Reservoir Oil in the Presence of a Water Film Considering the Swelling Effect. *Ener. Sources*. 39(1): 36–46.

Ghoroori, M., Shahrabadi, A and Jamialahmadi, M. (2017). Prediction of gas diffusion coefficient for reservoir oil in the presence of a water film considering the swelling effect. *Ener Sources, Part A: Recov, Util and Envir Effects*. 39(1): 36–46.

Gibbs, J. W. (1878). On the Equilibrium of Heterogeneous Substances. *Connecticut Acad. Art. Sci*. 3: 343 – 524.

Gotawala, D. R and Gates, I. D. (2008). Steam Fingering at the Edge of a Steam Chamber in a Heavy Oil Reservoir Surmount Athabasca Reservoir. *Can. J. Chem*. Eng. 86: 1011–1022.

Govind, P. A., Das, S., Srinivasan, S and Wheeler, T. J. (2008). Expanding Solvent SAGD in Heavy Oil Reservoirs. *SPE Inter. Thermal Oper. And Heavy Oil Symp*. Calgary, Alberta, Canada. October 20 - 23.

Granek, R and Hu, J.G. (1996). Buckling of amphiphilic monolayers induced by head–tail asymmetry. *J. Phys. II*. 6: 999–1022.

Granek, R., Ball, R and Cates, M. (1993). Dynamics of Spontaneous Emulsification. *J. Phys II*. 3 (6): 829–849.

Grimaldos, F. A. (2018). Measurement of Liquid-Liquid Diffusion in Solvent-Bitumen Systems, Master of Science thesis, University of Calgary, Calgary, Canada.

Grogan, A. T, and Pinczewski, W. V. (1987). The Role of Molecular Diffusion Processes in Tertiary CO_2 Flooding. *J. Pet. Tech*. 39(5): 591–602.

Grogan, A. T., Pinczewski, V. W., Ruskauff, G. J and Orr Jr, F. M. (1987). The Role of Molecular Diffusion Processes in Tertiary CO_2 Flooding. *J Pet Tech.* 39(5): 591–602.

Grogan, A.T., Pinczewski, V. W., Ruskauff, G. J, and Orr Jr, F. M. (2007). Diffusion of CO_2 at Reservoir Conditions: Models and Measurements. *SPE Reser. Eng J*. 3(01): 93–102.

Hejazi, S. H and Azaiez, J. (2012). Stability of Reactive Interfaces in Saturated Porous Media under Gravity in the Presence of Transverse Flows. *J. Fluid Mech*. 695: 439–466.

Hutchinson, E. (1947). Diffusion across Oil – Water Interfaces. *J. Phys. Colloidal Chem*. 52: 897 – 908.

Irani, M and Gates I. D. 2014. On the Stability of the Edge of a Steam Chamber. *SPE J*. 695: 280 – 288.

Isaacs, E.E and Chow, R. S. (1992). Practical Aspects of Emulsion Stability. *Amer. Chem. Soc*. Edmonton, Alberta, Canada.

Ito, Y and Ipek, G. (2005). Steam - Fingering Phenomenon during SAGD Process. *SPE Intern. Thermal Operations and Heavy Oil Symposium*. Calgary, Alberta, Canada. November 1 - 3.

Jafary, S., Puyan, B and Navid, D. (2019). Prediction of Dynamic Interfacial Tension of Bitumen-Water System Using a Reliable Approach: Application in Enhanced Bitumen Recovery. *Ener. Soures Part A: Recov. Util. and Env. Effects*. 42 (4): 497 - 504.

Jha, R. K., Kumar, M., Benson, I and Hanzlik, E. (2013). New Insights into Steam / Solvent-Coinjection-Process Mechanism. *SPE J*. 18: 867 – 877.

Ji, D., Dong, M and Chen, Z. (2015). Analysis of Steam-Solvent-Bitumen Phase Behavior and Solvent Mass Transfer for Improving the Performance of the ES-SAGD Process. *J Pet Sci Eng*. 133: 826–837.

Johnston, K. A., Schoeggl, F. F., Satyro, M. A., Taylor, S. D and Yarranton, H. W. (2017). Phase Behavior of Bitumen and *n*-pentane. *Fluid Phase Equilibria*. 442: 1 – 19.

Kabalnov, A. (1998). Thermodynamic and Theoretical Aspects of Emulsions and Their Stability. *Colloid and Inter. Sci.* 3(3): 270–75.

Keshavarz, M., Okuno, R. and Babadagli, T. (2014). Efficient Oil Displacement near the Chamber Edge in ES-SAGD. *J Pet Sci Eng.* 118: 99–113.

Keshavarz, M., Okuno, R. and Babadagli, T. (2015). Optimal Application Conditions for Steam/Solvent Coinjection. *SPE Reser Eval & Eng*. 18(01): 20–38.

Khaledi, R., Boone, T. J., Motahhari, H. R and Subramanian, G. (2015). Optimized Solvent for Solvent Assisted-Steam Assisted Gravity Drainage (SA-SAGD) Recovery Process. *SPE Can Heavy Oil Tech. Conf*. Calgary, Alberta, Canada. June 9 – 11.

Koretsky M. D. (2004). Engineering and Chemical Thermodynamics. *John Wiley & Sons, Inc*. New Delhi, India.

Koshmieder, E. L. (1974). Benard Convection. *Adv. Chem. Phys*. 26: 177-212.

Lake, L. W. (1989). Enhanced Oil Recovery. Prentice-Hall. Englewood Cliffs, New Jersey.

Langevin, D., Poteau, S., I Hénaut, I and Argillier, J. F. (2004). Crude Oil Emulsion Properties and Their Application to Heavy Oil Transportation. *Oil & Gas Sci. Tech*. 59(5): 511–21.

Lee, G. W. J and Tadros, Th. F. (1982). Formation and Stability of Emulsions Produced by Dilution of Emulsifiable Concentrates. Part I. An Investigation of the Dispersion on Dilution of Emulsifiable Concentrates Containing Cationic and Non-Ionic Surfactants. *Colloids and Surf*. 5: 105-115.

Li, W and Mamora, D. D. (2011). Solvent-Type and –Ratio Impacts on Solvent-Aided SAGD Process. *SPE Reser Eval & Eng*. 14(03): 320 – 331.

Lin, E. C, and Huang T.S. (2007). The Effect of Rock Wettability on Water Blocking During Miscible Displacement. *SPE Reser Eng*. 5(02): 205–12.

Lopez-Montilla, J. C., Herrera-Morales, P. E., Pandey, S and Shah, D. O. (2002). Spontaneous Emulsification: Mechanisms, Physicochemical Aspects, Modeling, and Applications. *J. Dispersion Sci. Tech*. 23(1–3): 219–68.

Lord Rayleigh. (1900). Investigation of the Character of the Equilibrium of an Incompressible Heavy Fluid of Variable Density. *Sci. Papers*. Cambridge Univ. Press, Cambridge, England. 2: 200.

Mailybaev, A. A. (2018). Toward Analytic Theory of the Rayleigh – Taylor Instability: Lessons from a Toy Model. Report from *Instituto Nacional de Matematica Pura e Aplicada*.

Marangoni, C. (1865). On the expansion of a Drop of Liquid Floating on the Surface of another Liquid. Tipographia dei fratelli Fusi, Pavia.

Mc Bain, J. W and Woo, T. (1937). Spontaneous Emulsification and Reactions Overshooting Equilibrium. *Proc. Roy. Soc. Lond*. A163: 182 – 188.

Mclean, J. D and Kilpatrick, P. K. (1997). Effects of Asphaltene Solvency on Stability of Water-in-Crude-Oil Emulsions. *J. Colloid Interface Sci*. 189: 242 – 253.

Memarzadeh, A and Rahnema, H. (2015). Thermodynamic Analysis of Solvent Assisted Steam Injection. *SPE Annual Tech. Conf. and Exhib*. Houston, Texas, USA. September 28 – 30.

Mendes – Tatsis, M. A and Perez de Ortiz, E. S. (1992). Spontaneous Interfacial Convection in Liquid-Liquid Binary Systems under Microgravity. *Proc. R. Soc. Lond*. 438: 389 – 396.

Meshkov, E. E. (1969). Instability of the interface of two gases accelerated by a shock wave. *Sov. Fluid Dyn*. 4: 101 – 108.

Miller, C.A and Scriven, L. E. (1970). Interfacial Instability Due to Electrical Forces in Double Layers. *J Colloid Interface Sci*. 33:360-370.

Miller, C.A. (2006). Spontaneous Emulsification: Recent Developments with Emphasis on Self - Emulsification. *Taylor & Francis Group, LLC*. Ch 2. 108 - 124.

Mirazimi, S., Rostami, B., Ghazanfari, M. H and Khosravi, M. (2017). Water Film Rupture in Blocked Oil Recovery by Gas Injection: Experimental and Modeling Study. *Chem. Eng. Sci*. 161: 288–298.

Mohammadzadeh, O and Chatzis, I. (2009). Pore-Level Investigation of Heavy Oil Recovery Using Steam Assisted Gravity Drainage (SAGD). *Intern. Pet. Tech. Conf*. Doha, Qatar. December 7 – 9.

Moilliet, M. J. (1976). *Emulsions in Retrospect and Prospect*. Port Sunlight Laboratory, England.

Muller, T and Lake, L. W. (2007). Theoretical Study of Water Blocking in Miscible Flooding. *SPE Reser. Eng*. 6(04): 445–451.

Motahhari, H., Schoeggl, F. F., Satyro, M. A and Yarranton, H. W. (2011). Prediction of the Viscosity of Solvent Diluted Live Bitumen at Temperatures up to 175°C. *SPE Can. Unconventional Conf*. Calgary, Alberta, Canada. November 15 – 17.

Nasr, N. T and Ayodele, O. R. (2006). New Hybrid Steam – Solvent Processes for the Recovery of Heavy Oil and Bitumen. *Intern. Pet. Exhib. and Conf*. Abu Dhabi, U.A.E. November 5 – 8.

Nasr, T. N., Beaulieu, G., Golbeck, H and Heck, G. (2003). Novel Expanding Solvent – SAGD Process "ES-SAGD". *Tech. Note JCPT*. 42 (1): 13 – 16.

Oballa, V., Butler, R. M. (1989). An Experimental Study of Diffusion in the Bitumen-Toluene System. *J. Can. Petr. Tech.*, 28: 62 - 69.

Olander, D. R and Reddy, L. B. (1963). The Effect of Concentration Driving Force on Liquid – Liquid Mass Transfer. *Chem. Eng. Sci*. 19: 67 - 73.

Orr, B. (2009). ES-SAGD; Past, Present and Future. *SPE Annual Tech. Conf. and Exhib*. New Orleans, Louisiana, USA. October 4 – 7.

Ostrovskii, V., Barenbaum, R. K and Abramson, A. A. (1970). *Colloids J. USSR*. 32 (4): 470.

Ouincke. G. (1879). About emulsion formation and the influence of bile on digestion. *Pülger Archiv für die Physiologie*. 19: 129- 144.

Perez de Ortiz, E. S and Sawistowki, H. (1973). Interfacial Stability of Binary Liquid – Liquid Systems – I. Stability Analysis. *Chem. Eng. Sci*. 28: 2051 – 2061.

Plesset, M. S and Whipple, C. G. (1974). Viscous Effects in Rayleigh-Taylor Instability. *The Phys. of Fluids*. 17(1): 1–7.

Popil, R. (1979). Experimental Investigation of the Rayleigh-Taylor Instability. Master of Science Thesis. The University of British Columbia. Vancouver, British Columbia, Canada.

Poiling, B. E., Prausnitz, J. M and O'Connell, J. P. (2001). *The Properties of Gases and Liquids*. 5th ed. McGraw-Hill.

Rane, J. P., Harbottle., Pauchard, V., Couzis., A and Banerjee, S. (2012). Adsorption Kinetics of Asphaltenes at the Oil − Water Interface and Nanoaggregation in the Bulk. *Amer. Chem. Soc*. 28: 9986 - 9995.

Rayleigh, Lord. (1883). Investigation of the Character of Equilibrium of an Incompressible Heavy Fluid of Variable Density. *Proc. Lond. Math. Soc*. 14: 170 – 177.

Rehbinder, P. (1957). *Proc. Intern. Congr. Surf. Act. London*, 1: 476.

Riazi, M., Jamiolahmady, M, and Sohrabi, M. (2011). Theoretical Investigation of Pore-Scale Mechanisms of Carbonated Water Injection. *J Pet. Sci. Eng*. 75(3–4): 312–26.

Richardson, W. D. (2017). Diffusivity of Light Hydrocarbon Gases in Bitumen, Ph.D. Dissertation, University of Calgary, Calgary, Canada.

Richtmyer, R. D. (1960). Taylor instability in shock acceleration of compressible fluids. *Comm. Pure Appl. Math.* 8: 297 - 319.

Ruckenstein, E and Berbente, C. (1964). The Occurrence of Interfacial Turbulence in the Case of Diffusion Accompanied by Chemical Reaction. *Chem. Eng. Sci*. 19: 329 - 347.

Rudin, J and Wasan, D. T. (1992). Interfacial Turbulence and Spontaneous Emulsification in Alkali - Acidic Oil Systems. *Chem. Eng. Sci*. 45 (12): 2225 - 2238.

Ruschak, K. J and Miller, C. A. (1972). Spontaneous Emulsification in Ternary Systems with Mass Transfer. *Ind. Eng. Chem. Fundam*. 11(4): 534 - 539.

Santana-Solano, J., Quezada, C. M., Ozuna-Chacón, S and Arauz-Lara, J. L. (2012). Spontaneous Emulsification at the Water/Oil Interface. *Colloids and Surfaces A: Physicochem. Eng. Asp*. 399: 78–82.

Schramm L. L. (1992) *Petroleum Emulsions*. Amer. Chem. Soc. Washington D.C, USA.

Shahidzadeh, N., Bonn, D and Meunier, J. (1997). A New Mechanism of Spontaneous Emulsification: Relation to Surfactant Properties. *Les Editions de Physique*. 40(4): 459–64.

Shahidzadeh, N., Bonn, D and Meunier, J. (2000). Dynamics of Spontaneous Emulsification for Fabrication of Oil in Water Emulsions. *Amer. Chem. Soc*. 16: 9703-9708.

Shaw, D. J. (1980). *Introduction to Colloid and Surface Chemistry*. 3rd Ed. Butterworths, London. England.

Sherwood, T. K and Wei, J. C. (1957). Interfacial Phenomena in Liquid Extraction. *Ind. Eng. Chem*. 49: 1030 – 1034.

Shinoda, K and Kunieda, H. (1972). Conditions to Produce So-called Microemulsions: Factors to Increase the Mutual Solubility of Oil and Water by Solubilizer. *J. Colloid and Interface Sci*. 42: 381-387.

Shu, G., Dong, M., Chen, S and Hassanzadeh, H. (2017). Mass transfer of CO_2 in a carbonated water-oil system at high pressures. *Ind. Eng. Chem. Research*. 56(1): 404 – 416.

Silva, P. S., Zhdanov, S., Starov, V. M and Holdich, R. G. (2017). Spontaneous Emulsification of Water in Oil at Appreciable Interfacial Tensions. Colloids. *Surf. Phys. Chem. Eng*. 521: 141–46.

Slavtchev, S and Mendes, M. A. (2004). Marangoni Instability in Binary Liquid – Liquid Systems. *Intern. J. Heat and Mass transf.* 47: 3269 – 3278.

Sørensen, T. S. (1978). Instabilities Induced by Mass Transfer, Low Surface Tension and Gravity at Isothermal and Deformable Fluid Interfaces. *Proc. Meeting. Univ. Denmark. 1 – 74*.

ST98: 2018. Alberta's Energy Reserves & Supply/Demand Outlook. AER.

Sterling, C. V and Scriven, L. E. (1959). Interfacial Turbulence: Hydrodynamic Instability and the Marangoni Effect. *A.I.Ch.E J*. 5 (4): 514-523.

Summer, C. G. *Clayton's The Theory of Emulsions and Their Technical Treatment*. 5th Ed, Blakiston, New York, USA.

Sztukowski, D. M and Yarranton, H. W. (2005). Oilfield Solids and Water-in-Oil Emulsion Stability. *J Colloid and Interface Sci*. 285: 821–33.

Tadros, T. F and Vincent, B. (1983*). In Encyclopedia of Emulsion Technology*. Ed. Becher, P. Marcel Dekker, New York, USA.

Tadros, T. F. (2009). *Emulsion Science and Technology: A General Introduction*. Wiley-VCH Verlag GmbH & Co. KGaA. Weinheim, Germany.

Tadros, T. F. (2013). *Emulsion Formation, Stability and Rheology*. Wiley-VCH Verlag GmbH & Co. KGaA. Weinheim, Germany.

Tan, X., Fenniri, H and Gray, M. R. (2009). Water Enhances the Aggregation of Model Asphaltenes in Solution via Hydrogen Bonding. *Energy & Fuels*. 15: 9080–9086.

Taylor, G. I. (1950). The Instability of Liquid Surfaces when Accelerated in a Direction Perpendicular to their Plates. *Proc. R. Soc. London Ser. A*. 201: 192.

Theissen, O and Gompper, G. (1999). Lattice-Boltzmann Study of Spontaneous Emulsification. *The European Phys. J*. 11 (1): 91-100.

Thomas, M, and Lake, L. W. (2007). Theoretical Study of Water Blocking in Miscible Flooding. *SPE Reser. Eng*. 6 (04): 445 - 451.

Thomson, J. (1855). On certain curious Motions Observable at the Surfaces of Wine and other Alcoholic Liquors. *Philosophical Magazine*. 10: 330-333.

Tsamantakis, C., Masliyah, J., Yeung, A and Gentzis, T. (2005). Investigation of the Interfacial Properties of Water-in-Diluted-Bitumen Emulsions Using Micropipette Techniques. *J Colloid and Interface Sci*. 284: 176–183.

Vali, J., Kazemzadeh, E., Bakhtiari, H. A., Khodabakhshi, M, and Esfahani, M. R. (2011). A Fast and Simple Method for Modeling of Oil Swelling in CO_2 Injection. *J Geope*. 1(2): 39–46.

Varadaraj, R, and Cornelius B. (2012). Molecular Origins of Crude Oil Interfacial Activity. Part 4: Oil − Water Interface Elasticity and Crude Oil Asphaltene Films. *Energy & Fuels*. 26: 7164 - 7169.

Veil, J. A and Quinn, J. J. (2008). Water Issues Associated with Heavy Oil Production. *Enviromental Science Division Technical Report*.

Wadell, J. T., Niederhaus, C. E and Jacobs, J. W. (2012). Experimental Study of Rayleigh – Taylor Instability: Low Atwood Number Liquid Systems with Single-Mode Initial Perturbations. *Physics of Fluids*. 13 (5): 1263 - 1273.

Ward, A. F. H and Brooks, L. H. (1952). Flattening of Meniscus between Water and Organic Solvents. *Nature. Publish Group*. 170: 118.

Wei, J. C. (1955). pH.D Dissertation. Massachusetts Institute of Technology. Cambridge.

Weir Lawrie, A. G. (2009). On Rayleigh-Taylor Mixing: Confinement by Stratification and Geometry. pH.D Dissertation. The University of Cambridge. Cambridge, England.

Wu, H., Li, Z., Lu, Y., Yang, M., Feng, H., Xu, D., Hou, J., Kang, W., Yang, H and Zhao, Y. A. (2018). Novel Ultra-Low IFT Spontaneous Emulsification System for Enhanced Oil Recovery in Low Permeability Reservoirs. *SPE EOR Conf. at Oil and Gas*. Muscat, Oman. 26-28 March.

Yarranton, H. W., Badamchi-Zadeh, A., Satyro, M. A and Maini, B. B. (2008). Phase Behaviour and Physical Properties of Athabasca Bitumen, Propane and CO_2. *SPE 59th Annual Technical Meeting*. Calgary, Alberta, Canada. June 17 – 19.

Yarranton, H. W., Hussein, H and Masliyah, J. H. (2000). Water-in-Hydrocarbon Emulsions Stabilized by Asphaltenes at Low Concentrations. *J Colloid Interface Sci*. 228: 52–63.

Yeung, A., Dabros, T., Czarnecki, J and Masliyah, J. (1999). On the Interfacial Properties of Micrometer - Sized Water Droplets in Crude Oil. *Proc. R. Soc. Lond*. 455: 3709 - 3723.

Zou, M., Han, Y. L., Qi, L and Chen, Y. (2007). Fast and accurate measurement of diffusion coefficient by Taylor's dispersion analysis. *Chinese Sci Bull.* 52 (24): 3325 – 3332.

APPENDIX A: BITUMEN DOME FITTED FUNCTION AND SYMMETRY TEST ON A SOLVENT/WATER/BITUMEN TEST AT 60°C

A toluene/water/bitumen (Figure A1 top) and a cyclohexane/water/bitumen system (Figure A1 bottom) both at 60°C were selected for a symmetry test of the bitumen dome. Photographs were taken at 0, 90°, 180° and 270° of each test at a single time. Then, the procedure from Section 3.3.1 was implemented to find the fitting correlation for the dome at each angle and calculate its volume. Results of the fitting correlation at each angle for both tests are shown in Figure A1. The dome volume for both tests at the four angles are provided in Table A1. The 95% confidence intervals for a single measurement in each case (the potential error from a non-representative profile) was determined from the standard deviation assuming a normal distribution and were ±0.09 cm^3 (±15%) for the toluene/water/bitumen system and ±0.018 cm^3 (±5%) for the cyclohexane/water/bitumen system.

Table A1. Dome volumes at 0, 90°, 180° and 270° for a toluene/ water/WC-B-A3 bitumen and a cyclohexane/ water/WC-B-A3 bitumen system each with a 1 cm unsaturated water layer at 60°C.

Angle	Dome Volume, cm^3	
	T/W/B	CH/W/B
0°	0.531	0.349
90°	0.571	0.361
180°	0.640	0.353
270°	0.601	0.370
Mean	0.586	0.358
Standard Deviation	0.046	0.009

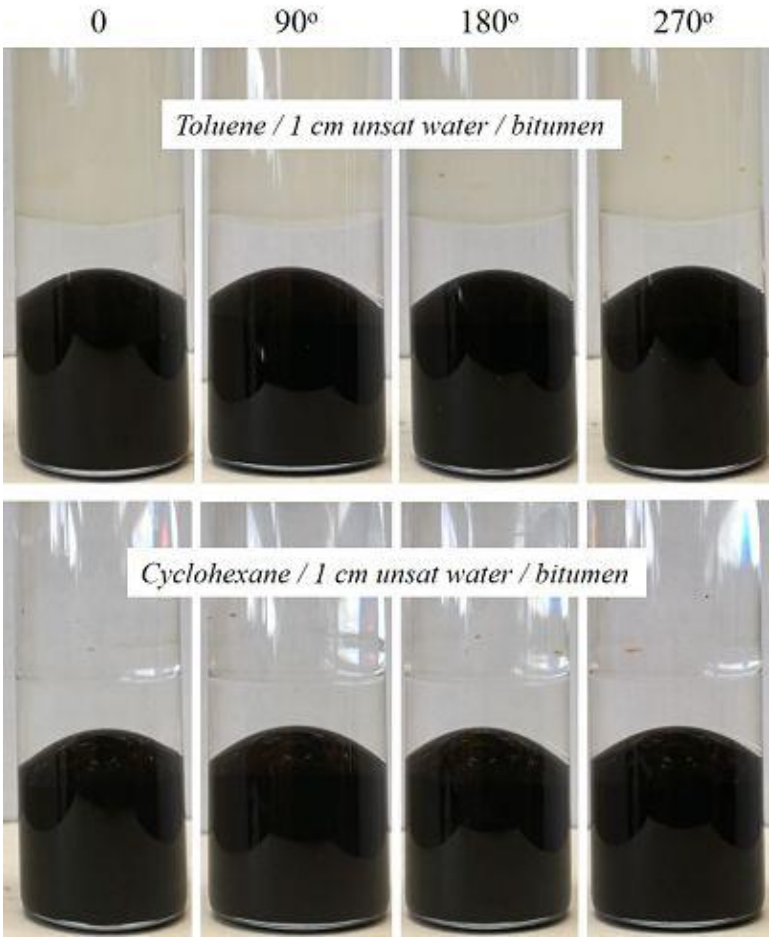

Figure A1. Photographs for a toluene/water/WC-B-A3 bitumen system with a 1.0 cm unsaturated water layer at 60°C and 209 hours (top) and a cyclohexane/ water/WC-B-A3 bitumen test with a 1.0 cm unsaturated water layer at 60°C and 306 hours (bottom).Each vial was rotated at 90° intervals to test the symmetry of the dome around the y-axis.

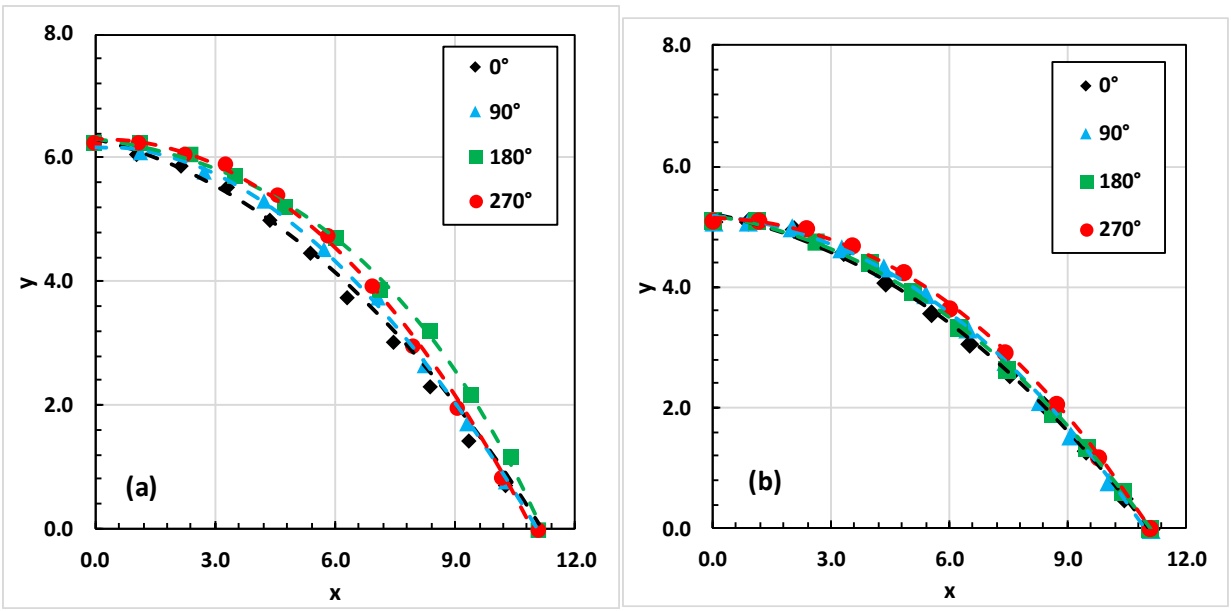

Figure A2. Contour points (closed symbols) and fitting correlation (dashed lines) of the bitumen dome at 0, 90°, 180° and 270° for (a) toluene/unsaturated water/WC-B-A3 bitumen at 60°C and (b) cyclohexane/unsaturated water/WC-B-A3 bitumen at 60°C.

APPENDIX B: REPEATABILITY OF WATER CONTENT AND MASS TRANSFER MEASUREMENTS

Water/Bitumen

Repeat experiments were performed for the water/WC-B-A3 bitumen system at the following conditions:

- unsaturated water, 1 cm water layer, 20°C; Figures B1 and B2a
- toluene saturated water, 1 cm water layer, 20°C; Figure B2b
- unsaturated water, 2 cm water layer, 20°C; Figure B3a
- toluene saturated water, 2 cm water layer, 20°C; Figure B3b
- unsaturated water, 1 cm water layer, 60°C; Figures B4 and B5a
- toluene saturated water, 1 cm water layer, 60°C; Figure B5b
- unsaturated water, 1.5 cm water layer, 60°C; Figure B6ab
- toluene saturated water, 1.5 cm water layer, 60°C; Figure B6b
- unsaturated water, 2 cm water layer, 60°C; Figure B7a
- toluene saturated water, 2 cm water layer, 60°C; Figure B7b

At 80°C, density of WC-B-A3 was lower than the density of water and the system was gravity unstable from the beginning of the test. Therefore, at this temperature, the repeatability was assessed for the WC-B-B5 bitumen instead; its density was approximately 0.01 g/cm^3 greater than the density of water. The following repeat experiment was done at this temperature:

- unsaturated water, 2 cm water layer, 80°C, Figure B8

The repeatability of the water contents was assessed. It was found that the runs at 20°C had a similar scatter to each other and that the runs at 60°C had a similar scatter to each other that was higher than the scatter at 20°C. Therefore, the confidence interval at 20°C was assessed from all of the deviations at 20°C together. The confidence interval at 60°C was assessed from all of the deviations at 60°C together.

The confidence interval was calculated from the paired measurements as follows. First, the average or sample mean of a set of measurements is defined as:

$$\bar{x} = \frac{\sum_{i=1}^{n} x_i}{n} \tag{B.1}$$

where x_i is each measurement in the sample and n is the number of measurements. The degree of scattering in the measurements is described by the sample variance defined as:

$$s^2 = \frac{\sum_{i=1}^{n}(x_i - \bar{x})^2}{n-1} \tag{B.2}$$

The standard deviation is the square root of the sample variance. The confidence interval for the average of the measurements is given by:

$$CI = \pm t_{(\alpha/2,\nu)} \frac{s}{\sqrt{n}} \tag{B.3}$$

where $\bar{x}$ is the correct mean, $\nu = n - 1$ and α is the significance level. The t-value can be found with a t-distribution table using the appropriate significance level and n - 1 degrees of freedom. For this thesis, $\alpha/2 = 0.05$ and thus the confidence level is 90%. The confidence interval for a single run was determined assuming a normal distribution with n = 1. In this case, the 90% confidence interval is given by:

$$CI = \pm 1.64s \tag{B.4}$$

The repeatabilities at 20°C and 60°C for the water/bitumen systems were ±0.24 wt% and 0.68 wt%, respectively. The confidence intervals for individual runs of water/bitumen tests at 20 and 60°C are plotted as error bars on Figures B2a to B7b.

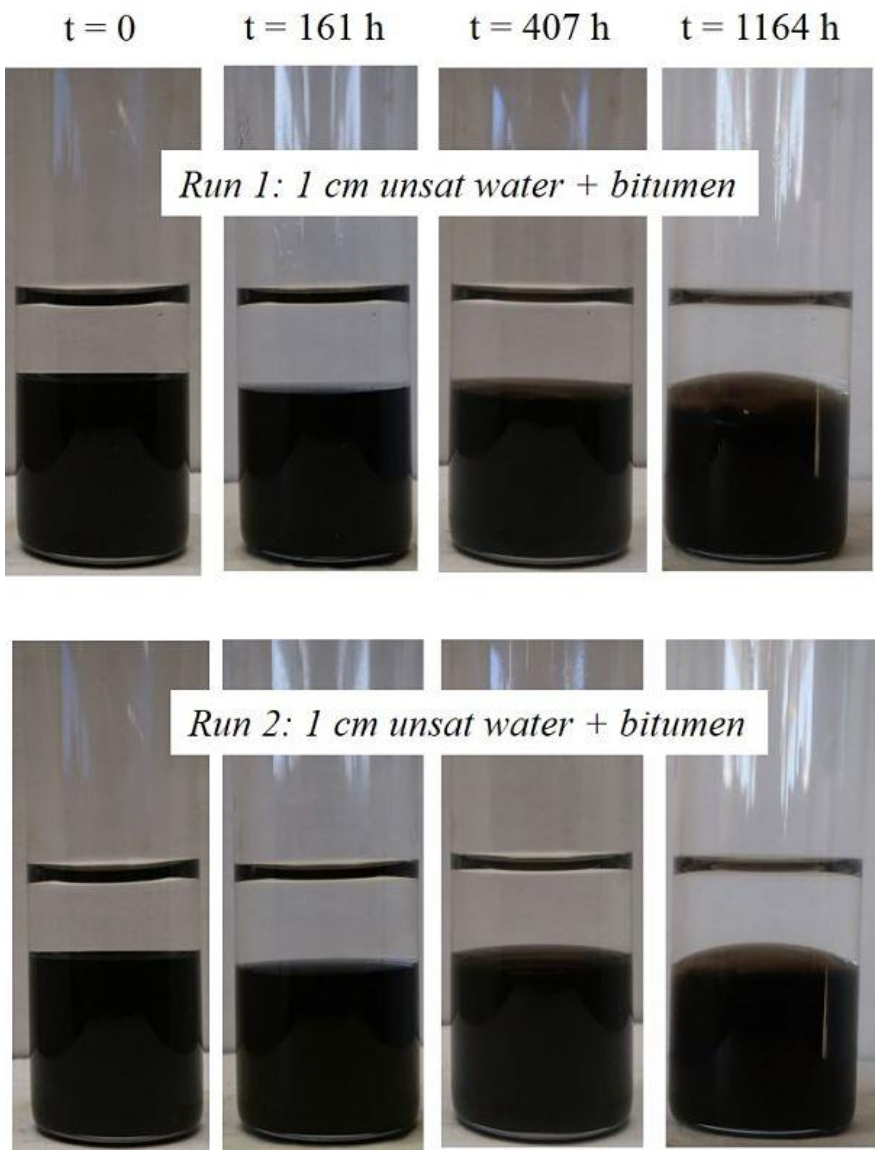

Figure B1. Photographs of repeated water/WC-B-A3 bitumen tests with 1 cm of unsaturated water at 20°C.

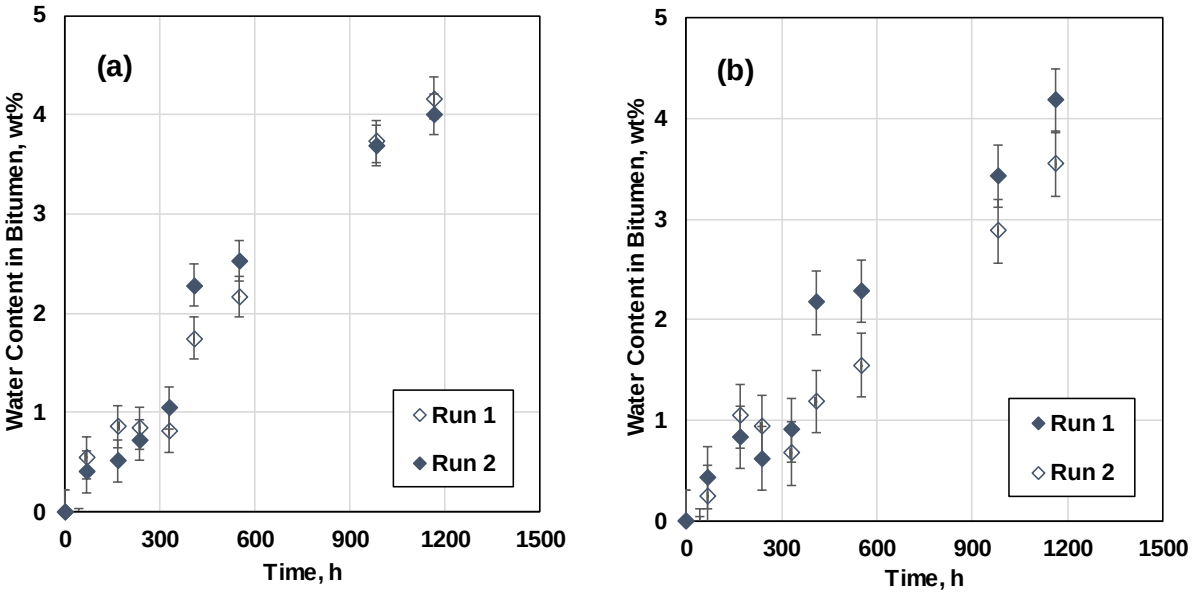

Figure B2. Water content in WC-B-A3 bitumen versus time for repeat water/bitumen runs at 20°C with a 1 cm water layer: a) unsaturated water; b) toluene saturated water.

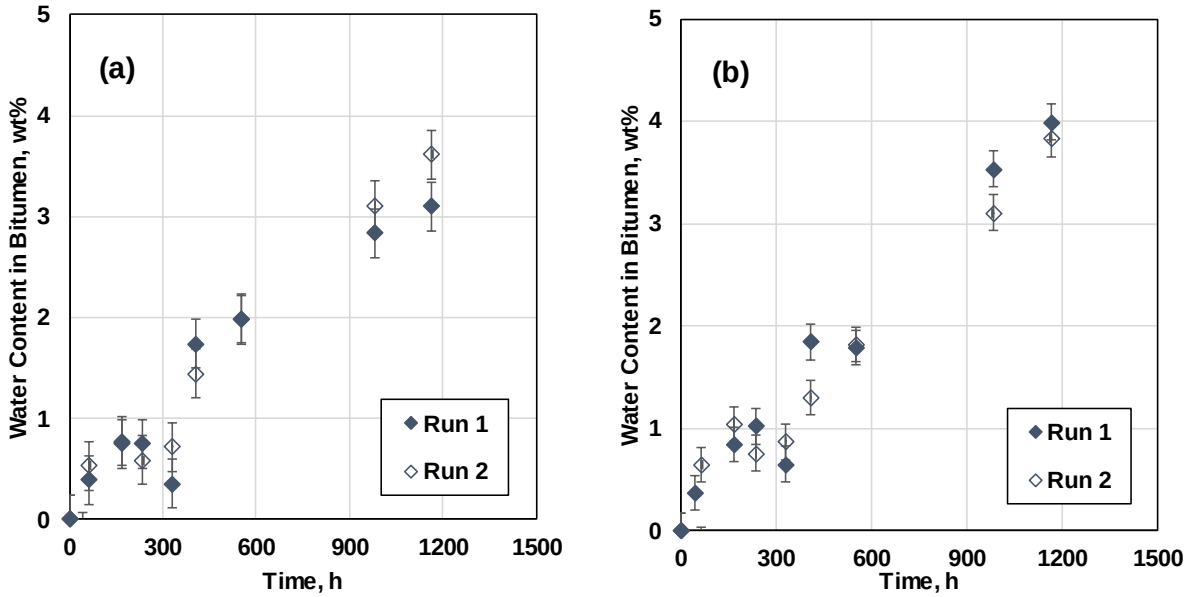

Figure B3. Water content in WC-B-A3 bitumen versus time for repeat water/bitumen runs at 20°C with a 2 cm water layer: a) unsaturated water; b) toluene saturated water.

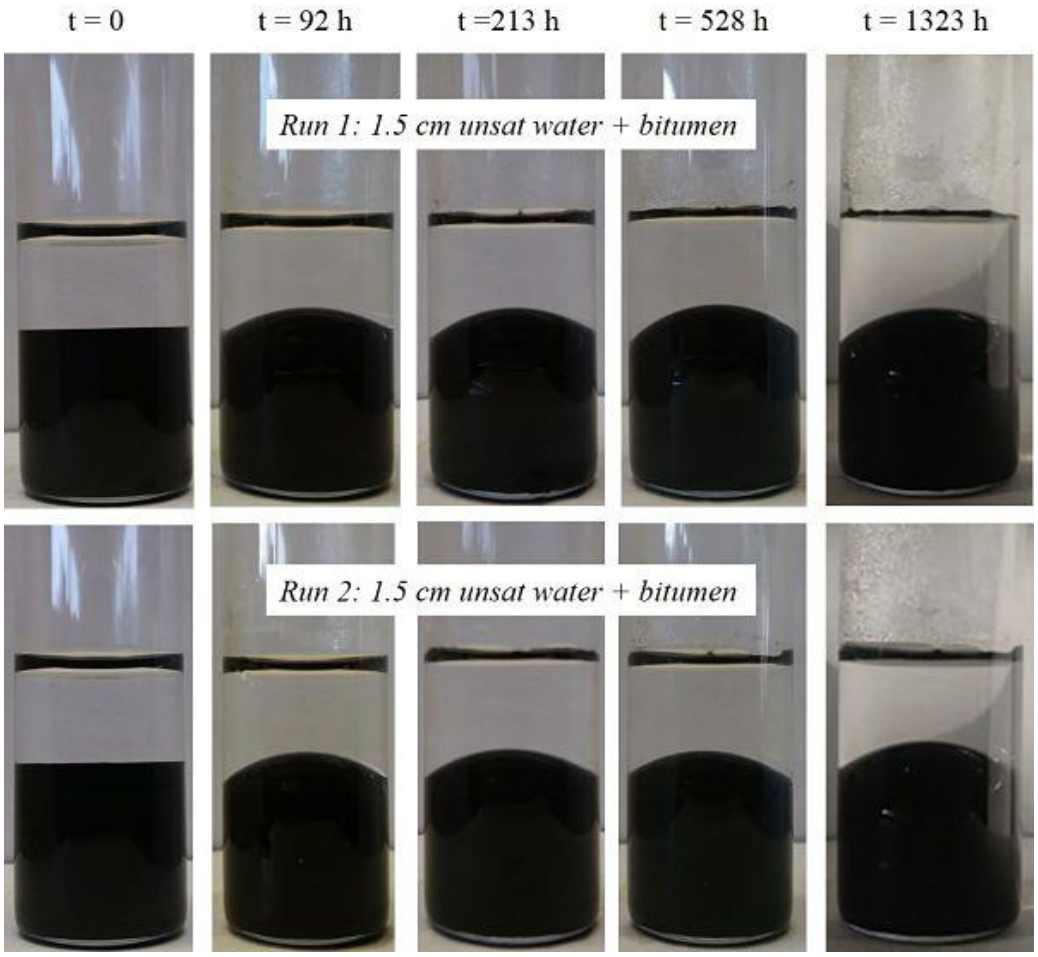

Figure B4. Photographs of repeated water/WC-B-A3 bitumen tests with 1.5 cm of unsaturated water at 60°C.

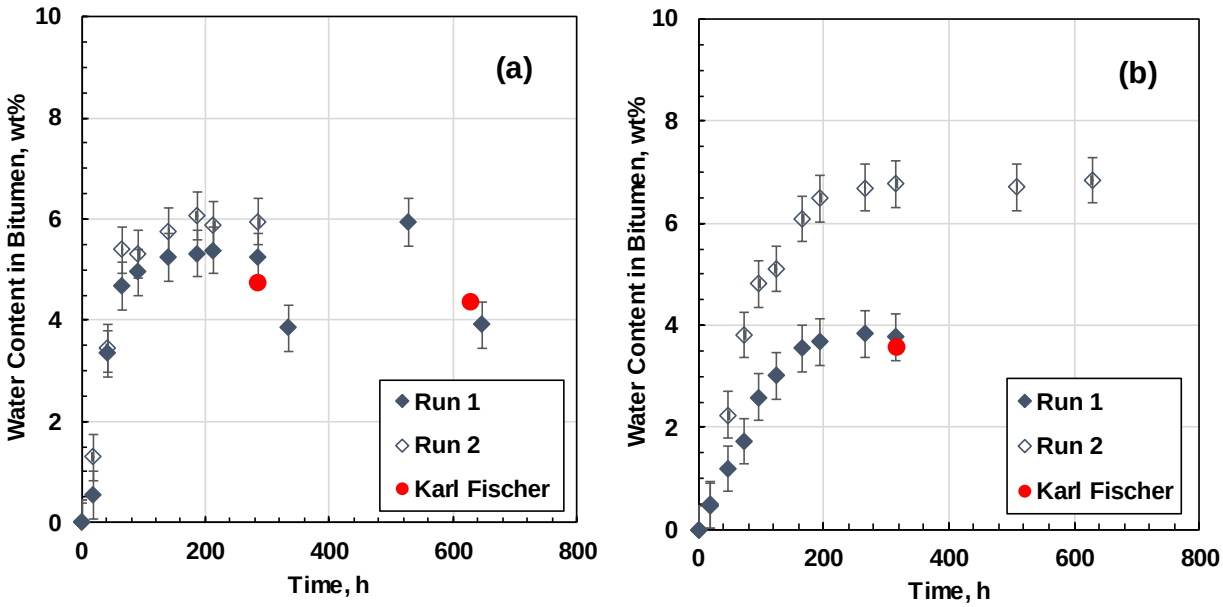

Figure B5. Water content in WC-B-A3 bitumen versus time for repeat water/bitumen runs at 60°C with a 1 cm water layer: a) unsaturated water; b) toluene saturated water.

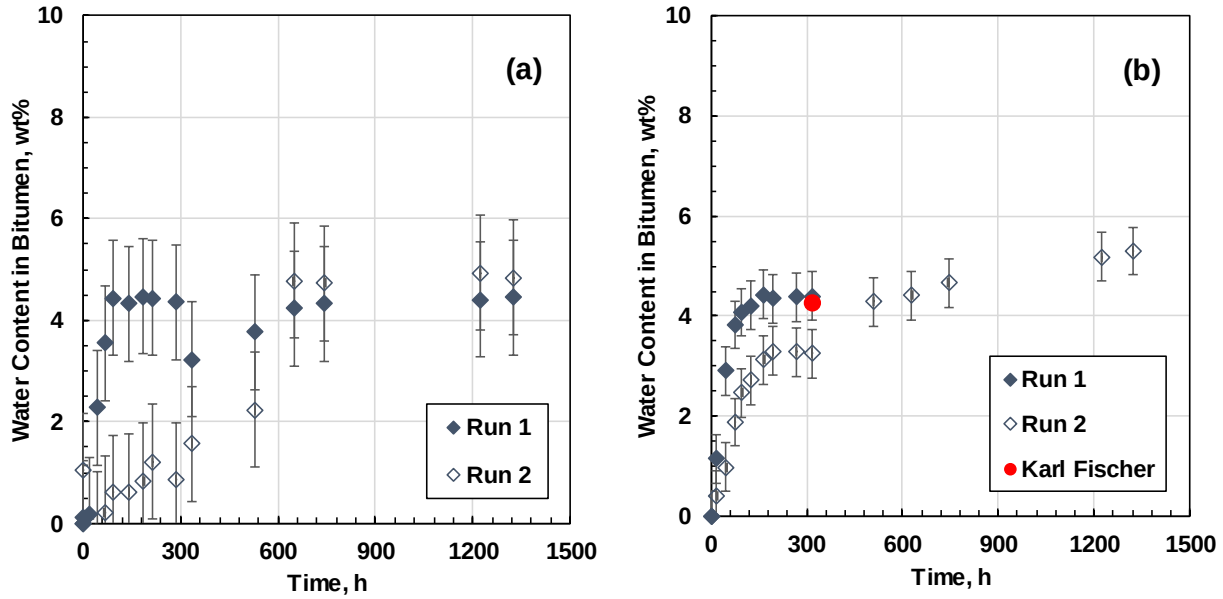

Figure B6. Water content in WC-B-B5 bitumen versus time for repeat water/bitumen runs at 60°C with a 1.5 cm water layer: a) unsaturated water; b) toluene saturated water.

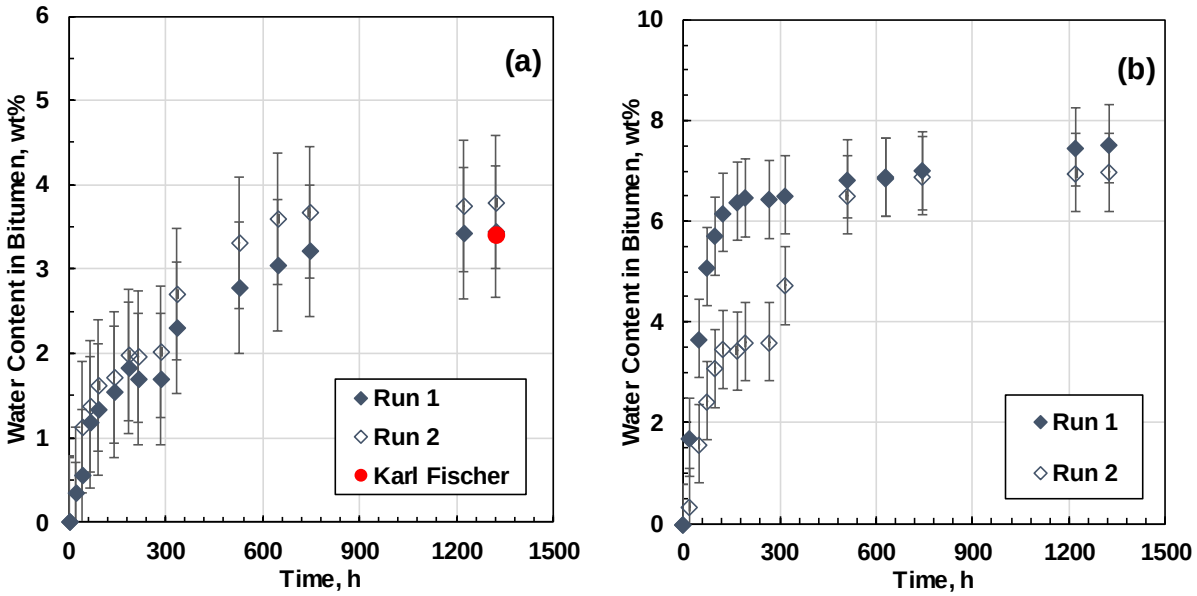

Figure B7. Water content in WC-B-A3 bitumen versus time for repeat water/bitumen runs at 60°C with a 2 cm water layer: a) unsaturated water; b) toluene saturated water.

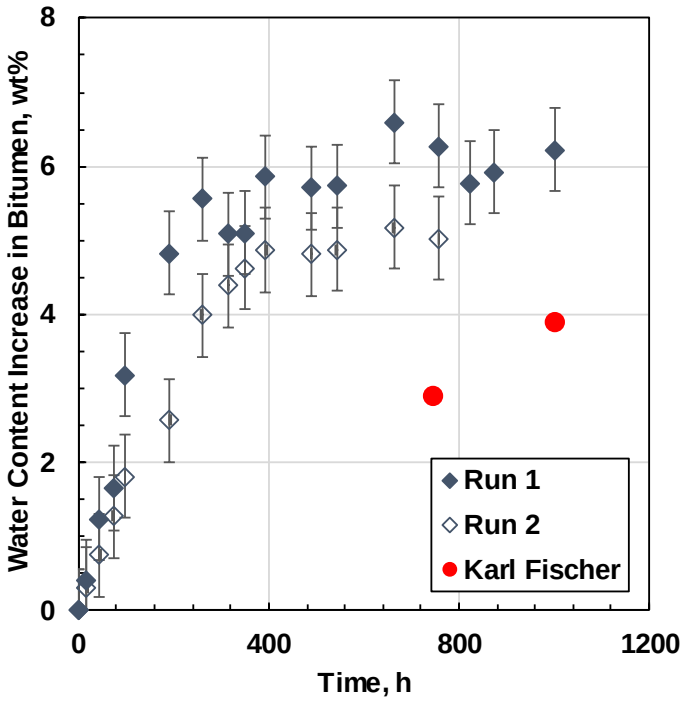

Figure B8. Water content in WC-B-A3 bitumen versus time for repeat water/bitumen runs at 80°C with a 2 cm unsaturated water layer.

Solvent/Water/Bitumen

Repeat experiments were performed for the solvent/water/WC-B-A3 bitumen system at the following conditions:

- unsaturated water, toluene/0.45 cm water layer, 20°C, Figure B9
- unsaturated water, n-pentane/0.3 cm water layer, 20°C, Figure B10 and B11.
- unsaturated water, toluene/1 cm water layer, 60°C; Figure B12a and B13.
- saturated water, toluene/1.5 cm water layer, 60°C; Figure B12b and B14.
- unsaturated water, toluene/2 cm water layer, 60°C; Figure B15.
- unsaturated water, cyclohexane/2 cm water layer, 60°C; Figure B16, B17 and B18.
- unsaturated water, *n*-heptane/0.5 cm water layer, 60°C; Figure B19, B20 and B21.

Repeatability analysis was done for the calculated bitumen and total volumes and for the solvent mass transfer rate and water content in bitumen. The calculated volumes, solvent and water content in bitumen for times on which the bitumen dome starts destabilizing were omitted for the statistical analysis due to a high uncertainty on these measurements. Average values for the volumes repeatability before instability for each system were calculated using Eq B.3 and are reported in table B1. Variations on the total volume repeatability for the evaluated systems are associated with the solvent solubility in water; any rise on the total volume is proportional to the solubility in water, lower repeatability values for *n*-heptane are associated with its lower solubility in water, which is 260 times lower than that of toluene.

Table B1. Uncertainty of the bitumen and total volumes at 60°C for the evaluated systems.

System	**Bitumen Volume cm³ (%)**	**Total Volume cm³ (%)**
Toluene/water/bitumen	±0.06 (±6.0)	±0.004 (±0.4)
Cyclohexane/water/bitumen	±0.04 (±4.0)	±0.007 (±0.7)
n-Heptane/water/bitumen	±0.003 (±0.3)	±0.002 (±0.2)

The average repeatability of the solvent/water/bitumen tests at 20 and 60°C for the evaluated systems is reported in Table B2. The repeatability of the solvent transferred is reported as an

absolute uncertainty (cm^3) because for the low solubility experiments the uncertainty is related to the absolute measurement error. The relative uncertainty (percentage unit) is also presented because, at higher solubilities, the difference in solvent transfer in each repeat arises from a difference in the transfer rate. The repeatability of the water content is reported as an absolute uncertainty (wt%) because the deviations were not proportional to the measured value.

Table B2. Average uncertainty of the solvent transferred and water content in bitumen at 20 and 60°C for the evaluated systems.

System	Solvent Transfer cm^3 (%)	Water Content wt%
Toluene/water/bitumen at 20°C	±0.038 (±22)	±0.18
n-Pentane/water/bitumen at 20°C	±0.067 (±34)	±1.35
Toluene/water/bitumen at 60°C	±0.057 (±35)	±4.25
Cyclohexane/water/bitumen at 60°C	±0.022 (±30)	±0.55
n-Heptane/water/bitumen at 60°C	±0.015 (±3.4)	±0.15

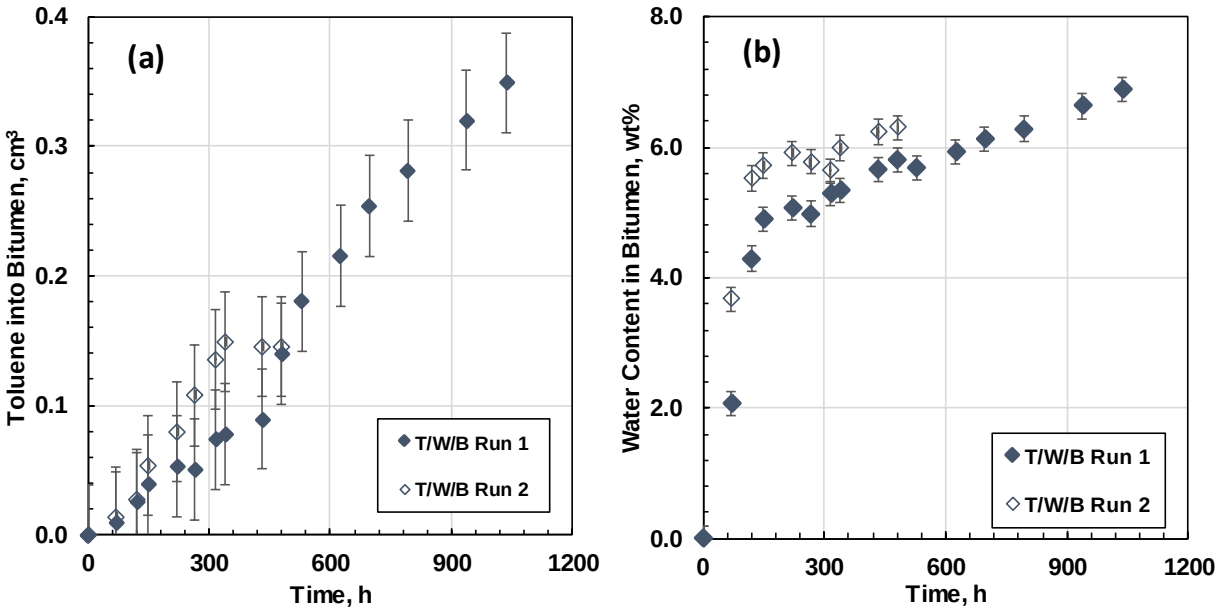

Figure B9. Toluene content (a) and water content (b) in bitumen over time for a toluene/water/WC-B-A3 bitumen system with a 0.45 cm unsaturated water layer at 20°C.

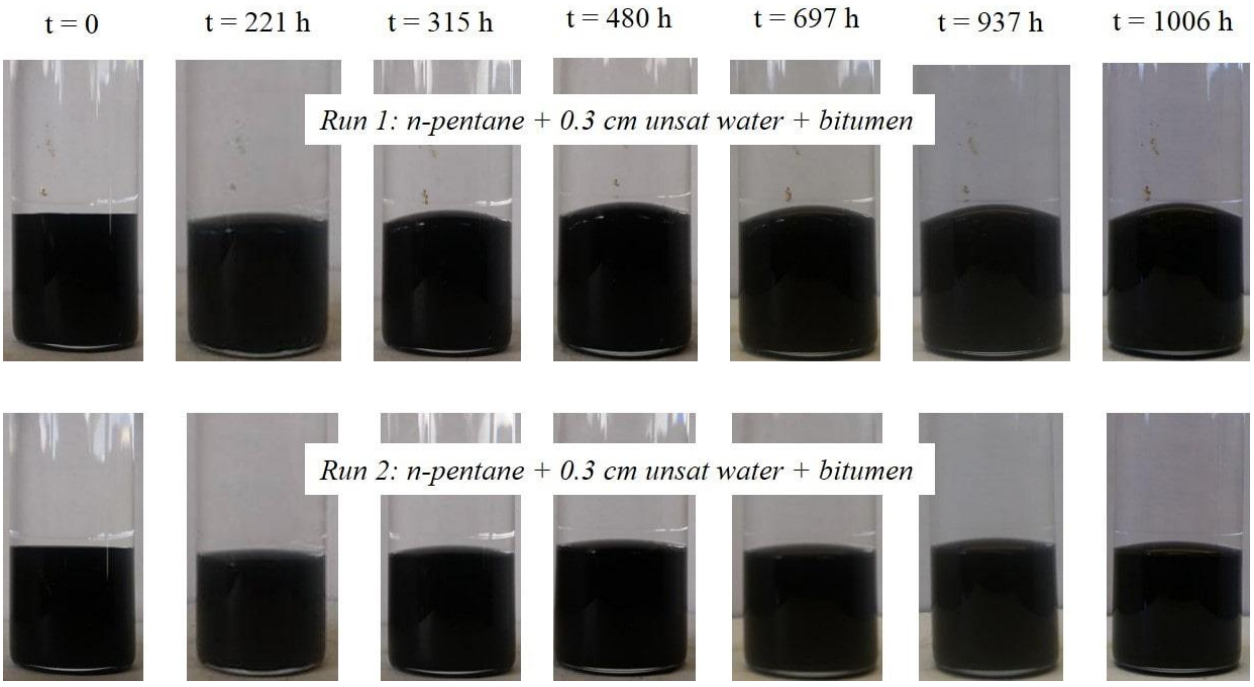

Figure B10. Photographs of repeated *n*-pentane/water/WC-B-A3 bitumen system tests with 0.3 cm of unsaturated water at 20°C.

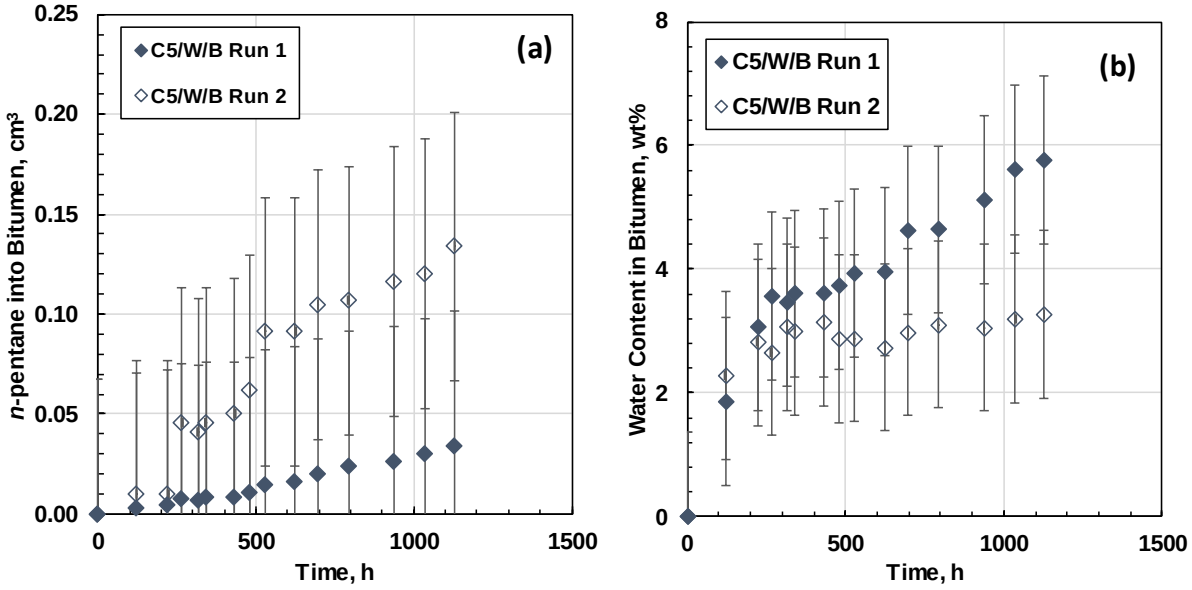

Figure B11. *n*-Pentane content (a) and water content (b) in bitumen over time for an *n*-pentane/water/WC-B-A3 bitumen system with a 0.3 cm unsaturated water layer at 20°C.

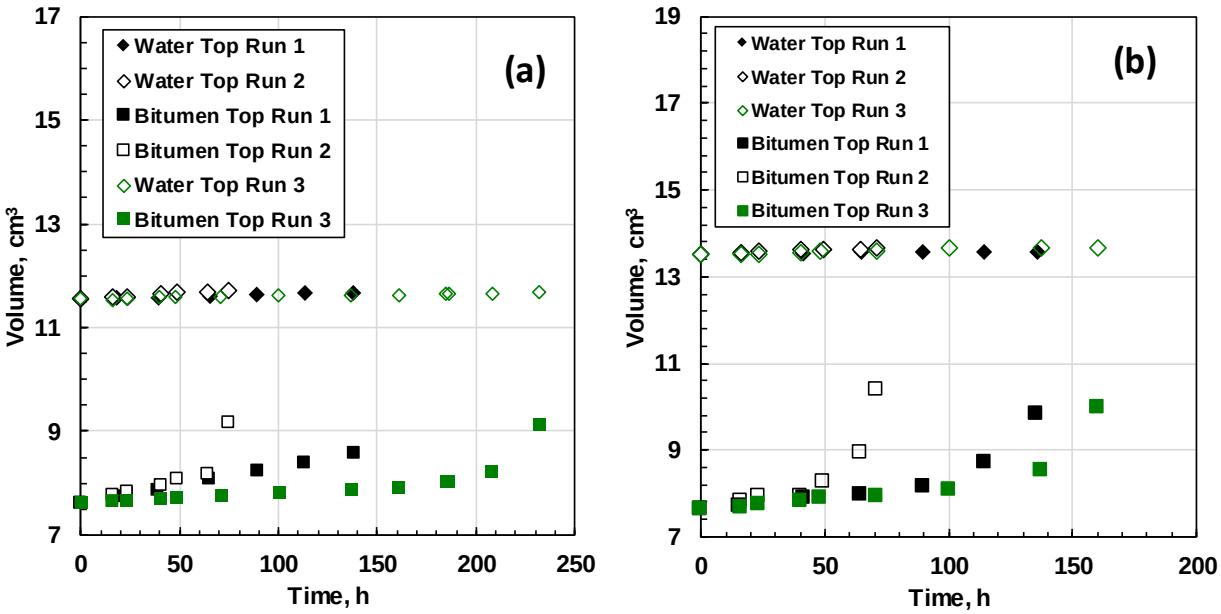

Figure B12. Bitumen volume and total volume over time for a toluene/water/WC-B-A3 bitumen system with (a) 1.0 cm unsaturated water layer and (b) 1.5 saturated water layer at 60°C.

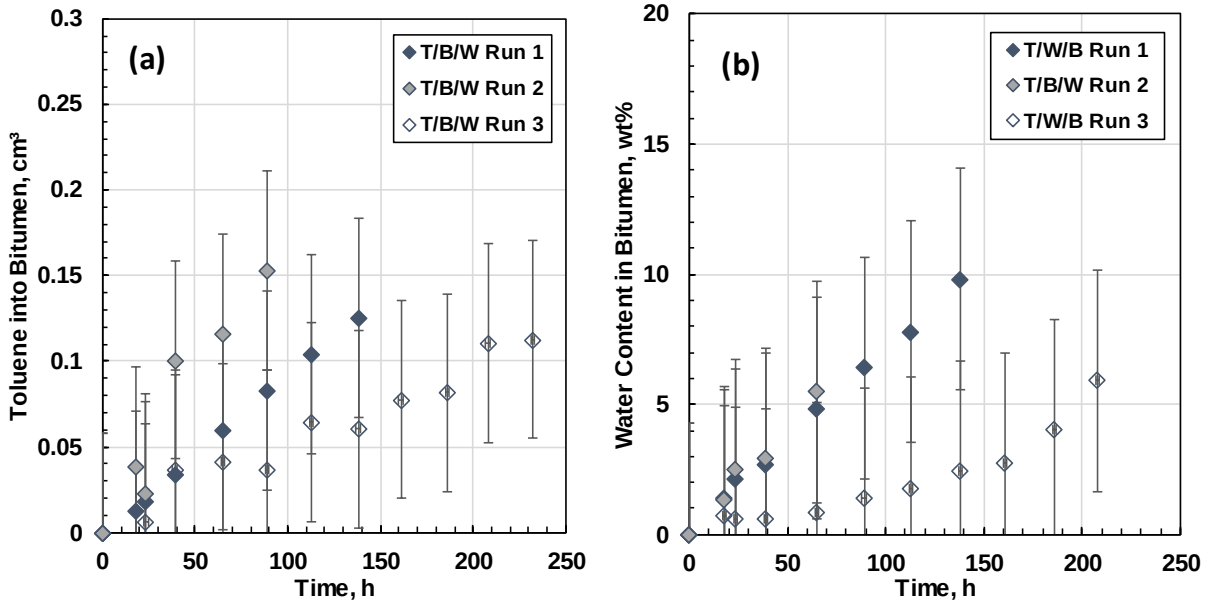

Figure B13. Toluene content (a) and water content (b) in bitumen over time for a toluene/water/WC-B-A3 bitumen system with a 1.0 cm unsaturated water layer at 60°C.

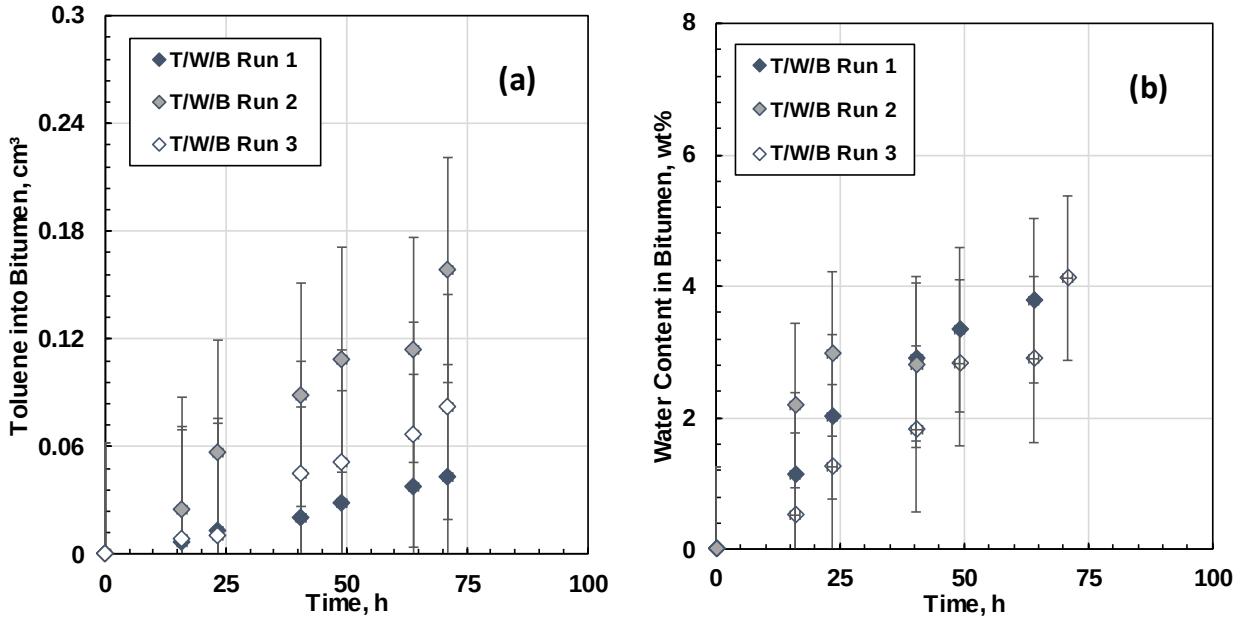

Figure B14. Toluene content (a) and water content (b) in bitumen over time for a toluene/water/WC-B-A3 bitumen system with a 1.5 cm saturated water layer at 60°C.

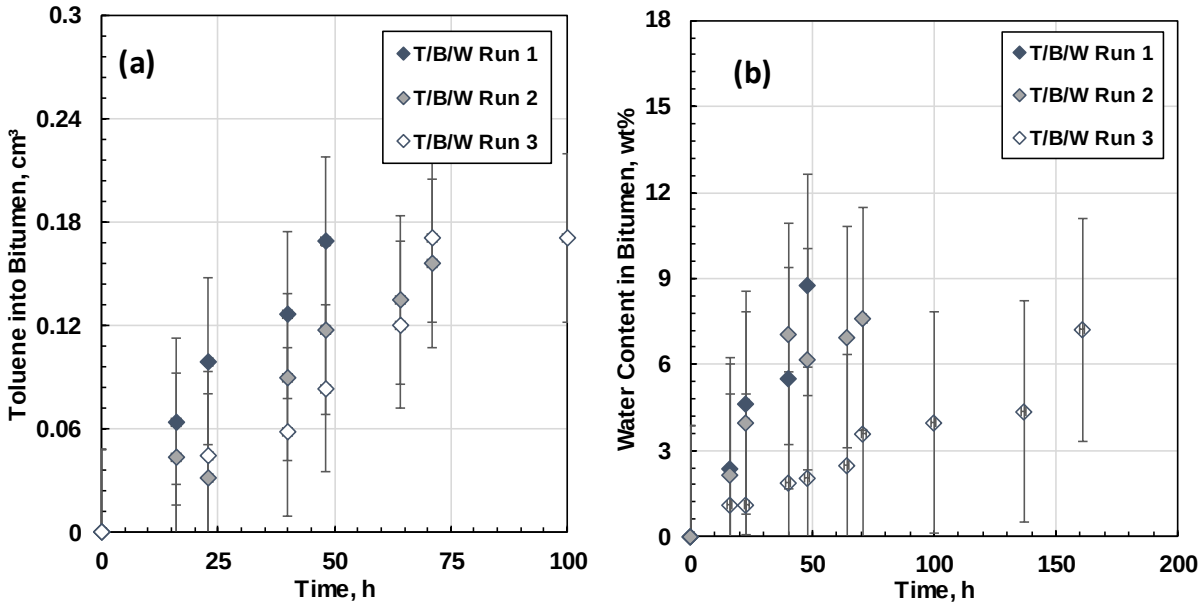

Figure B15. Toluene content (a) and water content (b) in bitumen over time for a toluene/water/WC-B-A3 bitumen system with a 2.0 cm unsaturated water layer at 60°C.

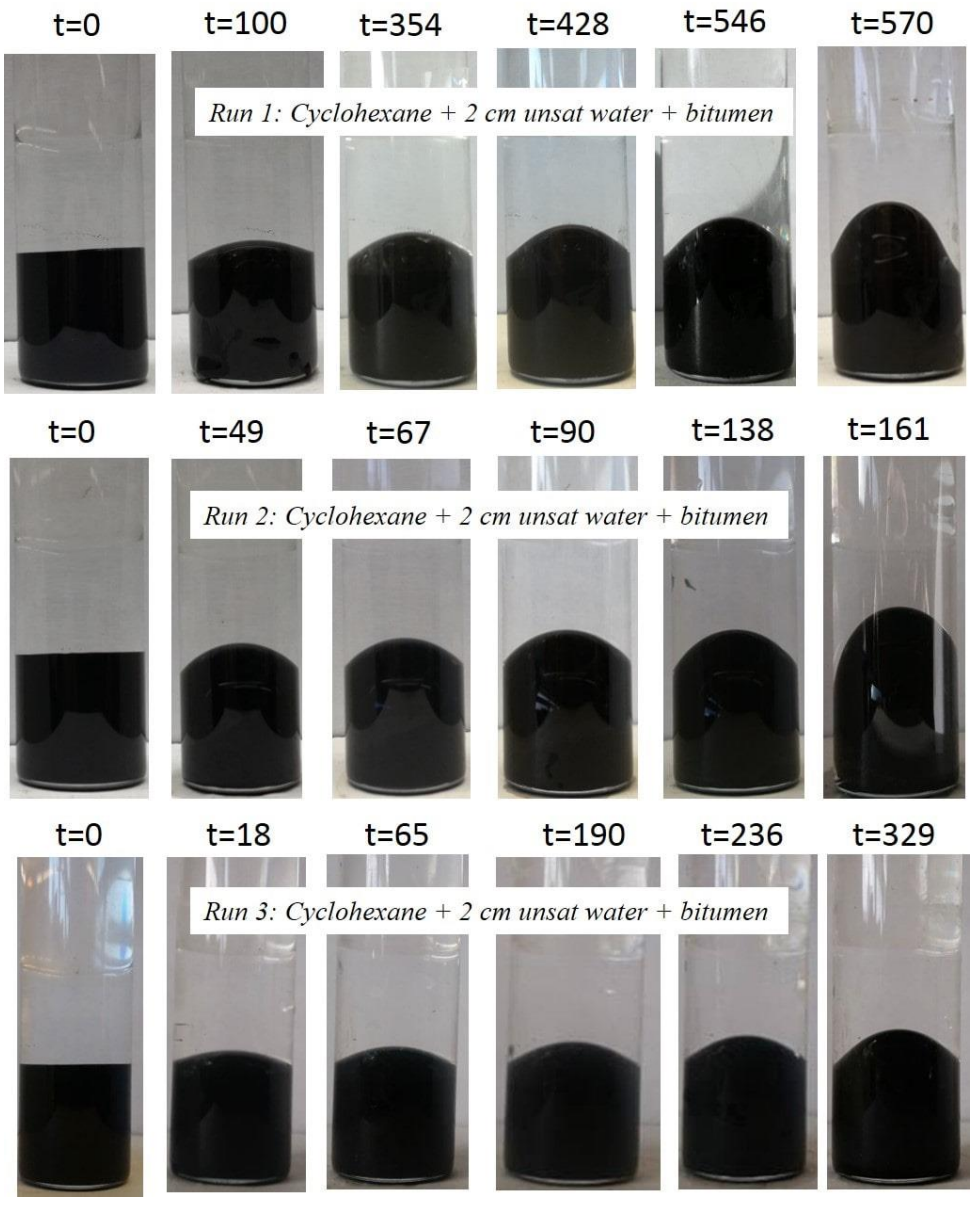

Figure B16. Photographs of repeated cyclohexane/water/WC-B-A3 bitumen tests with 2 cm of unsaturated water at 60°C.

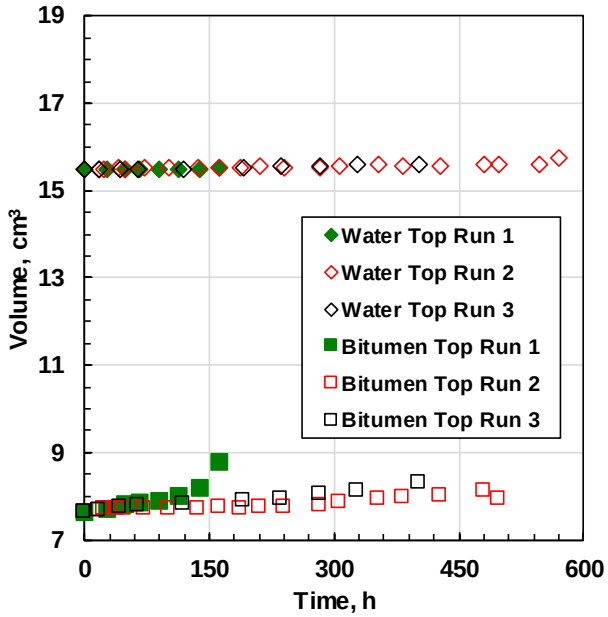

Figure B17. Bitumen volume and total volume over time for a cyclohexane/unsaturated water/WC-B-A3 bitumen system with a 2.0 cm unsaturated water layer at 60°C.

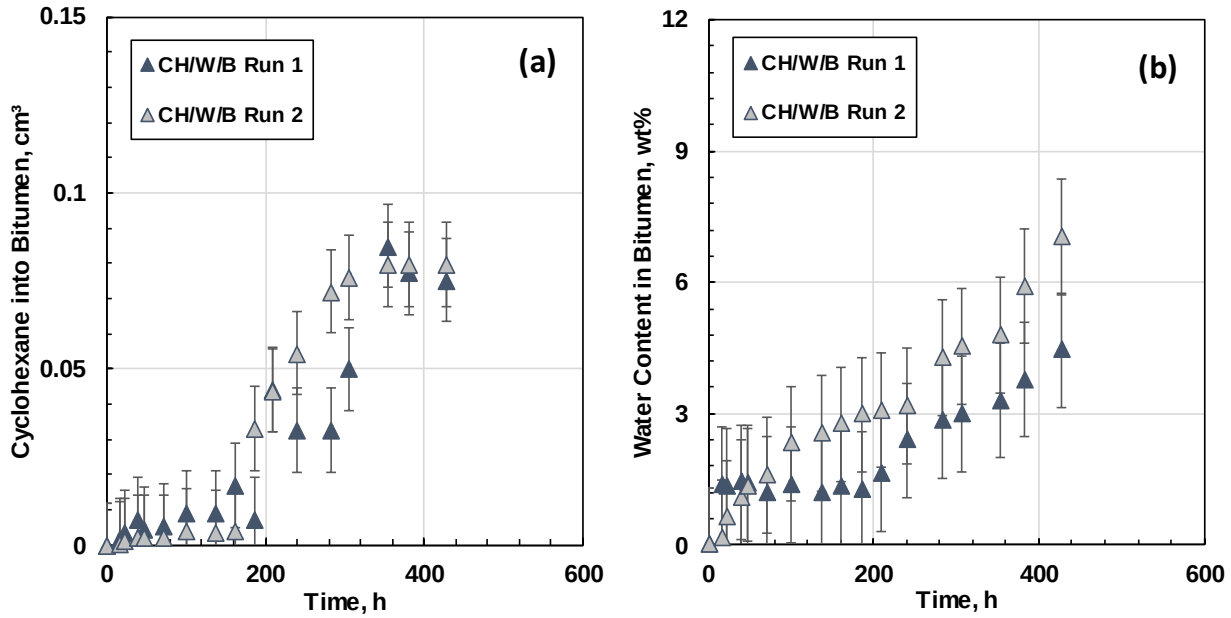

Figure B18. Cyclohexane content (a) and water content (b) in bitumen over time for a cyclohexane/water/WC-B-A3 bitumen system with a 2.0 cm unsaturated water layer at 60°C.

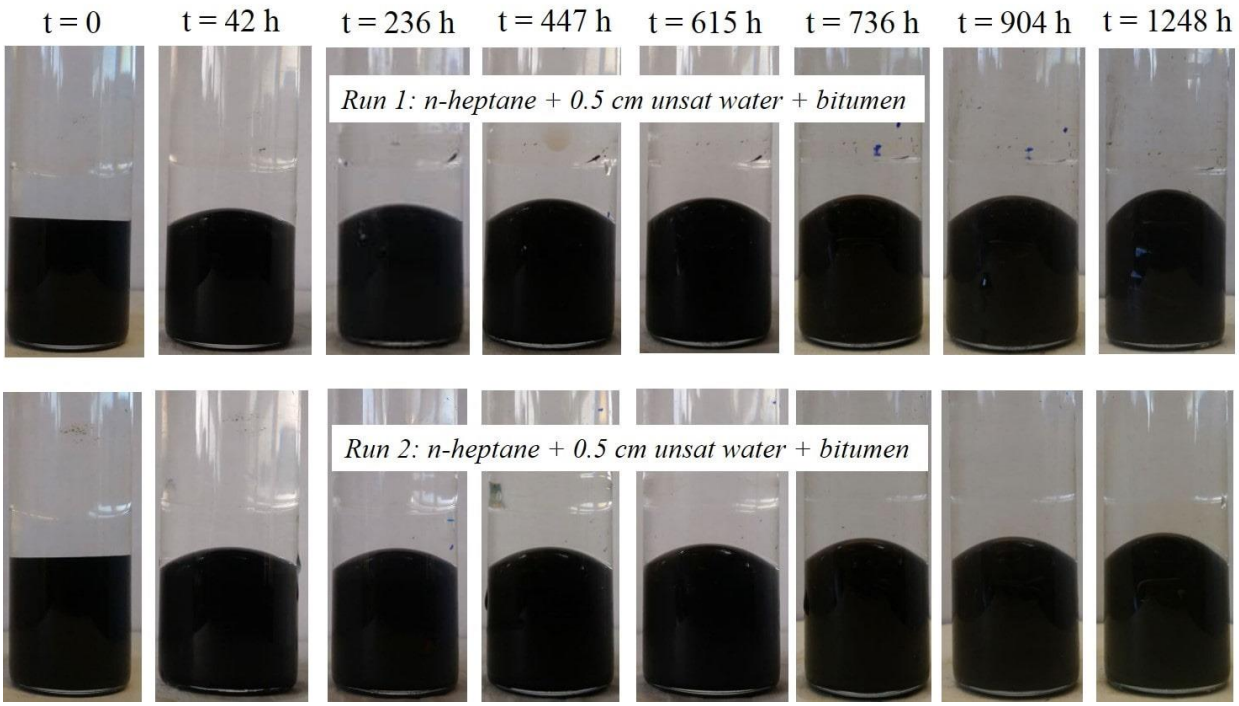

Figure B19. Photographs of repeated *n*-heptane/water/WC-B-A3 bitumen tests with 1 cm of unsaturated water at 60°C.

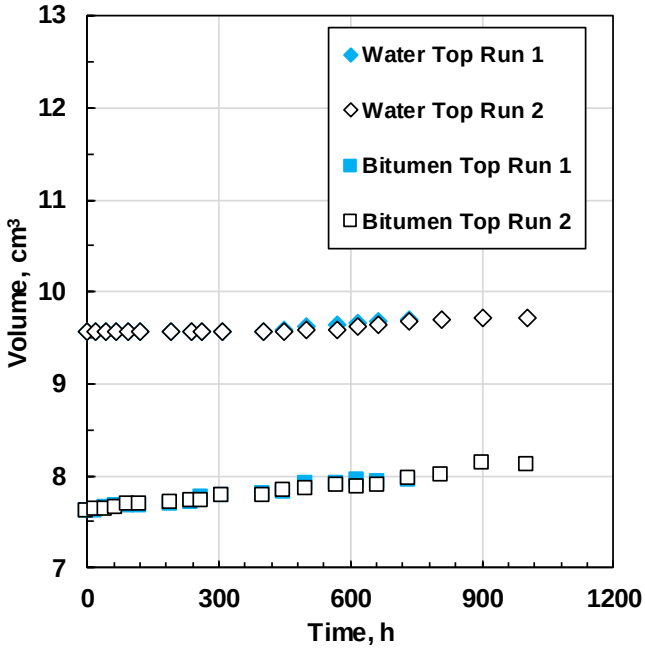

Figure B20. Bitumen volume and total volume over time for a *n*-heptane/unsaturated water/WC-B-A3 bitumen system with a 0.5 cm unsaturated water layer at 60°C.

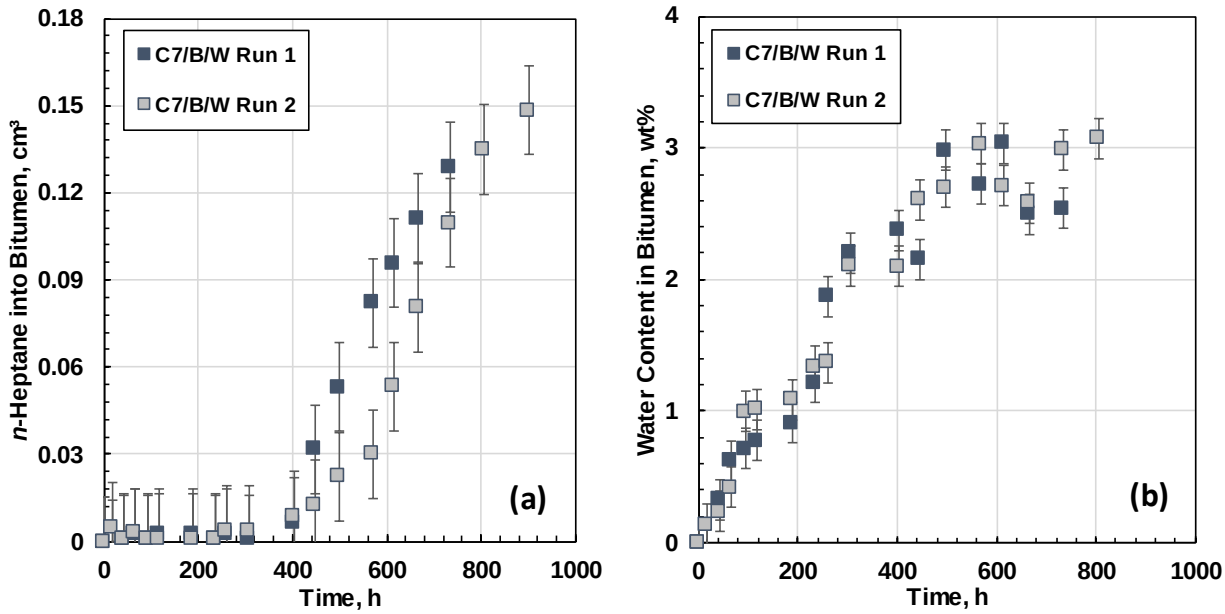

Figure B21. (a) *n*-heptane into bitumen versus time and (b) water content in bitumen versus time for a *n*-heptane /0.5 cm unsaturated water/WC-B-A3 bitumen at 60°C.

APPENDIX C: SOLUBILITY OF WATER IN BITUMEN

The procedure for estimating the solubility of water in bitumen by the method of Satyro *et al.*, (2013) is as follows:

1. Calculate the Watson-*K* (W_k) factor of the bitumen using the following equation:

$$W_k = \frac{T_{bp}^{1/3}}{SG} \tag{C.1}$$

where T_{bp} is the average boiling point of the bitumen in °R and *SG* is the bitumen specific gravity. In this thesis, the boiling point temperature was assumed to be the same as that of the Athabasca bitumen reported by Satyro *et al*, (2013); that is, 1408.14°R.

2. Calculate the interaction parameters ($a_{i,s}$, $b_{i,s}$, $c_{i,s}$, $\alpha_{i,s}$ and $\tau_{i,s}$) as a function of the specific gravity of the oil, Watson-*K* factor, and the NRTL model parameters, which are provided in Table C.1.

$$a_{i,s} = a_{1,s} + a_{2,s}SG + a_{3,s}W_k \tag{C.2}$$

$$b_{i,s} = b_{1,s} + b_{2,s}SG + b_{3,s}W_k \tag{C.3}$$

$$c_{i,s} = c_{1,s} + c_{2,s}SG + c_{3,s}W_k \tag{C.4}$$

$$\alpha_{i,s} = d_{1,s} + d_{2,s}SG + d_{3,s}W_k \tag{C.5}$$

$$\tau_{s,i} = e_{1,s} + e_{2,s}SG + e_{3,s}W_k \tag{C.6}$$

Table C1. NRTL model interaction parameters.

Parameter	1	2	3
a	80.55	10.05	-4.332
b	-1393	-2966	391.9
c	-6.912	-7.097	0.9115
d	-0.0189	-0.01282	0.001026
e	-57.47	74.82	-3.841

3. Calculate the interaction parameter between the water and bitumen ($\tau_{s,i}$).

$$\tau_{is} = a_{is} + \frac{b_{is}}{T} + c_{is}\ln T \tag{C.7}$$

where T is the temperature in K.

4. Calculate the infinite dilution activity coefficient of water in bitumen (γ_i^{∞}) using the NRTL model, given by:

$$\ln\gamma_i^{\infty} = \tau_{is}e^{-\alpha_{is}\tau_{is}} + \tau_{si} \tag{C.8}$$

5. Calculate the solubility of water in the bitumen. The solubility of sparingly soluble mixtures can be estimated as the inverse of the infinite dilution activity coefficient and the solubility of water in bitumen expressed as a mole fraction (x_i) is then given by:

$$x_i \approx \frac{1}{\gamma_i^{\infty}} \tag{C.9}$$

APPENDIX D: PHOTOGRAPHS OF WATER/BITUMEN AND SOLVENT/WATER/BITUMEN MASS TRANSFER EXPERIMENTS FOR THE ORIGINAL AND STRIPPED BITUMEN

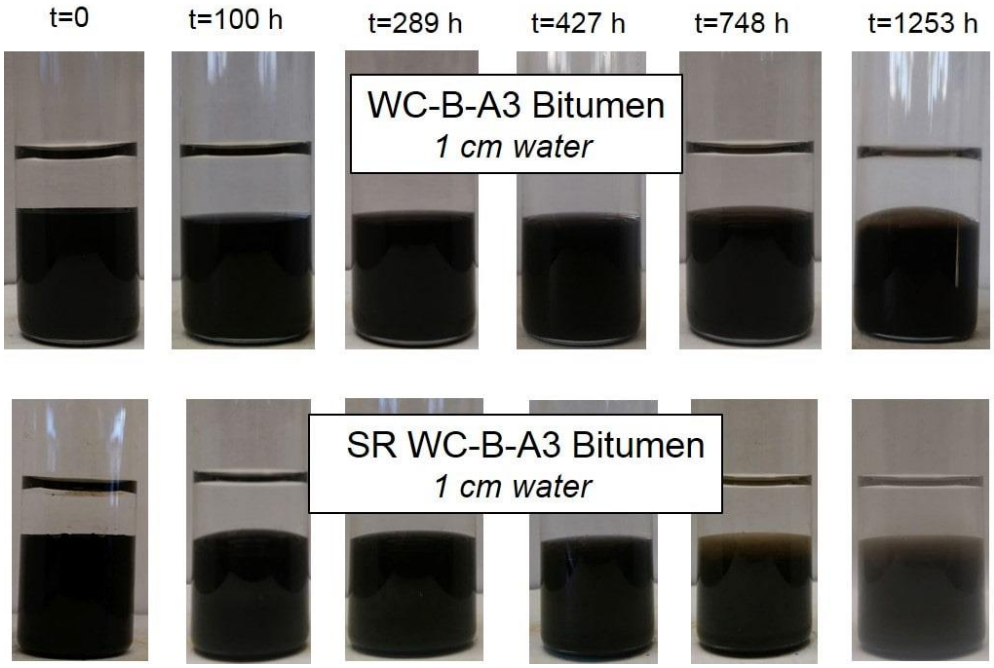

Figure D1. Photographs of water/WC-B-A3 and water/SR WC-B-A3 bitumen tests with 1.0 cm of unsaturated water at 20°C. (SR: Surfactant Reduced).

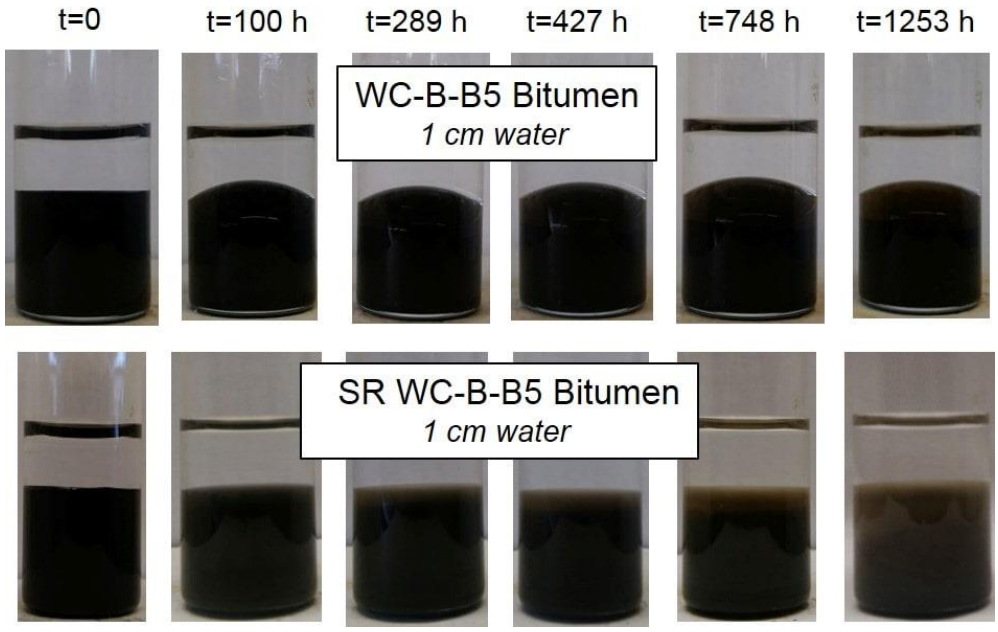

Figure D2. Photographs of water/WC-B-B5 and water/SR WC-B-B5 bitumen tests with 1.0 cm of unsaturated water at 20°C. (SR: Surfactant Reduced).

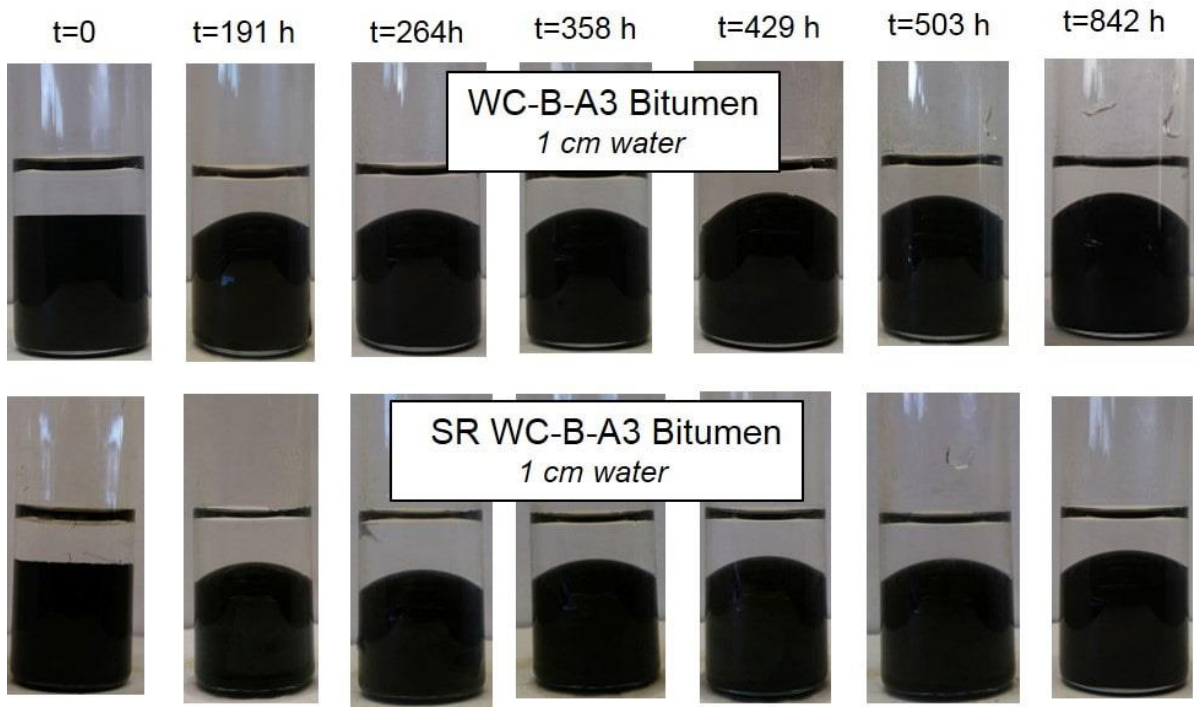

Figure D3. Photographs of water/WC-B-A3 and water/SR WC-B-A3 bitumen tests with 1.0 cm of unsaturated water at 60°C. (SR: Surfactant Reduced).

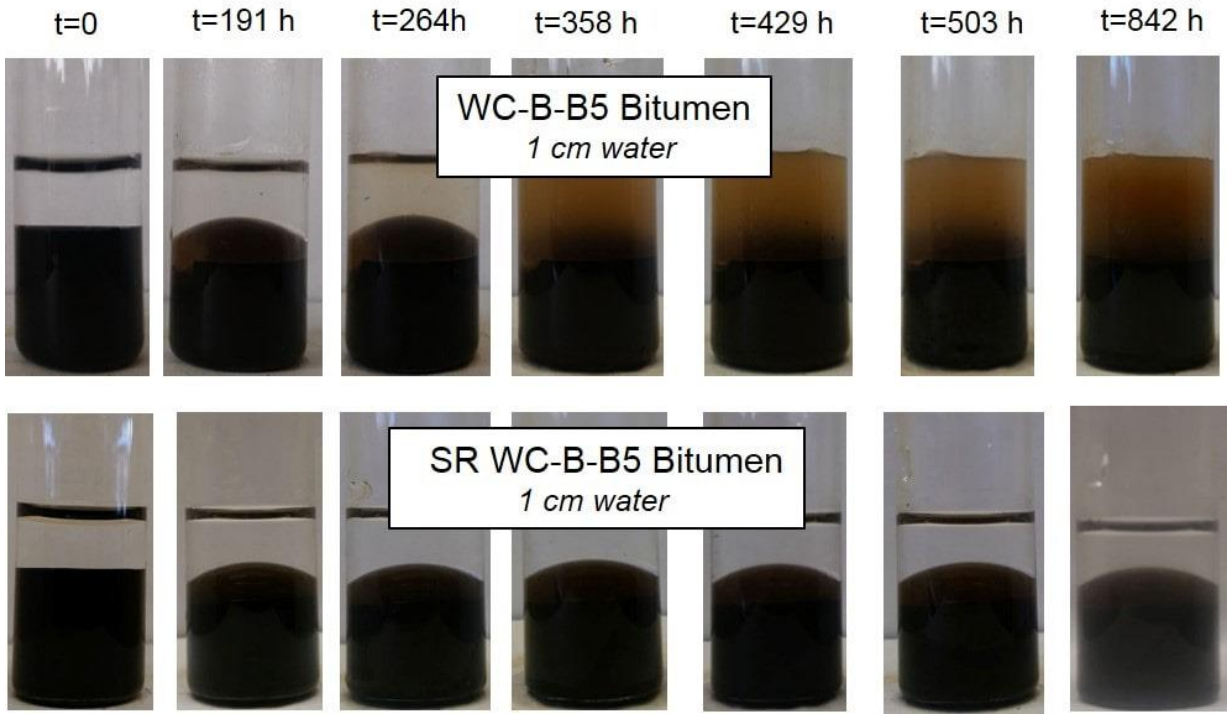

Figure D4. Photographs of water/WC-B-B5 and water/SR WC-B-B5 bitumen tests with 1.0 cm of unsaturated water at 60°C. (SR: Surfactant Reduced).

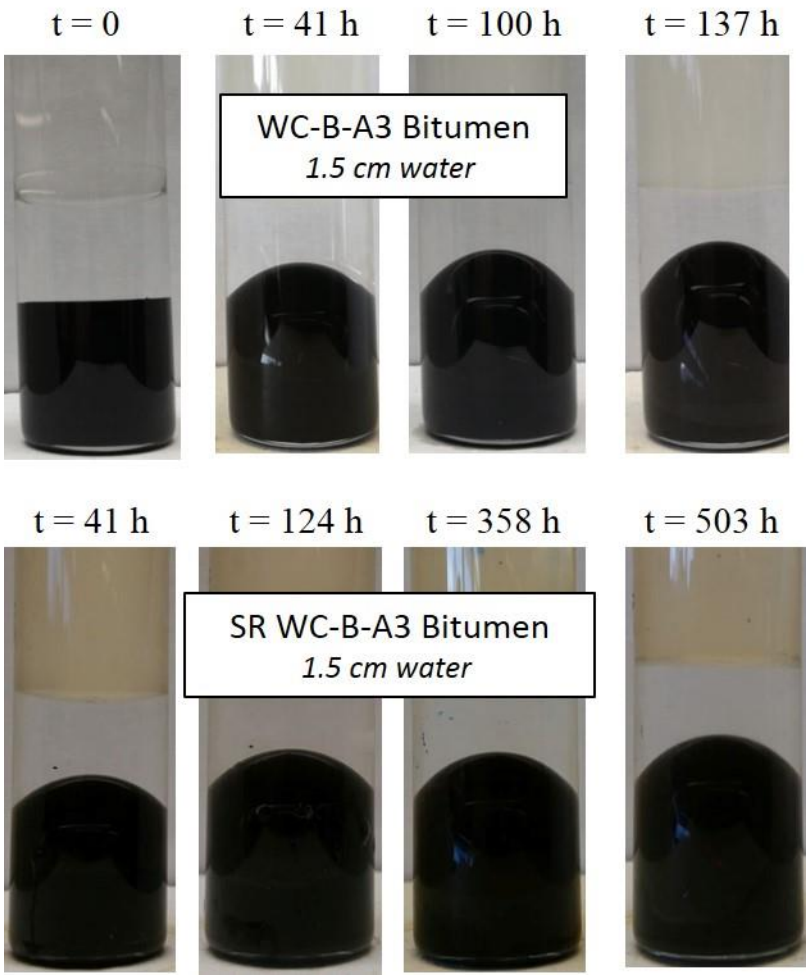

Figure D5. Photographs of toluene/water/WC-B-A3 and toluene/water/SR WC-B-A3 bitumen tests with 1.5 cm of unsaturated water at 60°C. (SR: Surfactant Reduced).

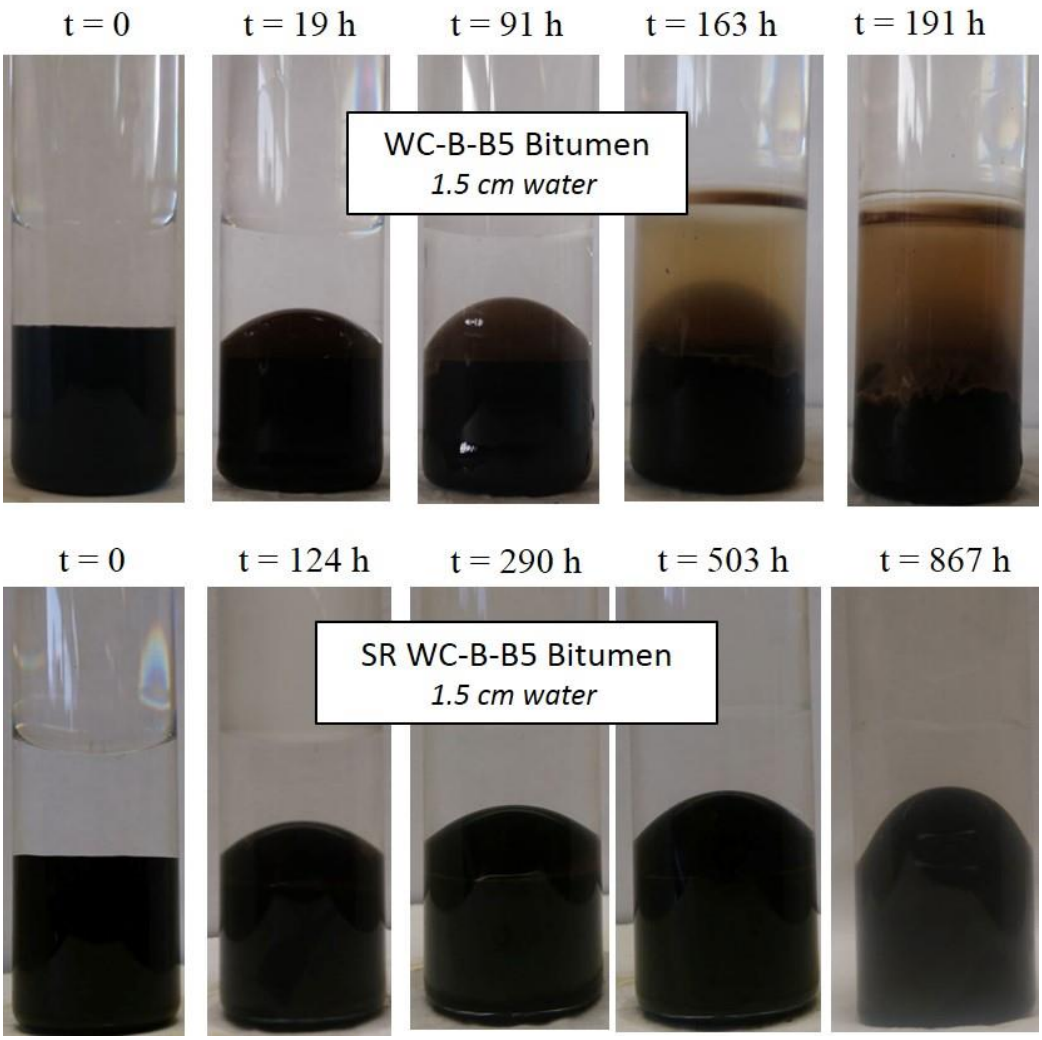

Figure D6. Photographs of toluene/water/WC-B-B5 and toluene/water/SR WC-B-B5 bitumen tests with 1.5 cm of unsaturated water at 60°C. (SR: Surfactant Reduced).

APPENDIX E: SOLVENT PENETRATION TIME

The solvent concentration profiles in water for the minimum (a) and maximum (b) water layer thickness are shown for the systems considered in this thesis in Figures E1 to E6.

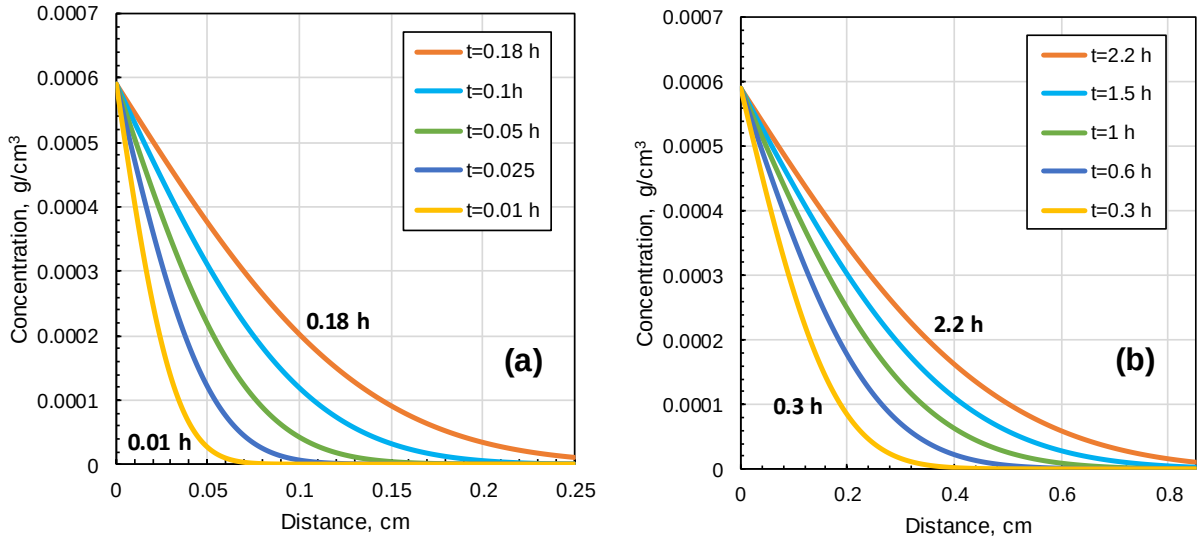

Figure E1. Solvent concentration profile in the water layer for a toluene/water/bitumen system at 20°C for water layer thicknesses of: a) 0.45 cm; b) 0.85 cm.

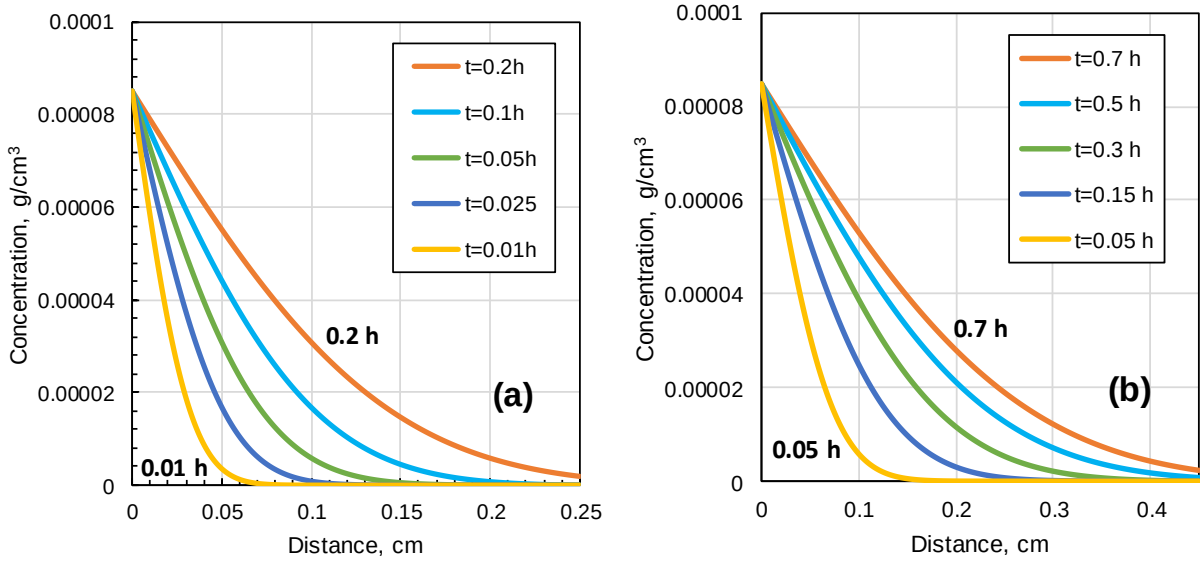

Figure E2. Solvent concentration profile in the water layer for a cyclohexane/water/bitumen system at 20°C for water layer thicknesses of: a) 0.25 cm; b) 0.45 cm.

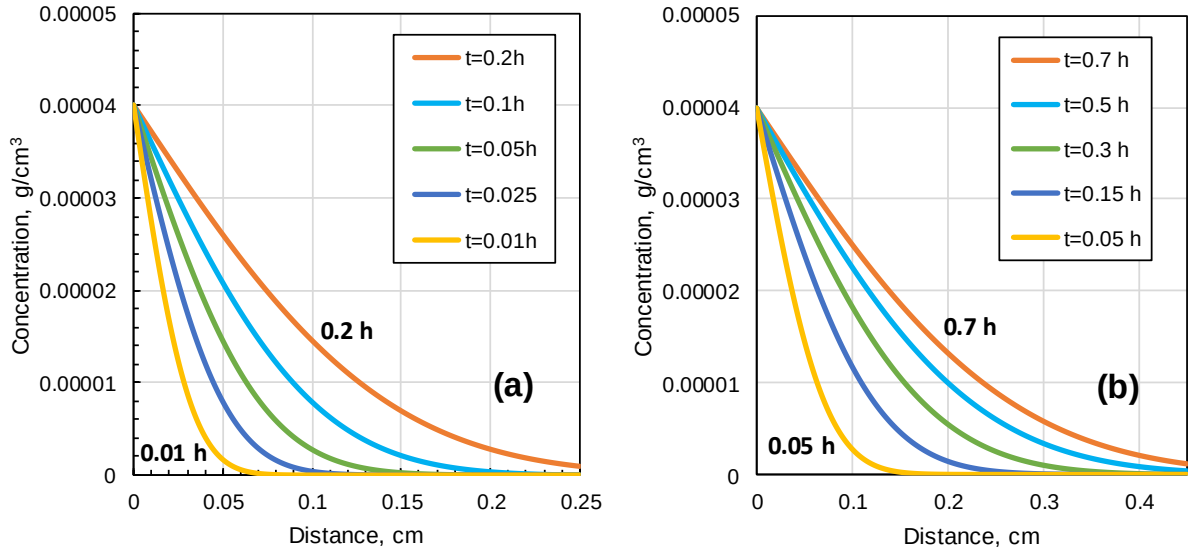

Figure E3. Solvent concentration profile in the water layer for a *n*-pentane/water/bitumen system at 20°C for water layer thicknesses of: a) 0.25 cm; b) 0.45 cm.

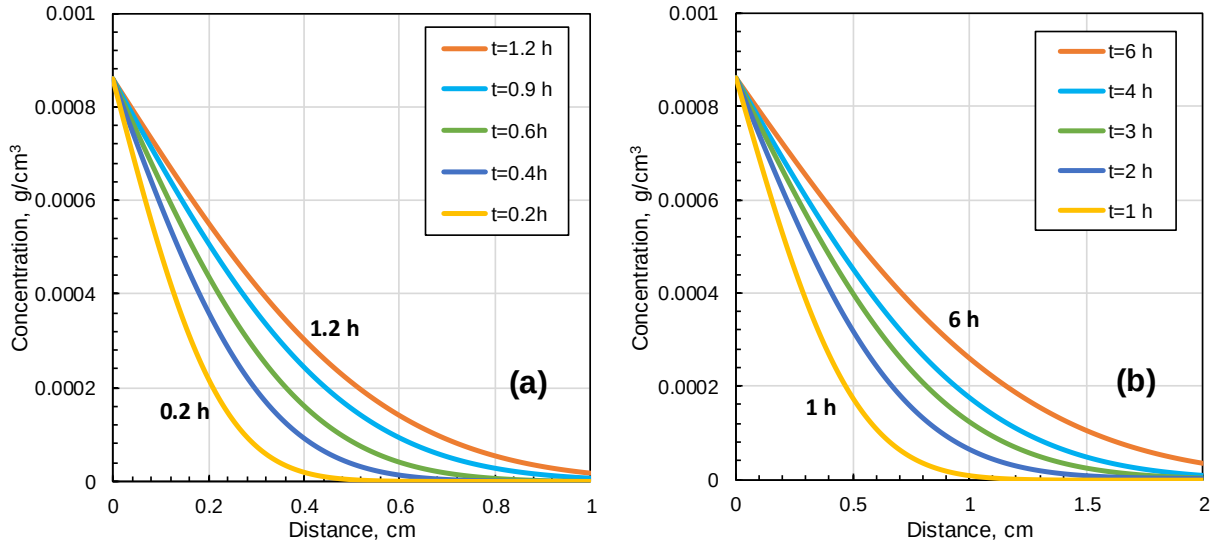

Figure E4. Solvent concentration profile in the water layer for a toluene/water/bitumen system at 60°C for water layer thicknesses of: a) 1.0 cm; b) 2.0 cm.

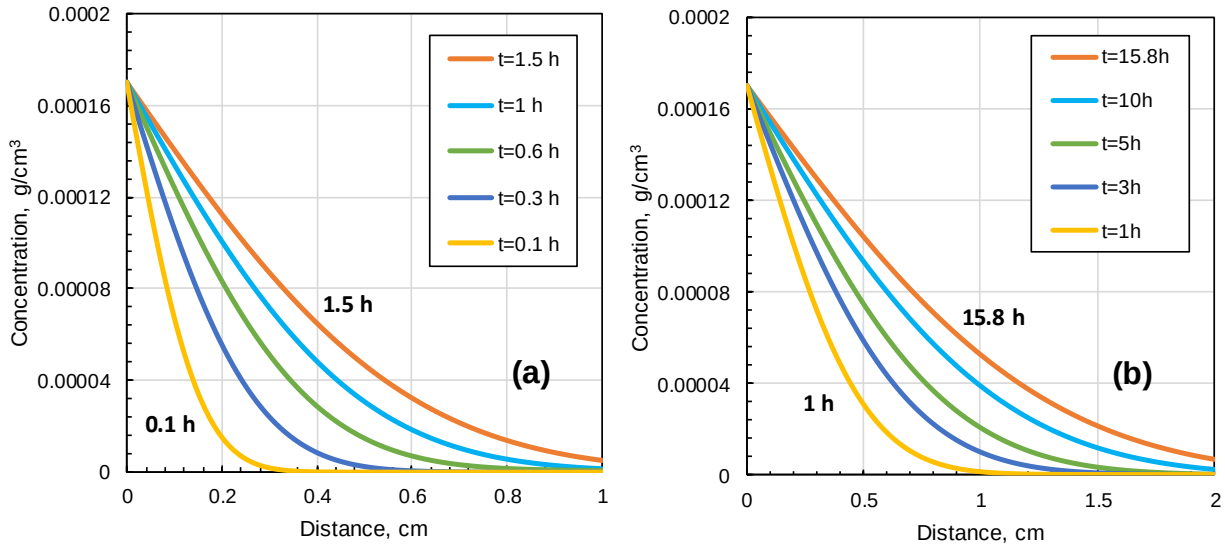

Figure E5. Solvent concentration profile in the water layer for a cyclohexane/water/bitumen system at 60°C for water layer thicknesses of: a) 1.0 cm; b) 2.0 cm.

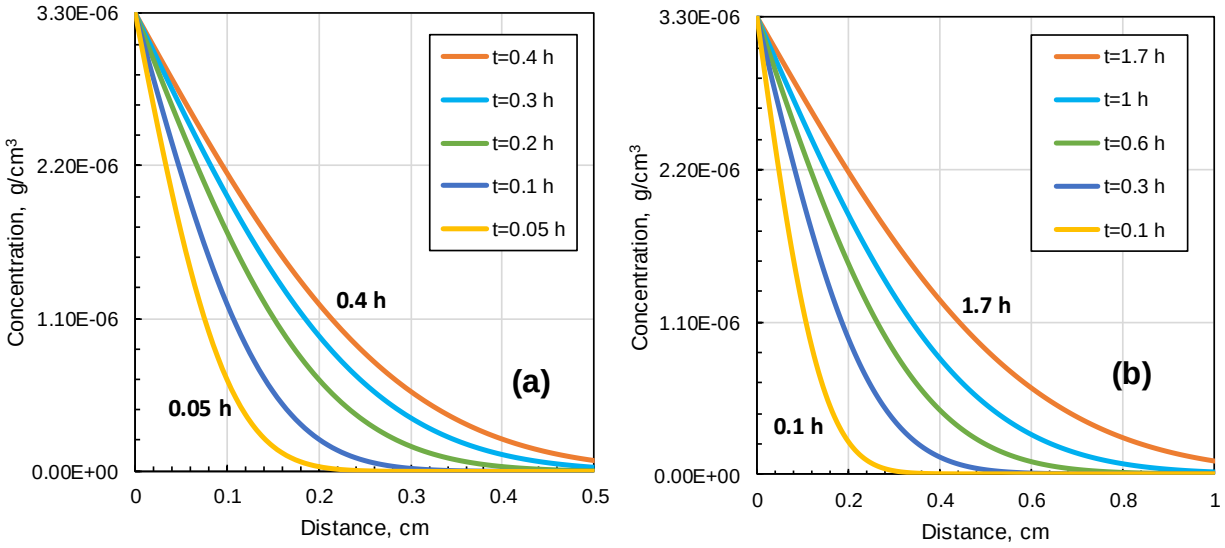

Figure E6. Solvent concentration profile in the water layer for a *n*-heptane/water/bitumen system at 60°C for water layer thicknesses of: a) 0.5 cm; b) 1.0 cm.

APPENDIX F: COMPARISON OF RESULTS FOR UNSATURATED AND SATURATED WATER FOR A TOLUENE/WATER/BITUMEN SYSTEM

Figures F1a and F1b compare the volume of toluene entering the bitumen and the incremental water content of the bitumen over time, respectively, for the toluene/water/WC-B-A3 bitumen systems prepared with saturate and unsaturated water at 20°C for a water layer thicknesses of 0.35. Figure F2 shows the same comparisons for a water layer height of 0.45 cm. The results with saturated and unsaturated water are the same within experimental error. Similar comparisons were observed at all other conditions considered in this thesis; that is, the difference between runs with saturated and unsaturated water were non-systematic and were well within the error of the measurements. Therefore, the initial saturation condition of the water was considered to have negligible effect on the experiments.

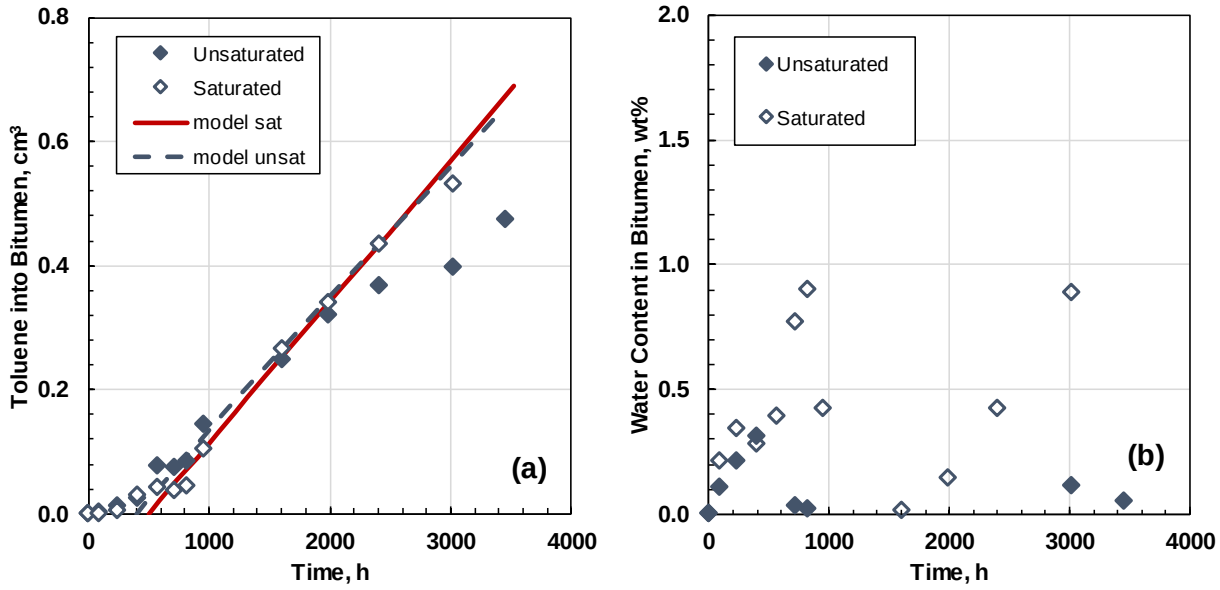

Figure F1. Comparison of results with saturated and unsaturated water for toluene/water/WC-B-A3 bitumen at 20°C with a water layer height of 0.35 cm: a) toluene volume entering bitumen layer; b) and incremental water content in the bitumen layer.

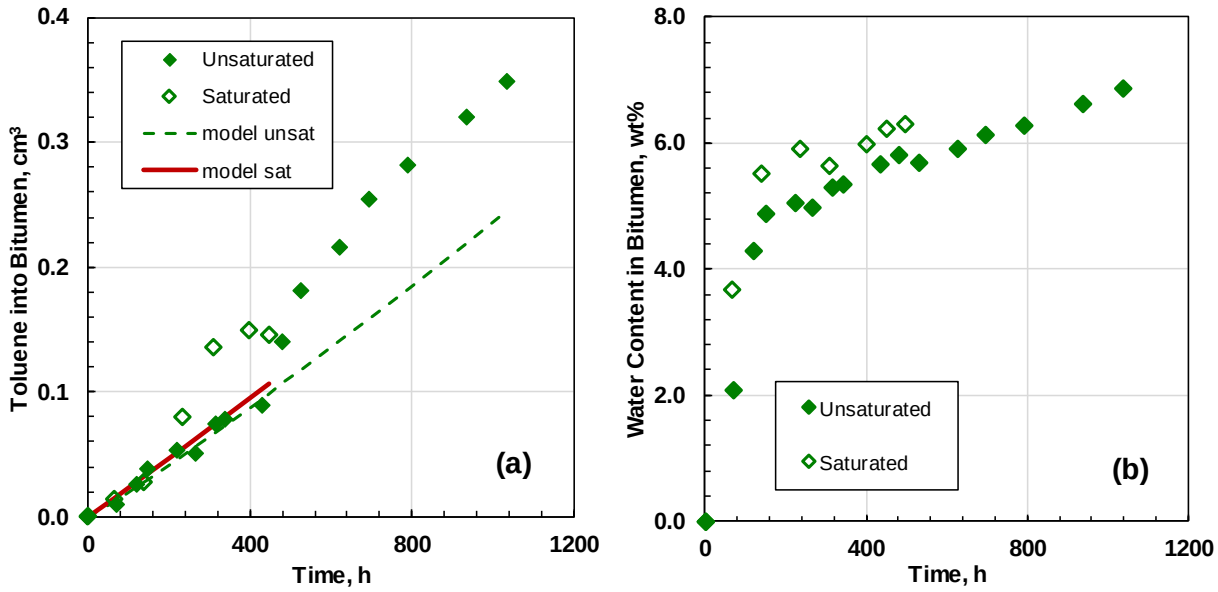

Figure F2. Comparison of results with saturated and unsaturated water for toluene/water/WC-B-A3 bitumen at 20°C with a water layer height of 0.45 cm: a) toluene volume entering bitumen layer; b) and incremental water content in the bitumen layer.